# OPTICAL FIBER BIOCHEMICAL SENSORS BASED ON MICRO-/NANO-STRUCTURED POLYMERIC COATINGS

**YIN MINGJIE**

**Ph.D**

**The Hong Kong Polytechnic University**

**2016**

# The Hong Kong Polytechnic University

## Department of Electrical Engineering


# Optical Fiber Biochemical Sensors Based on Micro-/Nano-Structured Polymeric Coatings


**YIN Mingjie**


A thesis submitted in partial fulfillment of the requirements for the degree of Doctor of Philosophy

**July 2015**

# CERTIFICATE OF ORIGINALITY

I hereby declare that this thesis is my own work and that, to the best of my knowledge and belief, it reproduces no material previously published or written, nor material that has been accepted for the award of any other degree or diploma, except where due acknowledgement has been made in the text.

_____ (Signed)

YIN Mingjie

_____ (Name of student)

# Abstract

Fiber-optic sensors have become one of the most enabling sensing technologies due to their distinctive advantages, such as small size, low cost, multiplexed detection and remote control capabilities. In recent years, new fiber-optic sensors for chemical and biological sensing have been drawn remarkable attentions due to their biocompatible properties as well as miniature size and high sensitivity. In this thesis, we present three kinds of new fiber-optic biochemical sensors through micro-/nano-engineering their polymeric coatings and demonstrate their applications in biological sensing.

We firstly developed a high-performance fiber-optic pH sensor through fabricating a nanoporous polyelectrolyte complex (PEC) film on the surface of a thin-core fiber modal interferometer (TCFMI) device. A monolayer self-assembly technique has been applied to make a high-quality PEC nano-structured film on the surface of TCFMI devices. Experimental results reveal that the sensor with nanoporous PEC film has a close sensitivity with the sensor coated with non-porous PEC film, but the former shows much fast response due to the nanoporous structures of the sensing film. The fabricated sensors break the common “trade-off” rule in sensor fabrication and show both superior pH sensing performance and fast response.

The second type of the developed fiber-optic biochemical sensor is a highly sensitive long-period grating (LPG) pH sensor. PAA ionic hydrogel has been periodically patterned on the surface of a tapered optical fiber with a diameter of 30 μm by using our own-developed maskless exposure setup and formed a strain-modulated grating structure. Experimental results revealed that this new kind of LPG pH sensor has much higher sensitivity than conventional LPG sensors whose grating structures are written in the photosensitive fiber core.

In order to exploit the fiber sensing technology in biological fields, we have developed a TCFMI biosensor based on polyelectrolyte multilayer nanocoatings for label-free DNA hybridization detection. With the layer-by-layer (LbL) self-assembly technique, multi-layered $(PEI/PAA)_{5(}PEI/ssDNA)_1$ sensing film has been coated on the surface of a TCFMI sensor for DNA detection. The sensor performance has been tested by using different kinds of ssDNA solutions with a concentration of 1 μM. Experimental results showed that the fabricated fiber-optic DNA sensor can precisely identify the number of match bases of ssDNA chains.

Finally, LPG sensors have been fabricated in small-diameter single mode fiber (SDSMF) and integrated into a microfluidic chip to develop an optofluidic biochip. With the point-by-point grating fabrication technique, LPG has been inscribed in a SDSMF by using high-intensity UV laser pulses.

LbL self-assembly technique was then adopted to coat $(PEI/PAA)_9(PEI/GOD)_1$multilayer sensing film on the LPG surface for glucose (GO) sensing. The influence of sensing film thickness on the GO sensors' performance was studied and compared. The fiber-optic GO sensor was finally integrated into the microfluidic channel to produce a biochip. Experimental results showed that the fiber sensor integrated biochip can detect GO concentration as low as 1 nM. Due to its point-of-care and real time analysis capabilities, such an ultrasensitive biochip has the potential for clinical applications.

# List of Publications

***Journal papers:***

1 **Mingjie Yin,** Mian Yao, Shaorui Gao, A. Ping Zhang, Hwayaw Tam, Pingkong Wai, Rapid 3D patterning of poly (acrylic acid) ionic hydrogel for miniature pH sensors, *Advanced Materials*, 28, 1394-1399, (2016).

2 **Mingjie Yin,** Bobo Huang, Shaorui Gao, A. Ping Zhang, Xuesong Ye, Optical fiber LPG biosensor integrated microfluidic chip for ultrasensitive glucose detection, accepted by *Biomedical Optics Express.*

3 **Mingjie Yin,** Chuang Wu, Liyang Shao, Wingkin Edward Chan, A. Ping Zhang, Chao Lu, Hwayaw Tam, Label-free, disposable fiber-optic biosensors for DNA hybridization detection, *Analyst*, 138, 1988-1994, (2013).

4 Qiang Zhao, **Mingjie Yin,** A. Ping Zhang, Simon Prescher, Markus Antonietti, Jiayin Yuan, Hierarchically structured nanoporous poly(ionic liquid) membranes: facile preparation and application in fiber-optic pH sensing, *J. Am. Chem. Soc.*, 135, 5549−5552, (2013).

5 Liyang Shao, **Mingjie Yin,** Hwayaw Tam, Jacques Albert, Fiber optic pH sensor with self-assembled polymer multilayer nanocoatings, *Sensors*, 13, 1425-1434, (2013).

6 Bobo Huang, **Mingjie Yin,** A. Ping Zhang, Xuesong Ye, *In-situ*

microfabrication of thermally controllable microvalves in microfluidic chip via optical maskless stereolithography, submitted to *Sensors and Actuators: A. Physical*.

***Conference papers:***

1 **Mingjie Yin**, A. Ping Zhang, Hwayaw Tam， Integrated microfluidic biochip with nanocoating self-assembled fiber-optic sensor, *15th International Conference on Nanotechnology (IEEE Nano 2015)*, Rome, Italy, 2015.

2 **Mingjie Yin**, A. Ping Zhang, Hwayaw Tam, Self-assembled biocompatible nanocoating for optical fiber biosensors, *The 4th Asian Biomaterials Congress,* Hong Kong, China, 2013.

3 Liyang Shao, **Mingjie Yin,** Hwayaw Tam, Jacques Albert, Fiber optic pH sensor with self-assembled multilayer nanocoatings on tilted FBG, 22nd *International Conference on Optical Fiber Sensor,* Beijing, China, 2012.

# Acknowledgements

First of all, in my heart of hearts, I would like to express my sincere gratitude to my chief supervisor, Dr. A. Ping Zhang, for his patient and valuable guidance during my graduate studies, from the establishment of research topic to the design of experiments, from the detail of experiments to the paper writing. Without his broad knowledge and deeply academic insight, I would not finish my study and research topic so smoothly. Without his nicely assistance in the aspects of my research and life, I would not complete my thesis successfully. More importantly, his zeal in research inspired me to broaden insight in the research area and master more knowledge about other subjects, which are very helpful in doing my research. It is a wealthy for my whole life.

I would appreciate the guidance and assistance from Prof. H.Y. Tam, my co-supervisor, who provided me the opportunity to pursuing my PhD degree at PolyU, his advice on my research made me quickly overcome the difficulties in the research.

I would also express my appreciation to Prof. Qingdong Zheng, who have given me the opportunity to learn more knowledge on the organic electronics. I have learnt a lot for his professional knowledge and experimental skills, which lay a foundation for my development in the future.

I am grateful to those who provided great help on finishing my experiments and the thesis. I thank to Mr. Cheng Xin, Mr. Wu Jushuai, Mr. Huang Bobo, Dr. Gao Shaorui, Mr. Yao Mian, Mr. Liu Zhengyong, Mr. Wang Jie, Mr. Yuan Tianhao, Dr. Wu Chuang, Dr. Zhao Qiang, Dr. Shao Liyang for their discussion and useful assistance in my experiments and thesis writing. I would also like to express my thanks to Dr. Yuan Jiayin, Dr. Xie Yizhu, Dr. Guo Xin, Dr. Pun Chifung, Mr. Du Jingyu for their help and discussion for my experiments. I am grateful to Mr. Xue Peng, Mr. Nie Yongquan, Mr. Liu Junwei, Mr. Guo Mingzhi, for their help and encouragements in my life and study.

Last but not the least, I am deeply indebted to my family and friends, for their selfless dedication, support and love. I give my special and deeply thanks to my mother, my aunt and my wife, for their encouragements and cares. They always gave support to me in time when I was in difficulty. It is their support encouraged me to finish my study. I would like to dedicate the thesis to my whole family.

# Table of Contents

***Page***

# List of Figures

# List of Tables

# List of Acronyms

| Acronyms | Description |
|---|---|
| TCFMI | Thin-core fiber modal interferometer |
| LPG | Long-period grating |
| SDSMF | Small-diameter single mode fiber |
| TOF | Tapered optical fiber |
| F-P | Fabry–Perot |
| LSPR | Localized surface plasmon resonance |
| TFBG | Tilted fiber Bragg gratings |
| OSA | Optical spectra analyzer |
| RI | Refractive index |
| FRET | Forster energy transfer |
| AFM | Atomic force microscope |
| SEM | Scanning electron microscopy |
| DMD | Digital-micromirror device |
| OMSL | Optical maskless setereolithography |
| RMS | Root mean square |
| LB | Langmuir–Blodgett |
| SAM | Self-assembled monolayers |

| | |
|---|---|
| LbL | Layer-by-layer |
| PCCA | Polymerized crystalline colloidal arrays |
| SCCBs | Silica colloidal crystal beads |
| CP | Conjugated polymer |
| PPMs | Porous polyelectrolyte membranes |
| PEC | Polyelectrolyte complex |
| MSO | Mercury-specific oligonucleotide |
| PIL | Polymerized ionic liquid |
| QDs | Quantum dots |
| DMF | Dimethylformamide |
| DNA | Deoxyribonucleic acid |
| ssDNA | Single-stranded DNA |
| PNA | Peptide nucleic acid |
| GO | Glucose |
| GOD | Glucose oxidase |
| GDH | Glucose dehydrogenase |
| Irgacure 2959 | 2-Hydroxy-4'-(2-hydroxyethoxy)-2-methylpropiophenone |
| AA | Acrylic acid |
| PAA | Poly (acrylic acid) |
| PEI | Poly (ethylenimine) |

| | |
|---|---|
| PSS | Poly (sodium-p-styrenesulfonate) |
| PAH | Poly (allylamine hydrochloride) |
| P4VP.HCl | Poly (N-ethyl-4-vinylpyridinium chloride) |
| HPTS | 1-Hydroxypyrene-3,6,8-trisulfonate |
| PCMVImTf2N | Poly [3-cyanomethyl-1-vinylimidazolium bis(trifluoro methanesulfonyl)imide] |
| PMNT | Poly (3-(3'-N, N, N-triethylamino-1'-propyloxy)-4-methyl-2, 5-thiophene hydrochloride) |

# *Chapter 1*

# Introduction

## 1.1 Background

'Optical Technologies for the 21st Century' was proposed by the German Agenda in 2002. It emphasized that optical technology will be an enabling technology for a great many of fields and applications in the future [1]. Particularly, optical sensors will play the key role in the development of almost every field, such as light barriers, automotive rain sensors, white light interferometers and high-resolution scanning near-field optical microscopes [2]. Optical sensors have become an attractive and hot research topic, and many kinds of optical sensors and biosensors have been demonstrated, such as gas sensors [3], ion sensors [4, 5], pH sensors [6-9], humidity sensors [10-12], small organic molecule detection [13], DNA biosensors [14-16], glucose biosensors [17, 18], cell based biosensors [19], and other biological sensors [20, 21]. Recently, much efforts have been devoted to developing miniaturize optical sensors and integrating them into biochips [22, 23]. Such biochips have many advantages: 1) on-site analysis, analysis in security areas; 2) extremely small sample consumption and fast response; 3) suitable for in vivo test because of compactness.

Optical fibers have become one of the best candidates for development of miniature optical sensors [22]. They have some competitive and attractive properties, including small size, biocompatibility, immune to electromagnetic interferences, multiplexed detection capability and potentially low-cost [24, 25]. So far, various kinds of fiber devices have been adopted for sensors development, such as long period grating [26], fiber Bragg grating [27], tapered fiber [28], thin-core fiber modal interferometer [5], Fabry-Perot cavity [18], photonic crystal fiber [29] and other specialty optical fibers [30]. Moreover, these fiber devices have been widely employed in chemical detection and biological fields. Since 2000, the ACS Journal 'Analytical Chemistry' has published the biannual review on the topic of 'fiber-optic chemical sensors and biosensors', which provides a concise but comprehensive reviews on the development of fiber-optic sensors and biosensors [31-36].

A key aspect of fiber-optic sensors fabrication is the ability to guide light propagation for both sensing and signal processing [37]. Fiber-optic biochemical sensors can be developed through interacting the sensing films with the propagating modes for conducting a range of measurements. Thus, it is quite appealing to deposit active and passive nanocoatings on the surface of optical fiber to achieve the chemical or biological sensing purposes [38].

The techniques used for preparation of thin sensing film deposition

becomes one of pivotal issues in the development of optical biochemical sensors [38]. A number of methods have been proposed for thin film deposition, such as self-assembled monolayer method, Langmuir–Blodgett technique [39], chemical vapor deposition [40], atomic layer deposition [41] and layer-by-layer (LbL) self-assembly technique [42]. In particular, the LbL self-assembly technique provides a versatile method to fabricate controlled layered nanostructures, with various kinds of functional materials, via very simple, inexpensive and rapid procedures. Since their rediscovery by Decher [43], numerous reports and reviews on their fundamental studies and applications have been published [42, 44-48]. The LbL self-assembly technique has been widely applied in physical fields (electrochemical capacitors [49], lithium-ion batteries [50], organic field-effect transistor [51] and solar cells [52]), chemical fields (self-healing [53], superhydrophobic surfaces [54], tunable degradation [55], sensors [25], catalysts [56] and permeability control [57]) and biomedical fields (controlled release [58], drug delivery [59], cell culture [60], biosensors [14] and cancer therapy [61]).

## 1.2 Objectives of Research

Though fiber-optic sensors have been studied for some years, most of them focused on physical sensors. The studies on fiber-optic biochemical sensors are not too many, and there is still spacious room for development in this

field, including high performance (including the sensitivity, response time and repeatability) and cost-saving fiber-optic biochemical sensors fabrication. In addition, special types of fiber-optic sensors are also needed to be developed for some emerging biochemical sensing applications. Moreover, fiber-optic sensors are very promising to be integrated within microfluidic chips to develop "lab-on-a-chip" devices for multi-parameter sensing and clinical diagnostics.

In this thesis, novel fiber-optic biomedical sensors, including novel types of fiber devices and new biomedical sensing coatings, are developed. Particularly, dramatic attention will be paid to enhance the performance of fiber-optic biomedical sensors, in terms of their sensitivity and response time. Several kinds of fiber-optic biosensors have been developed in accordance with different practical biochemical sensing applications. Eventually, fiber-optic biosensor is demonstrated to integrate with microfluidic chip to develop highly sensitive biochips for real-time, point-of-care and small-dose diagnosis.

## 1.3 Outline of Thesis

The chapters of my thesis are organized as follows:

Chapter 1: Introduction. In this chapter, the background of fiber-optic sensors and the sensing film deposition methods are introduced. The objectives of

the research are also introduced. Finally, the outline of the thesis is also presented.

Chapter 2: Overview of Optical Biochemical Sensing Technology. In this chapter, some kinds of fiber-optic refractive index sensors will be reviewed, and the development of optical biochemical sensors and their applications in biological field are summarized. Finally, the significance of developing fiber-optic biochemical sensors and their potential application in clinical diagnostics are discussed.

Chapter 3: Fiber-optic pH Sensors Based on Self-assembled Monolayer Nanoporous Sensing Coating. In this chapter, a high performance fiber-optic pH sensor based on TCFMI is developed by using monolayer self-assembly technology. Owing to the nanoporous sensing coating, both high sensitivity and fast response of the sensor have been achieved, which breaks the common “trade-off” rule in sensor fabrication.

Chapter 4: Optical Microfiber LPG pH Sensor Based on Micropatterned PAA Ionic Hydrogels. In this chapter, a novel long period fiber (LPG) grating pH sensors is developed by periodically patterning ionic hydrogels on the surface of a tapered optical fiber. An own-developed optical maskless exposure technology has been applied to fabricate a strain-modulated LPG structure. The results show that this new kind of PAA-LPG pH sensor has much higher sensitivity than conventional LPG sensors whose grating

structures are written in the fiber core

Chapter 5: Fiber-optic DNA Sensor Based on Self-assembled Multilayer Sensing Coating. In this chapter, a novel fiber-optic DNA sensor based on TCFMI is developed by layer-by-layer self-assembly $(PEI/PAA)_4(PEI/ssDNA)_1$ sensing coating. The performance of the sensor is studied in detail, and their sensitivity to target ssDNA with different match base numbers is investigated. The results show the sensor can even identify the DNA with two match base numbers.

Chapter 6: Optical Fiber Sensor Integrated Biochips for Ultrasensitive Glucose Detection. In this chapter, LPG inscribed in a small-diameter single mode fiber (SDSMF) is integrated into a microfluidic chip to develop biochips. Glucose oxidase containing sensing film was deposited on the surface of SDSMF-LPG. Thereafter, the LPG sensor are integrated into microfluidic channels to build a biochip for glucose detection. Experimental results reveal the biochip has a detection limit as low as 1 nM.

Chapter 7: Conclusions and Future Outlook. In this chapter, a summary of the research results is presented and the directions for future work and development are discussed.

*Chapter 2*

# Overview of Optical Biochemical Sensing Technology

## 2.1 Introduction

In this chapter, the fundamentals and recent progress in optical biochemical sensors are reviewed. Different types of fiber-optic RI sensors will be summarized and their performances will be compared. The optical biochemical sensors, including pH sensors, metal ions sensors, DNA sensors and glucose sensors, are also reviewed [31-37, 62, 63].

## 2.2 Fiber-Optic Refractive Index Sensors

### 2.2.1 Fundamentals of Fiber-Optic Biochemical Sensors

Fiber-optic biochemical sensors refer to the devices which adopt optical fibers as the transduction element, and use optical mechanisms for target analytes detection. Optical fiber is a kind of optical waveguide, which is generally with a shape of cylinder. It usually includes three parts: core, cladding, and coating. The coating is commonly made of polymer, for protection of the inner part of the fiber. The cladding part is usually made of silica, while the core is typically made of germanium-doped silica with enhanced refractive index (RI). The light propagates along the core by total

internal reflection, which light can be divided into the guided field in the core and the evanescent field in the cladding part. For a conventional optical fiber, the evanescent field usually decays to be zero within the cladding part. In order to fabricate fiber-optic sensors, the light will be exposed to the surrounding environment and directly or indirectly interact with the surrounding medium for sensing [64].

Optical fibers are originally developed for telecommunication which requires the light propagation with minimal loss. Thereafter, researchers found that optical fibers are also good candidates for sensor fabrication [31]. From then on, fiber-optic sensors have been a hot research topic due to their advantages of chemical-inertness, immunity to electromagnetic interferences, biocompatibility, multiplexed detection, remote sensing, and the ready availability of optoelectronic components. Up till now, different types of fiber-optic sensors have been designed and adopted for various kinds of applications [64].

However, most of those fiber-optic sensors are developed to detect physical parameters, such as temperature and pressure [65]. Therefore, much efforts are needed to developing fiber-optic biochemical sensors for bio-detection and chemo-detection by coating the fibers with micro-/nano-structured functional sensing film [37]. To fabricate the sensing film, thin film deposition techniques have been adopted, which offer the ability to

control the sensing film thickness on the nanometer scale. This capability is significant, as the penetration depth of light in fiber-optic sensors is usually in nanometer scale. In addition, it offers an approach to use optical responses of optical fiber to sense external stimulus. Some typical sensing film deposition techniques include Langmuir–Blodgett (LB) technique, self-assembled monolayers (SAM) , and layer-by-layer (LbL) self-assembly methods [37].

Table 2.1 Summary of different types of fiber-optic RI sensors: fiber types, principle, sensitivity and scheme.

| Fiber types | Principle | Sensitivity | RI Range | Scheme | Ref |
|---|---|---|---|---|---|
| LPG | RI modulation | 160 nm/RIU | 1.3-1.45 | 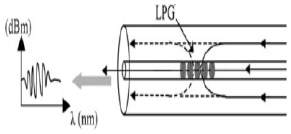 | [66] |
| TOF | evanescent field | 6008 nm/RIU | 1.337-1.347 | 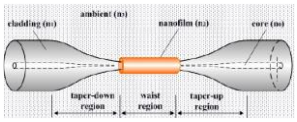 | [67] |
| F-P | optical path | 1130.887 nm/RIU | 1.333-1.395 | 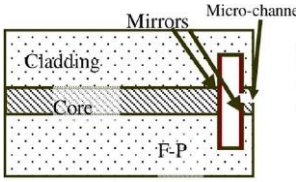 | [68] |
| LSPR | collective oscillation | 914 nm/RIU | 1.33-1.4 | 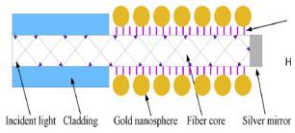 | [69] |
| TCFMI | mode mismatch | 138 nm/RIU | 1.33-1.39 | 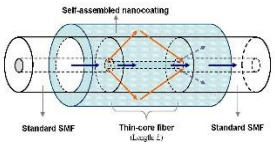 | [24] |

### 2.2.2 Long Period Fiber Gratings RI Sensors

Optical fiber long period grating (LPG) is a periodic modulation of the RI o of an optical fiber. It is usually fabricated by ultraviolet irradiation, and its period is typically in the range 100–1000 μm. The small grating wave-vector of the LPG enables the coupling of light from the guided modes of the fiber to cladding modes. Therefore, the transmission spectrum of a LPG consists of a number of attenuation dips according to different order modes [65]. Since cladding modes are sensitive to the surrounding RI change, so the LPG is an ideal candidate for biochemical sensors preparation by coating nanostructured sensing film on the surface.

### 2.2.3 Tapered Optical Fiber RI Sensors

Tapered optical fiber (TOF) has enhanced evanescent field and thus has great potential as optical biochemical sensors [64]. TOF can be fabricated through heating and drawn processes. TOF RI sensor is usually highly sensitive to surrounding medium through the evanescent field. Since the amount of evanescent field propagating in TOF depends on the RI difference between the TOF and the surrounding medium, one can even adopt output power as indication for detecting different kinds of analytes.

### 2.2.4 Fabry–Perot Cavity RI Sensors

Fabry–Perot (F-P) cavity based fiber-optic biochemical sensors can be

fabricated at the end-surface of optical fibers by depositing micro-structured sensing film. They have been demonstrated not only physical parameter measurements, including temperature, vibration and pressure [70], but also as low-cost, one-time biochemical sensors for e.g. ozone detection on Mars [71]. Using the optical fiber, one can directly use the fiber end-surface/film interface as the first mirror and the film/air interface as the second mirror. Thus the light launched into the fiber will form interference due to the F-P cavity. Once the target analyte changes the RI of sensing film, the interferometric fringe will shift due to the change of the effective optical path inside the F-P cavity. F-P cavity provides an ideal platform for sensor fabrication through engineering the RI or length of the cavity.

2.2.5 Fiber-based Localized Surface Plasmon Resonance RI Sensors

The localized surface plasmon resonance (LSPR) is an optical phenomenon generated by collective oscillations of electrons in metal nanostructures surrounded by a dielectric [72]. When a light irradiating on the metal nanostructures, a part of the incident photons is absorbed and the rest is scattered in different directions. Both absorption and scattering are greatly enhanced when LSPR is excited. If such a LSPR is excited on a fiber-based device, it will be extremely sensitive to RI change of surrounding mediums.

2.3.6 Thin-core Fiber Modal Interferometer as RI Sensors

Thin-core fiber modal interferometer (TCFMI) is an elaborate in-fiber

interferometer which can be quickly fabricated by fusion splicing a section of thin-core (2.5 μm) optical fiber between two standard single-mode fibers. Due to the mode mismatch, high-order cladding modes will be excited in the thin-core fiber and then recoupled back to single-mode fiber to form inter-modal interference. As the interference depends on cladding modes, its interferometric peaks are very sensitive to the surrounding medium's RI change. The sensing performance of such a fiber device is quite close to LPFG, while its advantage is ease of fabrication.

## 2.3 Optical Biochemical Sensors

Nowadays, a stringent problem mankind is confronted with is the increasing number of new diseases. Therefore, it is extremely appealing to develop new approaches to assess the status of health condition, disease onset and progression, and treatment outcome. Moreover, it is anticipated to achieve early disease diagnosis for patient survival and prognosis of disease. Therefore, it is important to develop a robust and convenient way to assess the status of health condition, disease onset and progression, and treatment outcome. And the method for the monitoring must meet the basic requirement of non-invasive and cost-efficiency. In addition, it is crucial to achieve early disease diagnosis for patient survival and successful prognosis of disease, which means that a highly sensitive and specific technique must

be developed. Therefore, biosensors technologies, including electronic biosensors, electrochemical biosensors, mechanical biosensors and optical biosensors, have made significant progress in the past years [73].

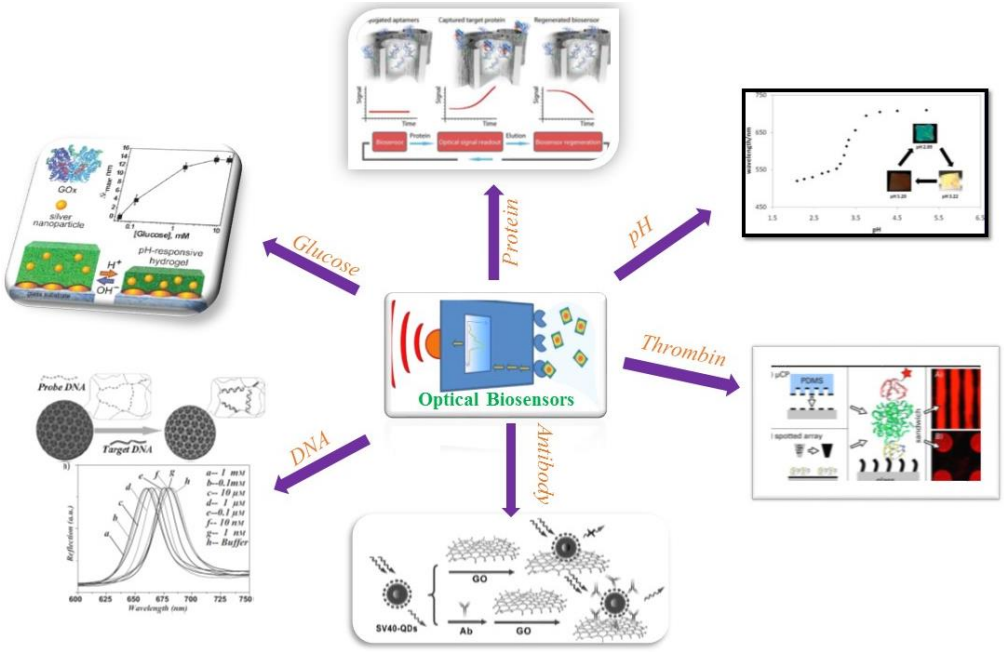


Figure 2.1 The applications of optical biosensors in the clinical field, such as protein detection [74], pH sensors [75], immunosensor [76], DNA tests [77], thrombin analysis [78], and glucose monitoring [79].

Recently, the demands for simple and disposable devices have been growing in the field of medical diagnostics. Moreover, the devices are desired to have the capabilities of fast response, biocompatibility, and ease of mass production. Optical biochemical sensors are very promising to meet those demands as optical signals are usually very sensitive to surrounding change and can be used for bio-sensing with very high precision. Fig. 2.1 shows some demonstrated applications of optical biosensors in the clinical

field. Particularly, fiber-optic sensors are promising to be integrated into microfluidic channels for biochip fabrication because of their small size. It has been demonstrated that fiber-optic biochemical sensors can be used as the point-of-care biosensors for biological parameter analysis in vivo, such as DNA, glucose, pH, antibody, cell and so on.

### 2.3.1 Optical pH Sensors

pH of a solution is defined as:

$$\mathrm{pH} = -\log[H^+]$$

where $[H^+]$ is the concentration of protons in the solutions. pH plays an important role in many applications, including medicine, environmental sciences, food science, agriculture, biotechnology, and the biological fields. For instance, the activities of enzymes depend on the pH of surrounding environments, the functions of cells are modulated by the pH, and pH of tissue is also a key physiological parameter, indicating the healthy conditions of the body [80]. Therefore, real-time pH monitoring is much desired for medical diagnosis and treatment.

Though the electrochemical pH sensors have been widely applied in many fields, they are usually too bulky for medical applications, especially for real-time monitoring. To solve the problem, optical methods have been proposed for pH sensing. Lee et al. [81] fabricated pH sensing multilayer

film by LbL self-assembling of poly (acrylic acid) (PAA) and poly (allylamine hydrochloride) (PAH), which contains pH responsive dyes,1-hydroxypyrene-3,6,8-trisulfonate (HPTS). By measuring the fluorescence emission spectra of the film, pH change from 1 to 13 could be detected. Although the sensor showed wide pH detection range, it is not suitable for biomedical use. Miesenbock et al. [82] demonstrated to use optical indicators for pH sensing to monitor vesicle exocytosis and recycling process. They developed pH-sensitive mutants of green fluorescent protein, which they called 'pHluorins', by structure-directed combinatorial mutagenesis. The green fluorescent protein, which has a bimodal excitation spectrum, was attached to different mutants. Their results showed that the protein displayed excitation ratio change with pH from 5.5 to 7.5, reversibly, due to the pH induced protonation–deprotonation process. They tested the pH values of endosomes and *trans*-Golgi network through excitation spectrum (Fig. 2.2). Though this kind of optical pH sensors exhibited good performance for biological measurements, it is still not suitable for in vivo tests as the leakage of dyes, the harm of UV light and the large size of instruments for the tests.

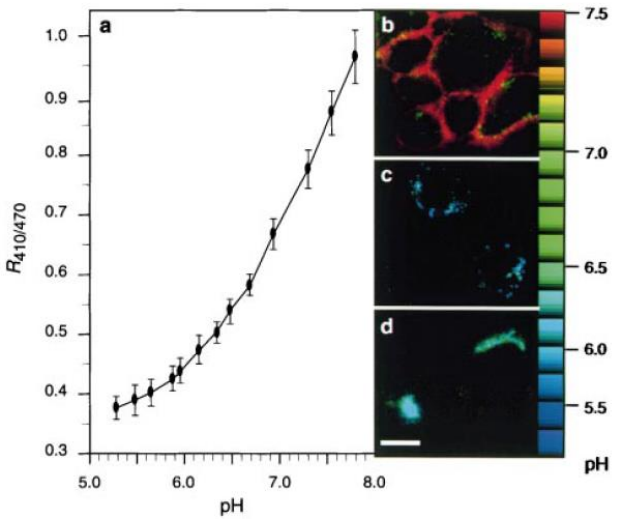


Figure 2.2 pH measurements with ratiometric pHluorin in HeLa cells. a, Calibration curve of $R_{410/470}$ (mean±s.d.). Cells expressing GPI-anchored ratiometric pHluorin at their surface ($n$=28) were imaged in buffers adjusted to pH values between 5.28 and 7.8. b–d, ratiometric pH measurements in subcellular compartments, colour-encoded according to the look-up table on the right. Targeting modules used: b, GPI anchor for delivery to the cell surface (at pH 7.40); c, cellubrevin for sorting to endosomes; d, TGN38 for localization to the *trans*-Golgi network. Scale bar, 10 μm [82].

Fiber-optic pH sensors have potential to solve the problem due to their small size and biocompatibility. Many efforts have been devoted to developing fiber-optic pH sensors by adopting new materials or novel type of fiber devices.

Commercial organic dyes are sensitive to pH and can be immobilized in gels and deposited on the optical fiber for fabrication of fiber-optic pH sensors. Beltran-Perez's group [83] developed fiber-optic pH sensors by depositing a $TiO_2$ doped with organic dyes (brilliant green, rhodamine 6G, rhodamine B and coumarin) sensing film on the end-surface of a multimode fiber. The sensor was able to detect a wide range of pH change, covering

from 2 to 12, by using the evanescent wave absorption variations. In another report, Dong et al. [84] immobilized a mixture of three pH sensitive indicators (cresol red, bromophenol blue and chlorophenol red) on an unclad fiber surface (the fiber was etched with HF solution to 60 μm in diameter) for pH sensing. The results showed that the transmitted power of the sensor changed linearly with pH varying from 4.5 to 13. Moreover, the response of the sensor is very fast, about 5s.

Though fiber-optic pH sensors organic using dyes show good performance, the spectra are usually too wide to detect tiny pH change. Quantum dots (QDs), as inorganic dyes, show very narrow emission peak. Maule et al. [85] synthesized mercaptopropionic acid capped CdTe QDs and deposited the QDs hybrid etraethoxysilane and phenyltriethoxysilane gels on the end-surface of optical fiber for pH sensing. The QDs had an emission peak at 635nm and its wavelength shifts with pH change. Its pH detection range was from 4.8 to 11. Kim's group [9] reported the near infrared QDs deposited on tapered optical fiber for pH sensing. A very wide pH range from 2 to 12 was demonstrated in the experiments.

One of the potential issues of the dye-based fiber-optic pH sensors is the dye leakage. Thus, it is necessary to fabricate fiber-optic pH sensors without dyes. One of promising solution is to use functional polymeric film to develop optical fiber pH sensors. In the thesis, we will design novel fiber-

optic pH sensors by using micro-/nano-structured sensing film without dyes.

### 2.3.2 Optical Metal Ion Sensors

Heavy metals are essential to our body in small dose, such as copper, zinc and iron. However, they will become harmful or even fatal if too many heavy metals exist in the body [86, 87]. For example, $Hg^{2+}$, $Pb^{2+}$ and $As^{3+}$ ions will affect the central nervous system, $Cu^{2+}$, $Cd^{2+}$, $Hg^{2+}$ and $Pb^{2+}$ have influence on the health of kidneys or liver, and some ions ($Ni^{2+}$, $Cu^{2+}$, $Cd^{2+}$ and $Cr^{3+}$ ions) will cause disease on the skin, bones and teeth. Moreover, the heavy metals will accumulate in the body without degrading. Therefore, it is desired to monitor the maximum contaminant levels in drink water by using metal ions sensors.

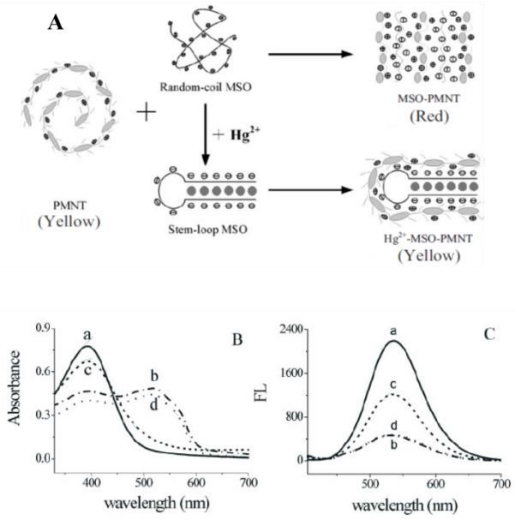


Figure 2.3 A) Description of the optical mercury sensing mechanism. B) UV-vis absorption spectra, and C) fluorescence spectra of aqueous solutions of PMNT (a), MSO-PMNT (b), $Hg^{2+}$-MSO-PMNT (c), and $Zn^{2+}$-MSO-PMNT (d). The metal ion concentrations are 450 μM, 25 μM, and 2.5 μM in B and C respectively, and that of PMNT is 1.7 μM on a monomeric-unit basis [88].

Liu et al. [88] proposed a "mix-and-detect" optical methods for mercury ions detection. They fabricated an optical $Hg^{2+}$ sensor using a water-soluble conjugated polymer, poly (3-(3'-*N*, *N*, *N*-triethylamino-1'-propyloxy)-4-methyl-2, 5-thiophene hydrochloride) (PMNT) and a mercury-specific oligonucleotide (MSO) probe. The MSO probe contains many thymines (T) and can form a stem-loop structure in the T–$Hg^{2+}$–T configuration with the existence of target $Hg^{2+}$ ions. The PMNT can bind to $Hg^{2+}$-free MSO and $Hg^{2+}$–MSO complex, and exhibits different fluorescence spectra (Fig. 2.3). The fluorescence intensities depend on $Hg^{2+}$ concentration. Therefore, the sensor can detect $Hg^{2+}$ in the concentration range from 0 to 1 mM.

However, conventional metal ions sensors are not suitable to be used in human bodies for clinical test. So it is much appealing to develop small sensor that is safe to human bodies. Due to its compactness and high sensitivity, fiber-optic sensors have been considered as a promising solution for trace metal ions detection in body.

Based on the quenching of fluorescence dyes, optical fibers have been used as a light propagation waveguide to develop optical metal ion sensors. Ueberfeld et al. [89] prepared permeation liquid membrane, and used it as both separation and preconcentration membrane for $Cu^{2+}$ detection. The fluorescence intensity change caused by copper ions concentration was

detected via multimode optical fibers. $Cu^{2+}$ concentration of 50 nM can be detected.

Besides, QDs and carbon dots have also been adopted for metal ions detection. Sung et al. [90] synthesized hydrophobic CdSe/ZnS QDs and encapsulated them into silica shell. After mixing with polyvinyl alcohol and depositing on the tip of optical fiber, a linear growth of fluorescence intensity with $Cu^{2+}$ concentration was achieved in the concentration range from 0 to 10 μM. Its detection limit is 0.09 μM.

Moreover, biological methods have also been proposed for metal ions detection. For example, Long et al. [4] developed an optical fiber DNA probe by depositing a sequence of T-T mismatch pairs. Probe DNA chain containing a short oligonucleotide sequence can hybridize with the complementary DNA chain labeled with a fluorescent. The mismatched pairs could bind with $Hg^{2+}$ ions and formed a T-$Hg^{2+}$-T complex by folding the DNA segments into a hairpin structure, and thus weaken the fluorescence signal. Such a fiber-optic sensor can detect $Hg^{2+}$ ions in the range from 0 to 2000 nM, and its detection limit is 2.1 nM. Moreover, the sensor could be reused after treating with 0.5% SDS solution.

Another way for trace metal ions detection is based on the swelling degree change of sensing film induced by metal ions. Therefore, the RI of sensing film will also change, which can be monitored by using e.g. TCFMI

sensors. With LbL self-assembly technique, P4VP and PAA can be deposited on the surface of TCFMI by hydrogen bonding [91]. The sensing film will be complexed with many kinds of heavy metal ions. It was demonstrated the $Fe^{2+}$, $Cu^{2+}$, and $Zn^{2+}$ detection, with a range from 10 nM to 0.1 M. The detection limit reached to be 9.6 nM. The sensors could be regenerated by treatment with ethylene-diamino-tetraacetic acid. But they did not have selectivity.

In order to improve selectivity of the sensor, another kind of fiber-optic $Hg^{2+}$ sensor was developed by depositing poly (N-ethyl-4-vinylpyridinium chloride) (P4VP·HCl) and poly (sodium-p-styrenesulfonate) (PSS) ultrathin sensing film on the surface of TCFMI [5]. The sensor exhibited high selectivity towards $Hg^{2+}$ ions, and its detection limit and response time are 1 nM and 30 s, respectively.

### 2.3.3 Optical Glucose Sensors

Diabetes mellitus is a kind of worldwide health problem induced by endocrine disorder of carbohydrate metabolism. It was reported by the World Health Organization that the number of diabetic patients will increase to be about 366 million by 2030 [92]. More importantly, many kinds of diseases are usually derived from diabetes, such as kidney failure, heart disease and blindness [93]. The main causes of the disease are hyperglycemia and insulin

deficiency in human bodies. Those two parameters can be measured by using blood glucose (GO) concentrations, with a normal range of 2-30 mM [94]. Therefore, it is very valuable to monitor the concentration of GO in human body for the diabetes mellitus prevention and treatment.

The first GO biosensors was proposed by Clark and Lyons in 1962 [95]. Thereafter, many kinds of high performance GO biosensors have been reported. However, most of those GO biosensors are based on electrochemical principles which might induce electroactive interference with some endogenous reducing species, such as ascorbic and uric acids and some drugs (e.g., acetaminophen) [93].

In order to exclude the influence of those interferences, Holtz et al. [96] fabricated a polymerized crystalline colloidal arrays (PCCA) based GO sensor. A three-dimensional periodic CCA of highly charged polystyrene spheres (100 nm in diameter) was adopted as the reporter. Glucose oxidase (GOD) was attached on those PCCA, with a spacing of 25 nm between enzymes. Based on Bragg's law, PCCA will swell and induce a redshift of the diffraction when GO reacts with GOD. Using such a sensor, the GO with concentration from 0.1 mM to 0.5 mM can be detected (Fig. 2.4). Besides, Tokarev et al. [79] fabricated pH responsive ionically cross-linked alginate–gelatin complex containing Ag nanoparticles for LSPR detection. The reaction of GO with GOD generates the gluconic acids which influence the

swelling property of alginate–gelatin complex film. Consequently, the induced change of the distances between Ag nanoparticles causes a shift of LSPR spectra. The detect limitation of the demonstrated GO sensor is 0.1 mM.

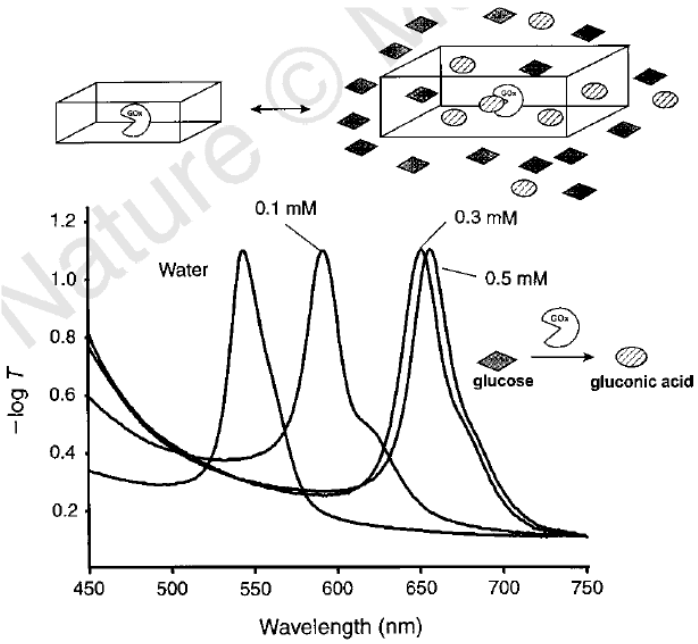


Figure 2.4 Visible extinction spectra showing how diffraction depends on the glucose concentration for the 125-mm-thick PCCA glucose sensor [96].

Unfortunately, those optical sensors are not suitable for in vivo tests and their fabrication costs are relatively high. In order to overcome those limitations, Corres et al. [97] demonstrated an optical fiber GO sensor through depositing enzyme glucose dehydrogenase (GDH), PEI and PSS multilayer sensing films on a tapered fiber. With $NAD^+$, GDH can catalyze glucose into NADH which has absorbance and fluorescence peaks at the wavelength of 340 nm and 450 nm, respectively. Both the absorption and

fluorescence spectral peak can be used to detect GO concentration. Saxl et al. [98] reported Badan (an environmentally sensitive fluorophore) labelled glucose/galactose binding protein can be attached onto Ni–nitrilotriacetic acid-functionalized agarose. The agarose was deposited on the end surface of the multimode fiber. It was observed that fluorescence lifetime increases with the GO concentration which can be used to detect GO concentration in the range from 1 mM to 100 mM.

Hydrogels' GO dependent swelling/deswelling transition can also be used for development of fiber-optic GO sensors. Tierney et al. [17] demonstrated a fiber-optic GO sensor by depositing hydrogel containing 3-phenylboronic acid and a tertiary amine, dimethylaminopropylacrylamide, on the head of an optical fiber. Using an interferometric technique, the swelling induced change of optical length can be precisely measured. Such a fiber-optic GO sensor can detect the concentration change ranging from 0 to 8 mM, and its response time is around 10 min.

Though fiber-optic GO sensors have good performance on GO sensing, relatively large amount of blood is usually consumed in the measurement. To solve the problem, we will develop a novel fiber-optic GO sensor with low detection limit and integrate it into a microfluidic channel for biochip fabrication, see Chapter 6.

### 2.3.4 Optical DNA Sensors

Deoxyribonucleic acid (DNA) is a kind of nucleic acid. It plays a very important role in the clinical tests and genetic engineering, because many diseases are induced by the sequence disorder of DNA. Thus, lots of efforts have been devoted to developing DNA sensors in the last decades [99]. The demonstrated approaches for DNA detection include electrochemical methods, QCM methods, mechanical methods, and optical methods. Among them, optical DNA biosensors provide a convenient way for DNA detection.

Gaylord et al. [100] synthesized a cationic water soluble conjugated polymer (CP), poly (9,9-bis(6'-N, N, N-trimethylammonium)-hexyl)-fluorene phenylene) which can be complexed with DNA chains based on electrostatic force. Since peptide nucleic acid (PNA) strand cannot be complexed due to its neutral property, it was labeled with a dye and then mixed with CP in aqueous solution. Therefore, when the fully matched ssDNA chains are added into the solution, those molecular chains can attach with each other, where CP complexes with ssDNA based on electrostatic force and PNA labeled with dye hybridizes with ssDNA. Consequently, the emission intensity will be enhanced due to Forster energy transfer (FRET) from CP to the dye. For the ssDNA chains that are not matched with PNA chain, the emission spectra have no change. Based on this principle, the DNA sensor can be fabricated for hybridization detection. However, this approach

can only detect whether the base sequence of ssDNA chains match with the probe PNA, but cannot reveal the concentration information of ssDNA. Zhao et al. [77] used ssDNA chains modified silica colloidal crystal beads (SCCBs) to fabricate photonic crystal sensors. When ssDNA chains hybridize with the probe ssDNA on the SCCBs, the swelling degree of hydrogels will change and thus induce a shift of peak wavelength of Bragg diffraction. The fabricated sensor can detect ssDNA with different concentration from 1 pM to 1 mM (Fig. 2.5).

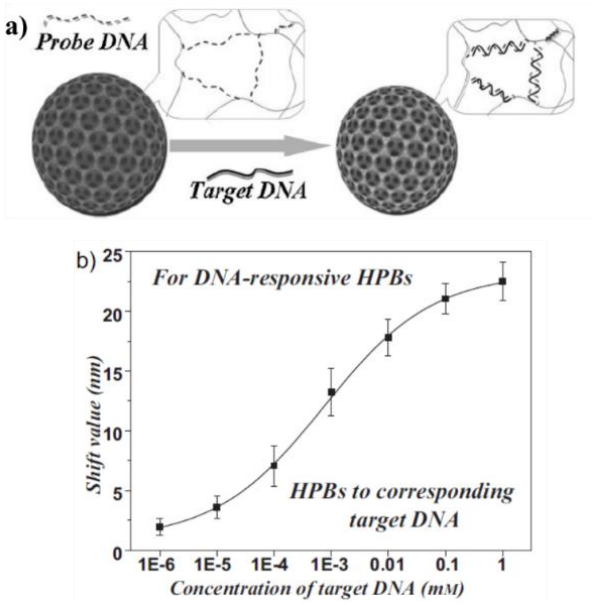


Figure 2.5 a) Schematic diagram of the label-free DNA detection based on the DNA-responsive hydrogel photonic beads. b) Bragg diffraction peak shifts of the DNA-responsive hydrogel photonic beads incubated in their corresponding target DNA with different concentrations [77].

In order to fabricate miniature sensor for DNA detection, fiber-optic DNA sensors has been demonstrated and showed promising future for clinical application. ssDNA labeled with fluorescent dyes is commonly

employed for fiber-optic DNA sensor fabrication. Krull's group [101] synthesized ethylene glycol derivatized thiazole orange dyes and linked them to ssDNA by covalent bond. The labeled ssDNA can enhance the fluorescence intensity by hybridizing with the complementary ssDNA. Based on this principle, they deposited the probe ssDNA onto an optical fiber for monitoring DNA hybridization. Niu et al. [102] synthesized a novel fluorescence indicator, $Fe(phen)_2 \cdot PHPIP \cdot 3ClO_4 \cdot 2H_2O$ for development of DNA sensors. $[Fe(phen)_2 \cdot PHPIP]^{3+}$ can intercalate into dsDNA double helix structures, thus, they can be used as indicator for DNA hybridization. The labeled probe ssDNA was deposited on the end surface of optical fiber and used for detecting the concentration of target ssDNA. Their experimental results showed that the sensor could detect target ssDNA concentration ranging from $4.98\times10^{-7}$ to $4.88\times10^{-6}$ M and its detection limit is $1.08\times10^{-7}$ M.

Moreover, some indirect labeled methods have also been suggested for development of fiber-optic DNA sensor. Zhang's group [103] demonstrated to deposit DNA probe and biotinylated target linked with streptavidin labeled horseradish peroxidase (streptavidin-HRP) on the etched optical fiber. With the catalysis of HRP, a fluorescent indicator, bi-p,p'-4-hydroxyphenylacetic acid was generated from 4-hydroxyphenylacetic acid (p-HPA). The target ssDNA can then be detected by monitoring the

fluorescence intensity. The sensor can detect low concentration of ssDNA from 1.69 pM to 169 pM and its detection limit is 1 pM.

As labeled methods are usually not suitable for clinical use, label-free methods have been attracted much attention in the field of fiber-optic DNA sensors. One of promising approaches to achieve this objective is to adopt optical fiber RI sensor for DNA sensing. In this thesis, we will develop a label-free fiber-optic sensor based on a self-assembled nanocoating for DNA detection.

## 2.4 Summary

In summary, optical approaches have been widely explored for sensors fabrication in the last several decades. Recently, fiber-optic biochemical sensors have attracted remarkable attentions for clinical applications due to their small size, low cost, biocompatibility and multiplexed detection capability.

Many kinds of fiber-based devices have been exploited for development of optical biochemical sensors, such as long period grating, fiber Bragg grating, tilted fiber Bragg grating, multimode or few mode fibers, tapered optical fibers, fiber based F-P cavity, microstructured optical fibers, and side-polished optical fibers. Although lots of efforts have been devoted to adopting labeled methods for development of biochemical sensors, few of

them are applicable for real clinical DNA and GO detection.

To overcome those issues, optical fiber RI sensors have been proposed to develop label-free biochemical sensors. After immobilized with different kinds of sensing films, these optical fiber RI sensors can be further developed to different kinds of sensing applications, including gas, ions, pH, humidity, dopamine, DNA, antigen, glucose and other biological species. Various film deposition techniques, e.g. monolayer self-assembly, layer-by-layer self-assembly, chemical vapor deposition, have been demonstrated to immobilize numerous polymer materials for development of fiber-optic biochemical sensors.

Moreover, fiber-optic sensors have advantages of rapid, remote, multiplex, in-line or on-line sense capabilities. Therefore, it is very appealing to develop novel low-cost and high-performance fiber-optic biochemical sensors. The trends of the development of fiber-optic biochemical sensors include: 1) fabricate high performance fiber-optic biochemical sensors by using novel optical fiber devices and new sensing mechanisms; 2) develop novel fiber-optic biochemical sensors using new sensing coating materials to detect more analytes, especially for clinical tests; 3) miniaturize fiber-optic sensors and integrate them into microfluidic chip to develop multiple functional biochips for practical clinical use.

# *Chapter 3*

# Fiber-optic pH Sensors Based on Self-assembled Monolayer Nanoporous Sensing Coating

In this chapter, a cationic polymerized ionic liquid (PIL), named poly [3-cyanomethyl-1-vinylimidazolium bis(trifluoro methanesulfonyl)imide] (PCMVIm$Tf_2N$), was synthesized and mixed with poly (acrylic acid) (PAA) to form nanostructured polyelectrolyte complex (PEC) film. The nanostructured film was coated on the surface of thin-core fiber modal interferometer (TCFMI) to fabricate the fiber-optic pH sensors by self-assembly monolayer technique, taking the advantages of nanoporous in the film. These kinds of pH sensors showed high performance in terms of their sensitivity and response time, due to the large thickness of sensing film and nanoporous structure. The sensing principle of the sensor can be explained by the swelling degree variation of sensing film with the pH solutions.

## 3.1 Introduction

Fiber-optic pH sensors have been widely studied as they have significant advantages over commercially available pH electrodes, including anti-interference to electromagnetic waves and high signal-to-noise ratio [104]. In addition, fiber-optic pH sensors also have great potential for clinical tests

because of their small sizes, biocompatible property, low-cost and multiplex detection capability [25].

So far, most fiber-optic pH sensors have been developed by adding pH indicators into the sensing gels [83, 84, 105, 106]. These fiber-optic pH sensors have some disadvantages, such as the loss of pH indicators after many test cycles and quenching of indicators by the interference materials [83, 84, 107]. To overcome the problems mentioned, the TCFMI based pH sensors have been suggested [7, 24, 25, 108]. These sensors are based on the swelling degree change of sensing film with the pH solutions. The variation of the sensing film could be reflected by the TCFMI, which is sensitive to the refractive index (RI) change of surrounding conditions. Though these sensors have shown good performance in pH monitoring, their performance displayed a trade-off phenomenon, that is, higher sensitivity with slower response or faster response with lower sensitivity. To break out the trade-off phenomenon, we propose to fabricate sensing film with larger thickness and nanopores, which can achieve large swelling degree while provide a channel for the solution flowing into the sensing film.

Porous polymeric films have been attracting researchers' interests for many years because they can provide a multifunctional platform for fundamental research and many practical uses [109-122]. From this point, porous polyelectrolyte membranes (PPMs) are very appealing as they can

introduce additional charges in the membrane. In addition, the PPMs have high stability in mechanical and chemical aspects, which make them versatile for devices fabrication and many other attractive applications, such as controlled release, separation, catalyst supports, bio-interfacing and sensors, just to name a few [123-125]. In addition, the ionic property of polyelectrolytes makes them suitable for biological application. So we will suggest a simple and efficient way for nanoporous PEC preparation and nano-engineering it for fiber-optic sensors fabrication. PEC sensing film can be prepared by electrostatic complexation between a cationic PILs and a polyanion, PAA. By coating the nanoporous PEC sensing film on the TCFMI via self-assembly method, fiber-optic pH sensors can be fabricated (Fig. 3.1 shows the scheme for sensor fabrication process), as the sensing film is sensitive to the pH change. The chemical structures of PCMVIm$Tf_2N$ and PAA are given in the inset of Fig. 3.2.

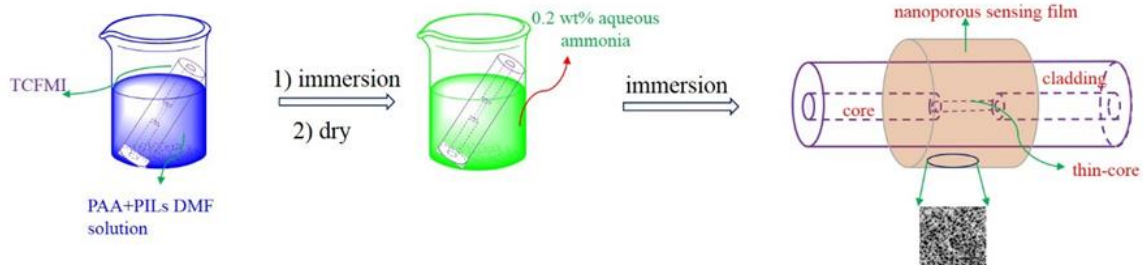


Figure 3.1 Process for the nanoporous sensing film based TCFMI pH sensor fabrication.

## 3.2 Nanoporous PEC Film Formation

### 3.2.1 Preparation of Nanoporous PEC Film

1.0 g PCMVIm$Tf_2$N PIL and 0.18 g of PAA ($M_W$ = 2000) were dissolved in dimethylformamide (DMF) to form homogeneous solution, which was subsequently casted onto a cleaned glass plate, dried at 80 $^oC$ for 1h, and soaked in 0.2 wt% aqueous ammonia (pH=10.8, 20 $^oC$, 2 h). After the soaking step, a yellowish and flexible free-standing membrane can be easily detached from the substrate. The PAA and PEC complex are characterized by FT-IR spectra (BioRad 6000 FT-IR spectrometer; samples were measured in solid state using a Single Reflection Diamond ATR). Fig. 3.2 shows the FT-IR spectrum change of PAA before and after forming complex with PCMVIm$Tf_2$N. It can be seen that the peak for -$COO^-$ appears after the treatment of film, which provides anions to form complex with PILs. The new peaks also indicate that the PEC complex has formed. The process of nanoporous PEC film fabrication is given in Fig. 3.3 (a) and the nanoporous PEC films are also shown in Fig. 3.3 (Scanning electron microscopy (SEM) was performed on a GEMINI LEO 1550 microscope at 3 kV).

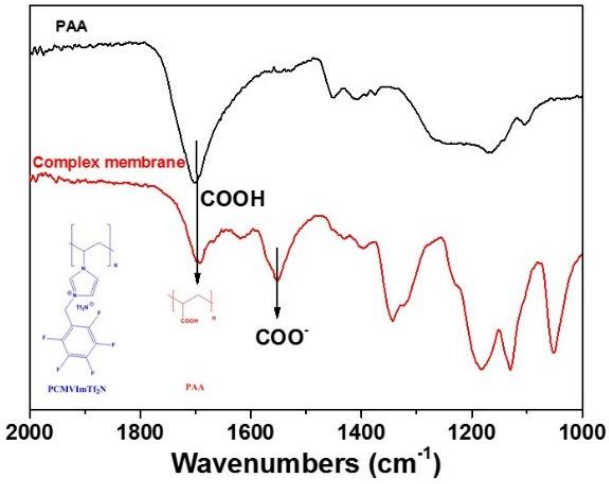


Figure 3.2 FT-IR spectrum of PCMVImTf2N-PAA complex membrane (red) and PAA polymer (black). The inset shows chemical structures of PCMVImTf2N and PAA used for nanoporous film preparation.

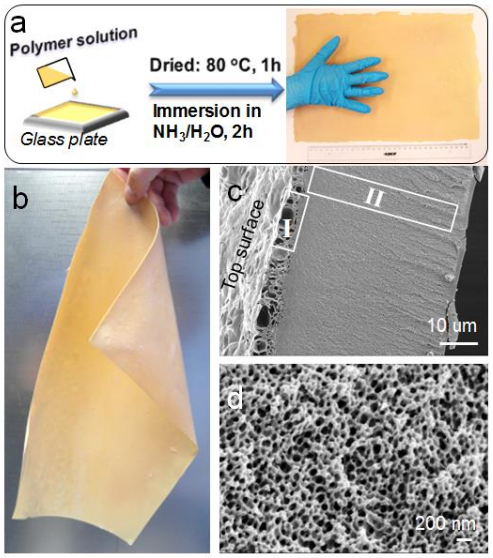


Figure 3.3 Preparation (a) and photographs (b) of nanoporous polyelectrolyte membrane made from PAA and PILs mixture solutions. (c) A representative SEM image of the cross-section area of the as-synthesized PPM. (d) SEM image of the nanoporous morphology observed in zone II in (c).

### 3.2.2 Nanopores Formation in the PEC Film

After treating the film with 0.2 wt% aqueous ammonia, the PEC was formed due to charging of the acrylic acid moieties. And during the PEC formation

process, the film was restructured on the nanoscale level. Finally, stable nanopores were formed within the film. In addition, the nanoporous PEC film is very flexible with high mechanical stability.

The nanoporous PEC film formation follows such a process: aqueous ammonia solution is in contact with the film surface and diffuses into the polymer matrix, deprotonating the carboxylic acid groups (COOH) of the PAA chains into carboxylate groups ($COO^-NH^{4+}$). As a result, it triggers an in-situ ionic complexation of PAA with surrounding PCMVIm$Tf_2N$ chains to build up the electrostatically cross-linked network film. Driven by this intrinsically spontaneous ionic complexation process, the polymer chains re-arrange themselves in the polymer matrix to achieve a high degree of charge complexation, which is only possible in a nanoporous state. Indeed, fluorescent confocal laser scanning microscopy (Fig. 3.4 (b)) was used to visualize the diffusion of Rhodamine B-labelled aqueous ammonia into the membrane cross-section. And the time dependent SEM examination also supports that large pore in zone I develops in the early stage of soaking while at the same time Zone II remains dense (Fig. 3.4 (c) ~ (d)). In later stages, zone I develops into its final macroporous morphology, while the nanopore system grows down into Zone II with increasing soaking time (Fig. 3.4 b).

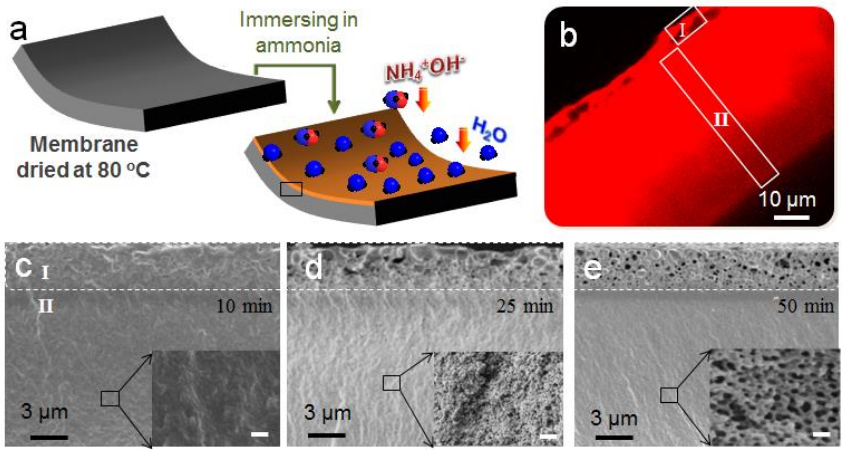


Figure 3.4 (a) A cartoon illustrating the diffusion of aqueous ammonia into the membrane, (b) fluorescent confocal laser scanning microscopy of the PPM cross-section after being soaked for 2 h in 0.2 wt% aqueous ammonia doped with 15 ppm of Rhodamine B. (c~e) Time-dependent cross-section structures of the membrane soaked in 0.2 wt% aqueous ammonia for 10, 25, and 50 min, respectively. Scale bar of the insertion is 100 nm.

## 3.3 TCFMI pH Sensor Based on Nano-structured Sensing Coating

### 3.3.1 TCFMI pH Sensor Fabrication by Self-assembly Monolayer Technique

The principle of the TCFMI sensor is based on the RI sensitivity of its transmission spectrum formed by multimode interference. The cladding modes of the fiber are excited because of the mode mismatch at the first hetero-core interface. And they will interfere with the core mode at the second hetero-core interface. As a result, they couple back to the core mode in the output single-mode fiber. A scheme for the light transmission path and RI sensing principle is given in Fig. 3.5. The dips observed in the output spectrum was caused by destructive interference and can be described as:

$$2\pi[n_{eff}^{co}(\lambda)-n_{eff}^{cl,j}(\lambda,n_{ext})]\frac{L}{\lambda_D}=(2k+1)\pi$$

where $n_{eff}^{co}$ is the effective index of the core mode, $n_{eff}^{cl,j}$ is the effective index of the j-th order cladding mode, $n_{ext}$ is the RI of the surrounding medium, L is the length of the inserted fiber, $\lambda_D$ is the wavelength of the transmission dip, and k is an integer. As the effective index of the cladding mode depends on the external RI, the spectrum dip will shift with external RI changes. Such a TCFMI-based sensor can be fabricated as a biochemical sensor if an appropriate sensing film is deposited on the surface of TCFMI.

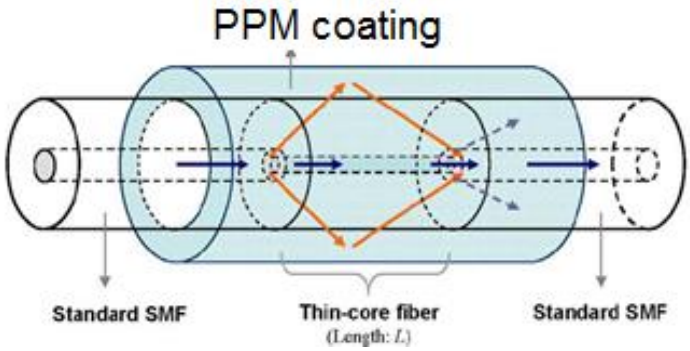


Figure 3.5 Scheme for the sensing principle of TCFMI based RI sensor.

The TCFMI RI sensor fabrication process is as follows: the TCFMI RI sensor can be quickly fabricated by fusion splicing a commercial 1.5 cm long thin-core optical fiber section (Nufern 460-HP, core diameter of the fiber is 2.5 μm, and the cutoff wavelength is ~450 nm) between two standard single-mode fibers. As we reported before [24, 25], the TCFMI is sensitive to RI change of surrounding environment. TCFMI pH sensors can be fabricated by coating nanoporous PEC sensing film on the surface of the TCFMI fibers.

TCFMI pH sensors fabrication by monolayer self-assembly technique:

TCFMI fiber was treated with piranha solution (8:2 v/v mixture of concentrated $H_2SO_4$ (98%) and 50% $H_2O_2$) for 20 min, followed by thoroughly rinsing with deionized water and drying with nitrogen. The fiber was then dipped into PCMVIm$Tf_2N$ and PAA blend solution for 1.5 h to coat a polymer layer onto the fiber surface by monolayer self-assembly method. Afterwards, the coated fiber was dried at 80 °C for 40 min, and soaked in 0.2 wt% aqueous ammonia for 1 h. Then it was immersed into DI water for 10 min.

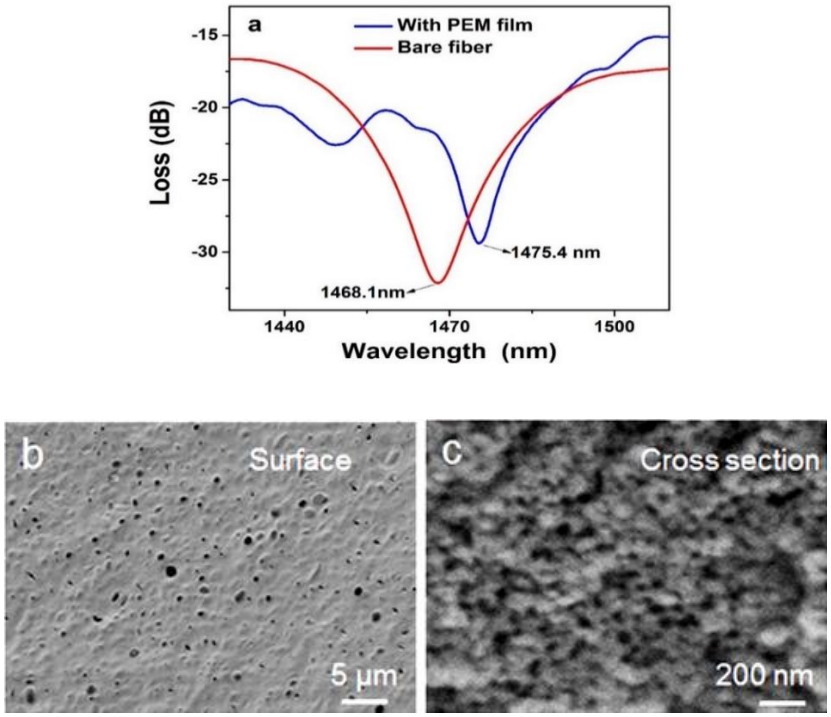


Figure 3.6 (a) Transmission spectrum of a optic fiber before (red line) and after (blue) being coated with nanoporous PEC film, (b) and (c) are porous morphologies of PCMVIm$Tf_2N$-PAA PEC film coated on the fiber.

Fig. 3.6 (a) shows the evolution of transmission spectra for TCFMI,

before and after the PEC sensing film coating by dipping the fiber into the PCMVIm$Tf_2$N-PAA blend solution for 1.5 h. It can be seen a red shift happens after depositing the PEC sensing film, with the wavelength change of 7 nm. The change can be attributed to the RI increasing as the sensing film displacing the air surrounding the TCFMI. It also proves that the PEC sensing film has been successfully coated on the surface of TCFMI. In addition, the surface morphologies of PEC film have also been tested after depositing it on the TCFMI. Fig. 3.6 (b) and (c) show the morphologies of PCMVIm$Tf_2$N-PAA film on the surface and at the cross section, respectively. It can be seen nanoporous appear both on the surface and inside the film. It suggests that the nanoporous PEC film can form, independing on the substrate. As a result, the TCFMI based pH sensors have been successfully fabricated.

### 3.3.2 Dipping Time Effect

We first fabricated the TCFMI based pH sensors by dipping the fiber into PCMVIm$Tf_2$N-PAA blend solution for 3 h. The sensor was tested by connecting the sensor with optical spectra analyzer (OSA) and broadband light source. The interferometer peak could appear on the OSA. The sensors were tested with different pH solutions from 2 to 10.

The results for the sensors' performance are given in Fig. 3.7. It can

be seen the wavelength has almost no change with pH increasing, neither in the acidic region nor in the alkaline region. The results indicate that no or little nanoporous PEC sensing film have formed on the surface of TCFMI. So the fiber has no response to pH values change. The reason is that with too long time dipping, the film may be redissolved by DMF. So it is necessary to decrease the dipping time during the sensors fabrication.

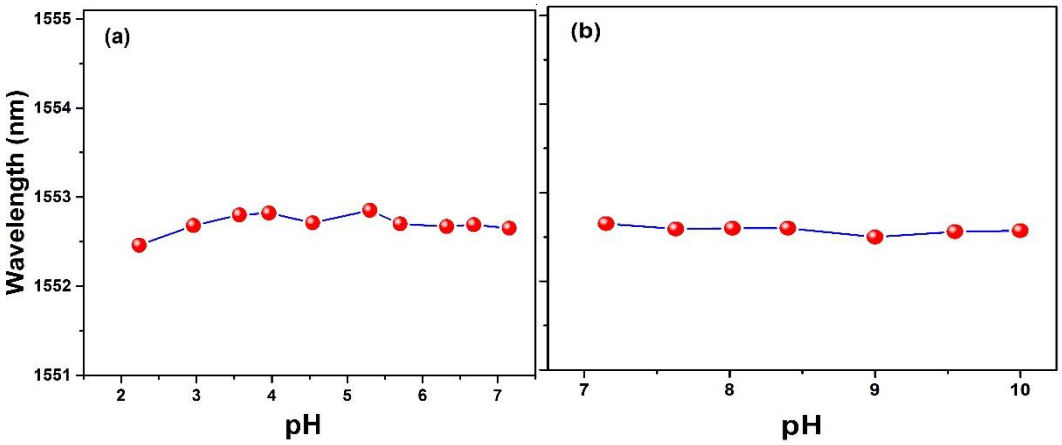


Figure 3.7 Wavelength evolution of TCFMI based pH sensors (with nonoporous PEC sensing film, dipping into PCMVImTf$_2$N-PAA blend solution for 3 h) to pH: (a) pH change from 2 to 7; (b) pH change from 7 to 10.

### 3.3.3 Testing of TCFMI pH sensor with Nanoporous Coating

The TCFMI based pH sensors, dipping the fiber into PCMVImTf$_2$N-PAA blend solution for 1.5 h, were fabricated. Performance of the freshly prepared fiber-optic sensor was also tested with increasing pH values from 2 to 10. As observed in Fig. 3.8, the transmission wavelength of the TCFMI sensor first increases and then decreases linearly with pH before and after a turning point

at pH=7. This non-monotonic change of wavelength versus pH has been well-known in sensing devices reported in previous works [24, 25], because the electrostatic complexation is the strongest at neutral pH. The change of wavelength for the sensor is due to the swelling degree change with pH solutions. With the pH increasing from 2 to 7, the hydrophility of nanoporous PEC sensing film decreases. It is attributed to the deprotonation of COOH group of PAA leads to larger electrostatic force between PCMVIm$Tf_2N$ and PAA. As a result, the swelling degree of the PEC sensing film decreases. In other words, the RI of PEC sensing film increases with pH changing from 2 to 7. So the wavelength shifted towards large wavelength. However, as the pH still increases, more surplus $COO^-$ groups appeare on the PAA chains, leading to the hydrophilicity of PEC sensing film increaseing. And the swelling degree of PEC sensing film also increases. That means the RI of sensing film decreases, and leads to the blueshift of the wavelength of the sensors. Consequently, the wavelength of the sensor reaches the largest value at pH=7 as it has the least swollen and the highest RI at this turing point. The spectra of TCFMI based pH sensor are shown in Fig. 3.8 in different pH solutions. The pH variation will change the refractive index of the sensing film, which thus alters the optical distribution of the excide cladding modes. Therefore, the light intensity coupled back from the thin-core optical fiber to the standard single-mode fiber will vary, which results in an alteration of the

amplitude of the interference spectrum. The sensitivity of the present TCFMI pH sensor is particularly high, 2.04 and -2.48 nm/pH unit in the acidic (2~7) and alkaline region (7~10), respectively. The sensitivity is much higher than other TCFMI based pH sensors reported before. And a comparation has been made in Table 3.1. The high sensitivity can be attribute to the large thickness of the sensing film.

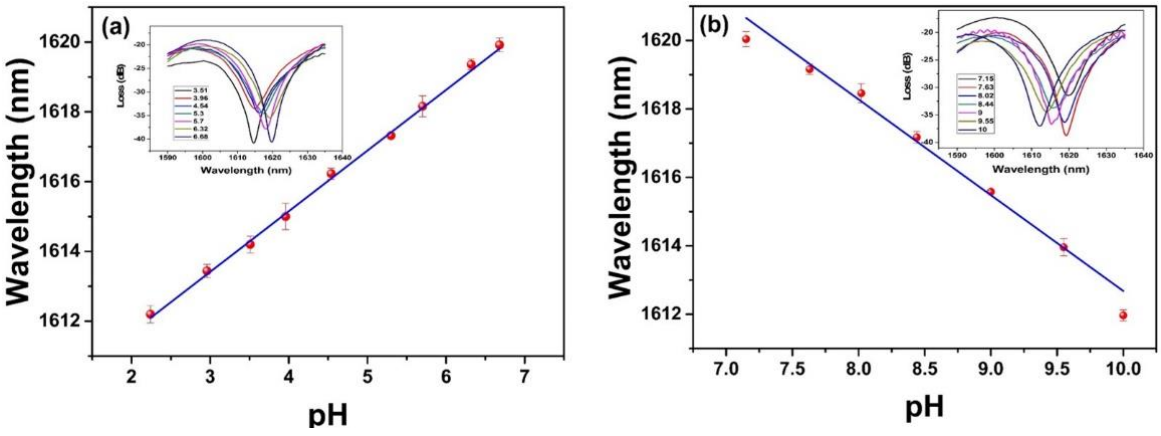


Figure 3.8 Wavelength change of TCFMI based pH sensors (with nonoporous PEC sensing film, dipping into PCMVImTf2N-PAA blend solution for 1.5 h) to pH: (a) pH change from 2 to 7; (b) pH change from 7 to 10. The inset gives the spectral evolution of TCFMI based pH sensor and the error bar is also given.

The dynamic response of the sensor has also been tested. The sensor was alternatively immersed into pH solutions (pH=3.96 and pH=6.68). The results are shown in Fig. 3.9. Remarkably, the response of the sensor is very fast. For example, a stable signal is observed within 5 s only after varying pH from 3.96 to 6.68 ($t_r$), and 12 s from 6.68 back to 3.96 ($t_f$). The response is much faster than any other TCFMI based fiber-optic sensors, which

usually required tens to hundreds of seconds [24]. The fast response can be attibuted to the nonopores of the PEC sensing film, which provides a channel for pH solutions to fast diffusing into or diffusing out of the film.

Table 3.1 Sensor performance (sensitivity and response time) of some other TCFMI pH sensors. It is seen that nanoporous PEC film sensor in this study is superior in terms of both the sensitivity and response time.

| Polymer coating | Sensitivity [a] | Response time | Ref |
|---|---|---|---|
| $(PAH/PAA)_{25}$ | 0.32 nm/pH, −0.45 nm/pH | $T_r$=120s; $T_f$=200 s | [24] |
| $(PDDA/PAA)_{10}$ | 0.32 nm/pH, ----- | $T_r$=240 s; $T_f$=160 s | [126] |
| $(PEC/PDDA)_{10}$ | 0.60 nm/pH , −0.85 nm/pH | $T_r$=30 s; $T_f$=50 s | [25] |
| $(PDDA/PAA)_{10}$ | 0.25 nm/pH, ------ | $T_r$=20 s; $T_f$=15 s | [126] |
| PCMVIm$Tf_2$N-PAA | 2.04 nm/pH, −2.48 nm/pH | $T_r$=5 s; $T_f$=12 s | This work |

Note: sensitivity in acid and base region, respectively.

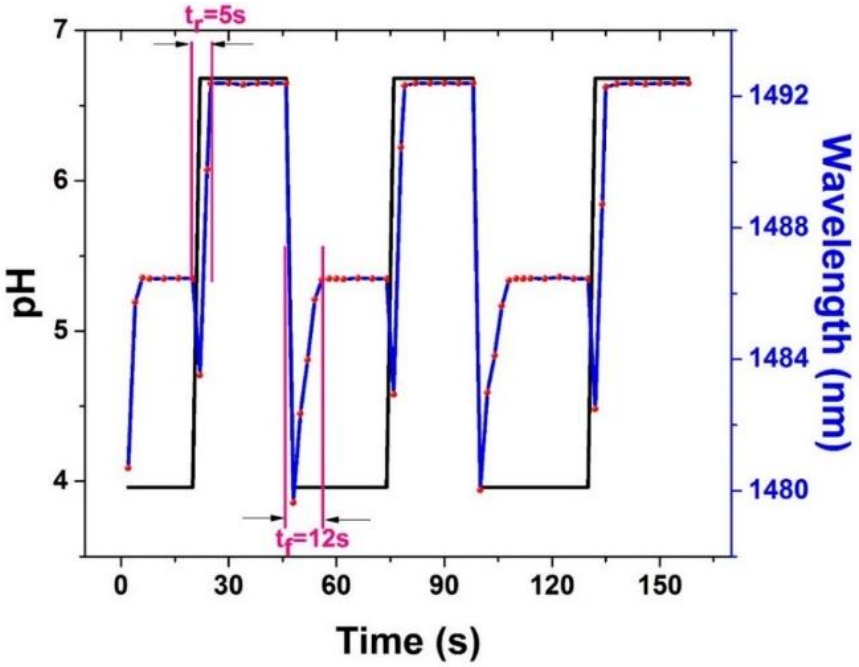


Figure 3.9 Dynamic responses of the TCFMI pH sensor (with nonoporous PEC sensing film, dipping into PCMVImTf$_2$N-PAA blend solution for 1.5 h) to pH change from 3.96 to 6.68 forwards and backwards several times.

The reversible performance of the sensor to pH changing from 2 to 10 forwards and backwards is given in Fig. 3.10. As observed, the wavelength of the TCFMI based pH sensor has no or only a little change when immersed into the same pH solution again. And the change is within the error range. The PEC sensing film is very stable, and cannot be dissociated at the solutions within the specified range of pH values. It means that the sensor can be used for long time. Thus, we can make a conclusion that the sensor is able to be used repeatedly, with little degradation of its performance. It has great potential for real applications, such as for clinical diagnosis.

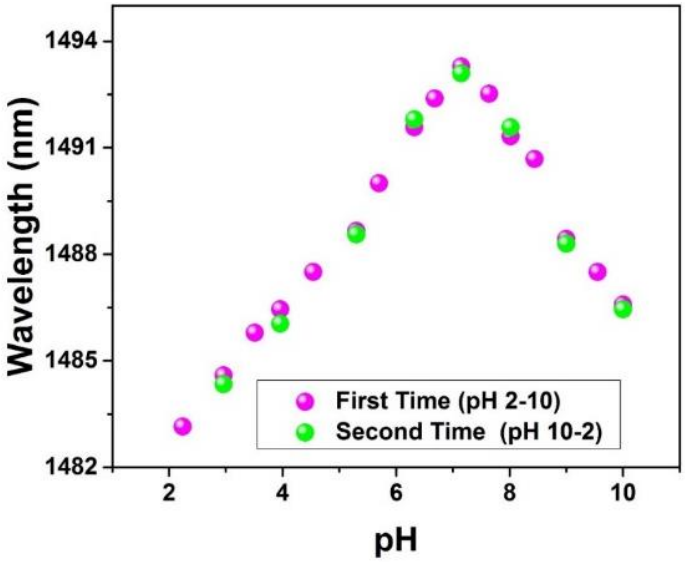


Figure 3.10 Reversible performance tests of TCFMI pH sensor (with nonoporous PEC sensing film, dipping into PCMVIm$Tf_2$N-PAA blend solution for 1.5 h) by increasing pH from 2 to 10 and reversibly.

### 3.3.4 Testing of TCFMI pH sensor with Nonporous Coating

In addition, another TCFMI based pH sensor has also been fabricated by monolayer self-assembly non-porous PEC coating on the fiber, to compare with the nanoporous PEC film sensors. To control the experiment accurately, the sensor was also fabricated by dipping the sensor into PCMVIm$Tf_2$N-PAA blend solution for 1.5 h and dried, but, without the 0.2 wt% aqueous ammonia treatment.

Similarly, the sensor was tested in different pH solutions, also from 2 to 10. The wavelength change with pH is displayed in Fig. 3.11. As we can see from the figures that the variation trend of nonporous PEC film to pH is the same with that of nanoporous PEC film. Also, the largest wavelength

reaches at pH=7. The sensitivity was calculated by fitting the data with linear relationship. The sensitivity of the nonporous PEC sensing film based TCFMI pH sensor is similar to that of the nanoporous PEC sensing film, 1.75 and -2.82 nm/pH unit in the acidic (2~7) and alkaline region (7~10), respectively. It indicates that the thickness of sensing film, both nanoporous and nonporous, is also similar, and the monolayer self-assembly deposition method provides a repeatable way for sensor fabrciation. The spectra evolution of the sensors are shown in the inset of Fig. 3.11.

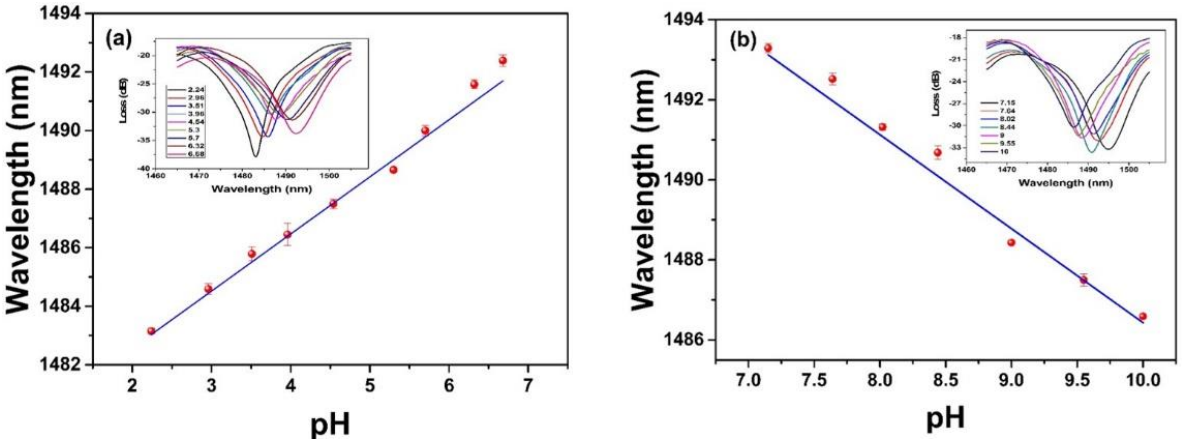


Figure 3.11 Wavelength change of TCFMI based pH sensors (with nonporous PEC sensing film, dipping into PCMVImTf2N-PAA blend solution for 1.5 h) to pH: (a) pH change from 2 to 7; (b) pH change from 7 to 10. The inset gives the spectra evolution of TCFMI based pH sensor and the error bar is also given.

Fig. 3.12 gives the dynamic response of nonporous PEC sensing film. The test was conducted by alternatively immersing the sensor into pH solutions (pH=3.96 and pH=6.68). The response times for $t_r$ and $t_f$ are 45s

and 120s, respectively. The dynamic response also suggests that the sensor has good repeatability. The response time of non-porous PEC sensing film is much longer, compared with nanoporous PEC sensing film. The slow response is due to the swelling/deswelling of sensing film needs long time [127], for the pH solutions diffusing into the sensing film very slowly. Therefore, the nanoporous PEC coating based pH sensor has better performance compared with nonporous PEC coating based sensor. And the former is more suitable for the real application, in terms of their performance.

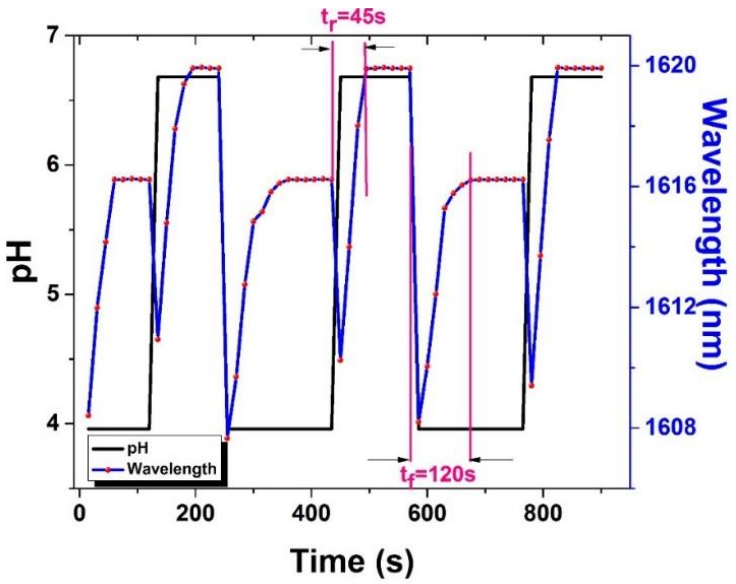


Figure 3.12 Dynamic responses of the TCFMI pH sensor (with nonporous PEC sensing film, dipping into PCMVIm$Tf_2$N-PAA blend solution for 1.5 h) to pH change from 3.96 to 6.68 forwards and backwards several times.

## 3.4 Summary

In summary, we introduced a template-free and scalable method to prepare hierarchically nanostructured PEC film in a simple film-casting and solution

immersion/activation procedure. The nanostructured film was adopted for fiber-optic pH sensors fabrication. The TCFMI fiber was coated with the nanoporous PEC sensing coating by monolayer self-assembly method. The sensor was capable of breaking the common “trade-off” rule in sensor applications, showing a superior pH sensing performance with a fast response ($t_r$ = 5 s, $t_f$ = 12 s) and high sensitivity (2.04 nm/pH unit, -2.48 nm/pH unit). And we also compared the nanoporous PEC coating sensor with nonporous PEC coating sensor, the results showed that their sensitivities were similar, but the former gave very fast response due to the nanoporous property of the sensing film. So the nanoporous PEC coating pH sensor has greatly potential for application in biological fields.

## *Chapter 4*

# Optical Microfiber LPG pH Sensor Based on Micropatterned PAA Ionic Hydrogels

In this chapter, a novel, rapid and maskless 3D printing technique based on a digital-micromirror device (DMD), called optical maskless setereolithography (OMSL) has been adopted to fabricate poly (acrylic acid) (PAA) ionic hydrogels microstructure arrays. The PAA ionic hydrogel microstructures were *in-situ*, periodically patterned to enclose 2-cm length tapered micro-fiber for fiber-optic pH sensor fabrication. The PAA microstructures were formed by photopolymerizing acrylic acid (AA) in the existence of photoinitiators. Various 2D and 3D complex microstructure arrays, including both concave and convex microstructures, were fabricated. The microstructure arrays were characterized by 3D laser scanning confocal microscope. The results indicate that microstructures with the size ranging from several to hundreds of micrometers can be fabricated by OMSL system. Moreover, these microstructure arrays could be rapidly fabricated on a large scale. Taking the advantages of our 3D printing technique, novel long-period grating (LPG) pH sensors were printed for the first time, using pH sensitive PAA hydrogels. The LPG pH sensors showed very high sensitivity and fast response.

## 4.1 Introduction

pH is a key parameter for regulating the functions of different organs of human. For example, the activities of enzymes depend on the pH of surrounding environments, the functions of cells are modulated by the pH, and pH of tissue is also a key physiological parameter which indicates the healthy conditions of the body. Thus, pH sensor is necessary for monitoring the pH values of different parts in humans. Though electrochemical pH sensors have been widely used in many areas, they are too bulky to be applied in vivo. And the signals of electrochemical pH sensors are not very stable and calibrations are also needed before use, which is inconvenient for in vivo applications.

To solve the problems mentioned above, fiber-optic pH sensors have been developed and shown great potential for clinical applications [84, 128]. However, fiber-optic pH sensors usually adopt organic dyes for pH sensing, which introduces another problem of dyes leakage. Therefore, LPG refractive index (RI) sensor provides a platform to achieve miniaturized pH sensor without dyes by coating pH sensitive nano-structured films [37]. Chiang et al. [129] studied coating PVA/PAA sensing film on the surface of LPG for fiber-optic pH sensor fabrication. The pH sensor detected pH ranging from 2 to 6, with the highest sensitivity of 2.6 nm/pH. But they make the LPG by UV inscribing technique, which was time-consuming and

inconvenient. Dip coating [130] and $CO_2$ laser machining [131] have been reported to fabricate tapered fiber based LPG, however, all of them involved "point by point" scribing processes, which limited the production efficiency. To solve the problem, ICP dry etching technique was proposed to fabricate LPG [132]. Though improving the efficiency, it still took many steps and long time to complete the fabrication process. In addition, all the LPGs fabricated were not chemical sensors or biosensors, while LPGs have great potential in sensors application. Ionic hydrogels, a subclass of hydrogels, are stimuli-responsive polymers, which are high water content and with swelling degree from several to hundreds of times [133, 134]. They are among the best candidates for sensors, because they can achieve the transduction from chemical signal to optical or electrical signals.

PAA, as a kind of ionic hydrogel, has been studied a lot [135-152], especially as sensors [38, 91, 126, 127, 138, 141, 153-155]. And many studies have explored to pattern PAA ionic hydrogel, to extend its applications or improving its performance [146, 156-160]. Moreover, the high density of carboxylic acids makes it suitable for physical and chemical modification to form bio-functional surfaces, and thus, PAA has great potential to be deployed in rapidly emerging fields, such as biosensors and biomedical devices.

In our study, we propose, for the first time, to rapidly pattern 3D

microstructure arrays of PAA ionic hydrogels by OMSL technique. And it is adopted to fabricate LPG on tapered optical fiber. Our PAA hydrogels based LPG itself is sensitive to environmental change, such as pH, without further surface modification by other functional materials. In addition, the sensor shows outstanding high sensitivity to pH change. Meanwhile, the PAA hydrogels based LPG sensors can be applied in vivo as PAA is biocompatible.

## 4.2 Micropatterning of PAA Ionic Hydrogels

### 4.2.1 Fabrication of PAA Microstructures

The setup of OMSL used for microstructures fabrication is shown in Fig. 4.1 (a). And the microstructures fabrication process is as follows: photoinitiator, 2-hydroxy-4'-(2-hydroxyethoxy)-2-methylpropiophenone (Irgacure 2959), was dissolved into AA with a concentration of 10 wt%. The solutions were first prepolymerized in the oven at the temperature of 110 $^{o}$C for 5 minutes. Then an own-established OMsL setup was used for micropatterning process. With a spacer, a cover glass was placed upon the AA solution that was dropped on another glass slide. UV light will penetrate the cover glass and photopolymerize AA on the bottom side of the cover glass. The pre-designed microstructures were converted into own-defined image data and then loaded onto the DMD chip for generation of optical patterns. UV light source (365 nm) was used in the OMsL setup for photopolymerization of AA solutions.

The intensities of UV light for 2D and 3D microstructure patterning are 103.12 mW/cm$^2$ and 51.56 mW/cm$^2$, respectively. The total exposure time is around 5 to 30 s. The exposed micropatterns were developed by using DI water and IPA, sequentially.

The mechanism for the photopolymerization of PAA is given in Fig. 4.1 (b). It can be seen that the photoinitiator is decomposed to generate highly active radicals with the UV light. In this way, the monomer, AA, reacts with the active radicals due to the double bonds are also active for the reaction. And the PAA can form in very short time as the radical polymerization is a fast way for polymer preparation.

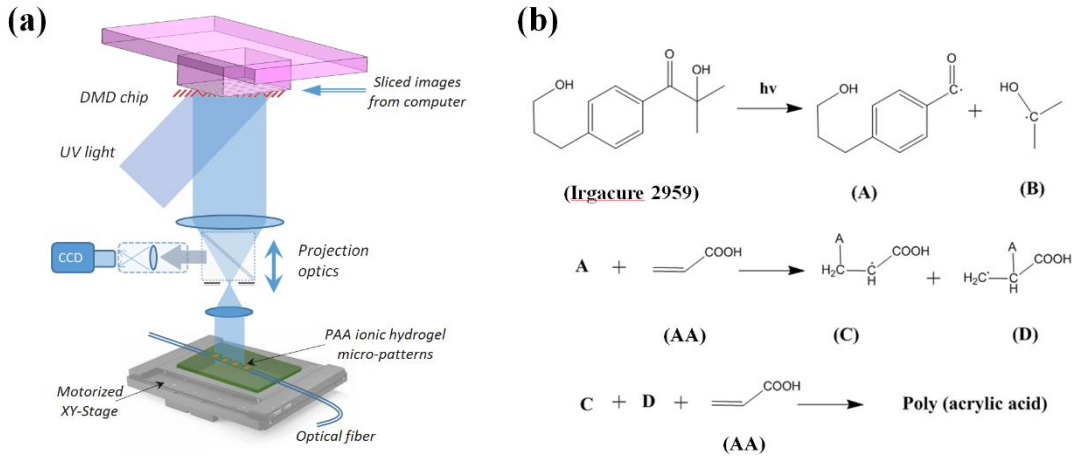


Figure 4.1 (a) Schematic diagram of the OMSL system: the UV light illuminates the DMD chip, and the generated optical pattern is projected on the photo-sensitive polymer for fabrication of microstructures. (b) The reaction process for the photopolymerization of AA in the presence of photoinitiator.

### 4.2.2 PAA Microstructures Characterization

The microstructures were fabricated by irradiating the prepolymerized AA solutions through the OMSL system. It is important to prepolymerize the solution by heating. On one hand, the time for microstructures fabrication were very long (several minutes). On the other hand, the microstructures were not as we designed, for some parts were overexposure while some parts were not irradiated enough. By heating the solution in the oven for prepolymerization, fine microstructure arrays could be reached by OMSL technique in very short time.

The microstructure arrays of PAA were characterized by 3D laser scanning confocal microscope (VK-X200, KEYENCE, manufactured in Japan). It was a non-contact scan. The magnification of lens used for scanning was 50×. Fig. 4.2 (a), (b) and (c) show some 2D microstructures with different line widths, ranging from 6 μm to 200 μm. The 2D microstructures are (a) lattice grid; (b) honeycomb pattern; and (c) our university logo. They are all fabricated in between 10 s and 20 s. It can be seen from the pictures that the surface of all microstructures are much smooth compared with other 3D printing hydrogels [161, 162]. However, the rims of microstructure are not so vertical due to the weak mechanical property of PAA hydrogel [163]. Experimental results reveal that the lithography process can quickly pattern complex microstructrues with

different feature sizes. Due to the inherent water-absorption property of hyrdogel, the joint points of thick microstructure will appear slightly swell, Fig. 2(c).

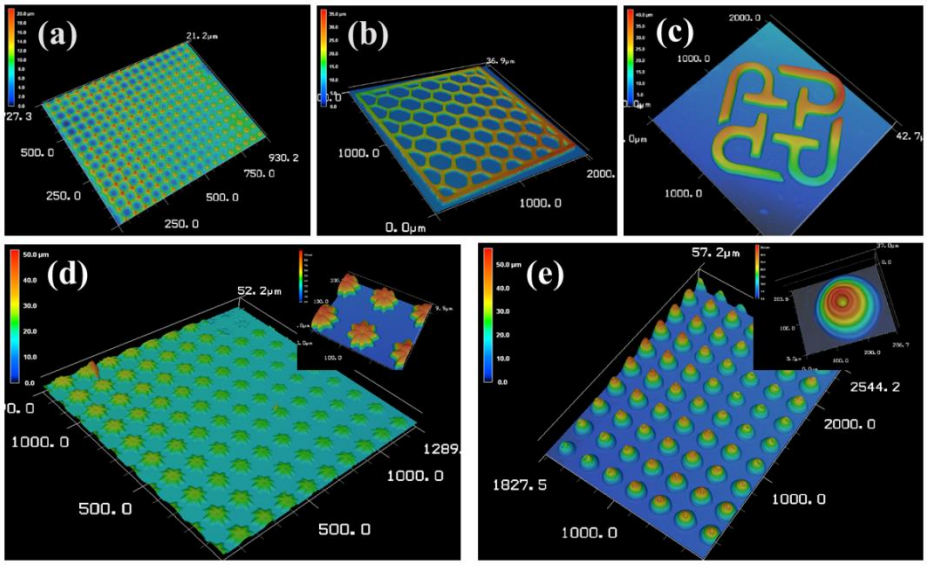


Figure 4.2 Laser scanning confocal images of the 3D patterned PAA microstructures: (a) lattice grid; (b) honeycomb pattern; (c) PolyU logo; (d) flower-like microstructure; and (e) Hanoi-tower microarray.

The advantages of OMSL system are the 3D microstructures fabrication without mask and the fast fabrication speed. So OMSL system is adopted for fabricating some more complex 3D microstructures. Though photopolymerization of PAA hydrogels have been reported before [142, 143, 163, 164], 3D printing of them has not been studied so far. Fig.4.2 (d) and (e) show the 3D printed flower-like microstructures and Hanoi-tower microarray. Compared with 2D microstructures, those 3D microstructures need eo be exposured for longer time (around 30 s). The flower-like microstructure

contains 8 petals, and its height gradually decreases from the center. The whole size of such a 3D flower microstructure is 75 μm. The exposure time for Hanoi-tower is longer than that for 2D microstructures. It is composed of 5 concentric rings with graded heights, and the size of a single microstructure is 200 μm. The surface of the fabricated 3D PAA microstructures are pretty smooth. Those results indicate that the OMSL technology is very promising to fabricate 3D PAA microstructures and devices.Though the time used for 3D microstructures is longer than 2D microstructures fabrication, it is much more rapid than other 3D printing techniques [133, 165, 166]. The lateral and depth resolutions of the platform for patterning PAA are around 4.8 and 0.2 μm, respectively.

### 4.2.3 Swelling Properties of PAA Ionic Hydrogels in pH Solutions

Four kinds of discoidal PAA ionic hydrogels were prepared using OMSL system, they were fabricated by controlling irradiation time: 5s, 7.5s, 10s and 15s. These hydrogels were immersed into different pH solutions for 2 hours for each pH solution. After equilibrium, the mass of these samples was weighed. The swelling degree was calculated from the ratio of the mass of the hydrogel in the swollen and dried states based on the average from two measurements. It can be seen from Fig. 4.3 that the swelling degree of PAA ionic hydrogel increases with pH increasing from 2 to 7. Moreover, PAA

ionic hydrogels prepared with different irradiation time have different swelling degrees. The shorter time for ionic hydrogel preparation, the larger the swelling degree is. The phenomenon is due to the molecular weight of PAA is smaller in shorter time preparation than that in longer time, and the hydrophilicity is also larger [167, 168]. It is noteworthy that there is no significant difference for PAA micropatterns irradiated for 10 s and 15 s. It means that the molecular weight of the PAA micropattern irradiated for 10 s has become comparatively large, and longer-time irradiation will not lead to significant change of PAA molecular weight.

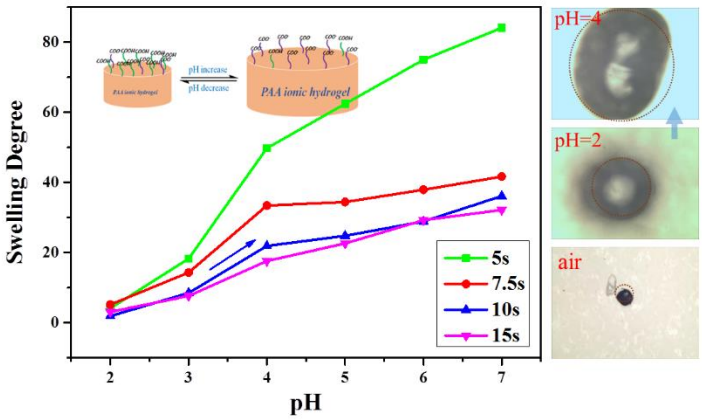


Figure 4.3 Swelling degree change of PAA ionic hydrogel with pH increasing: the right pictures shows the microscopic pictures of discoidal PAA ionic hydrogels fabricated in 10s: they are hydrogels immersed into pH=4 solution, pH=2 solution and dried hydrogels, respectively, from top to bottom.

The inset of Fig. 4.3 gives scheme for swelling degree change with pH. As the pH increases, the -COOH group of PAA is deprotonated to become $–COO^-$ group, and the hydrophilicity of PAA ionic hydrogels also

increases with it [138, 154]. In other words, more water can diffuse into the hydrogels, leading to the swelling degree of the PAA ionic hydrogel increasing with pH. In addition, the swelling/deswelling transition is reversible though the time needed for the process is very long.

## 4.3 Fabrication of PAA-LPG pH Sensor on Optical Microfibers

### 4.3.1 3D Printing PAA Ionic Hydrogel on Optical Microfibers

Tapered optical fibers were drawn by LZM-100 LAZERMaster™ Laser Splicing System (Fujikura Ltd., Japan). The tapered optical fibers are commercial single mode fibers (SMF-28e, Corning). The fibers were drawn to be 30 μm in diameter and 2 cm in length.

To utilize the pH responsive behavior of PAA ionic hydrogel, the OMSL technique was used to *in-situ* fabricate PAA micropatterns, encapsulating a tapered optical fiber to develop highly sensitive optical pH sensors. Fig. 4.4 (a) shows the schematic diagram of the fiber-optic pH sensor. The standard optical fiber is tapered to enhance the sensitivity of the sensor, as shown in Fig. 4.4 (b). PAA micropatterns are periodically fabricated on the fiber surface to form a LPG device. In order to properly excite the resonant scattering of cladding modes at the wavelength of ~1430 nm, the grating period of LPGs has been chosen to be 650 μm. The irradiation time for each PAA micropattern has been chosen to be 10 s to

ensure the repeatability of fabrication and a relatively large dynamic range of detection. Fig. 4.4 ($c_1$ – $c_3$) are the confocal microscopic images of three examples of PAA micropads patterned on a microfiber. The periods of the PAA gratings are all 650 μm, with duty cycles of 1:1. But the sizes of them are different, so we name them as LPG-X-Y, where X represents the size of each PAA grating, Y represents the duty cycle of the LPG grating, for short. Therefore, the devices from $c_1$ to $c_3$ are LPG-100-1:1, LPG-300-1:1, and LPG-600-1:1, respectively. One can see that the PAA ionic hydrogels have been precisely patterned to encapsulate the tapered micro-fiber for all these devices. The surfaces of the PAA patterns are very smooth and the grating pitches along the fiber are uniform. More importantly, the micro-fiber surface is totally encapsulated for each grating pitch, which is a key point to form the LPG.

The transmission spectra of LPGs are measured by an OSA and a broadband light source. Experimental results reveal that the width of PAA micropatterns has significant influences on the spectra of the LPG devices. Fig. 4.5 shows the spectra of LPGs with different sizes of PAA ionic hydrogel grating pitch. It can be seen the LPG resonant peak becomes deeper and deeper with increasing the size of PAA ionic hydrogel. It indicates that LPG-600-1:1 is better for sensors, for the narrower loss band. Meanwhile, the central resonant wavelength appears blue shift with the PAA ionic

hydrogel size increasing. So the shape of the resonant peak can be adjusted by changing the size of PAA ionic hydrogel, which provides a convenient way to control LPG spectra. One can see that the OMSL is very flexible and able to pattern PAA ionic hydrogel to customize micro-structured device.

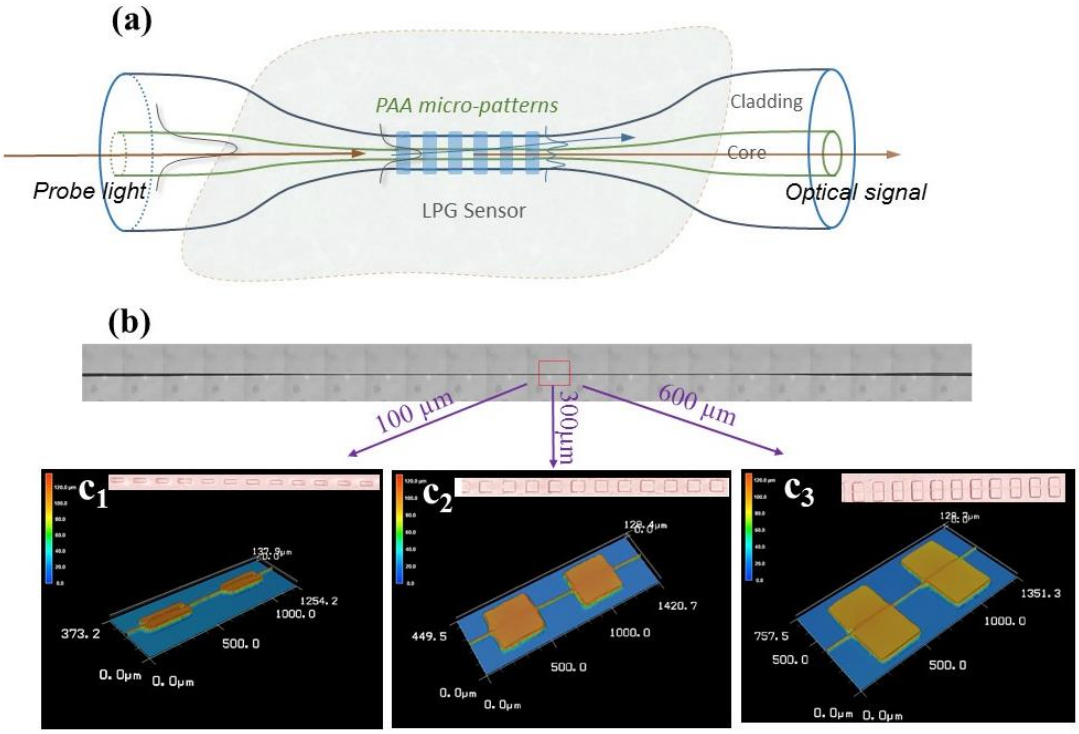


Figure 4.4 (a) Scheme of the optical transimission path through PAA ionic hydrogels patterned tapered fiber. (b) Tapered optical fiber with a diameter of 30μm (2cm in length). (c) 3D microstructures of PAA ionic hydrogels gratings used for encapsulating tapered fiber: LPG-100-1:1 ($c_1$), LPG-300-1:1 ($c_2$), and LPG-600-1:1 ($c_3$) fabricated by OMSL system in 10s measured with 3D laser scanning microscope. The inset pictures of (c) are microarray gratings taken by optical microscope.

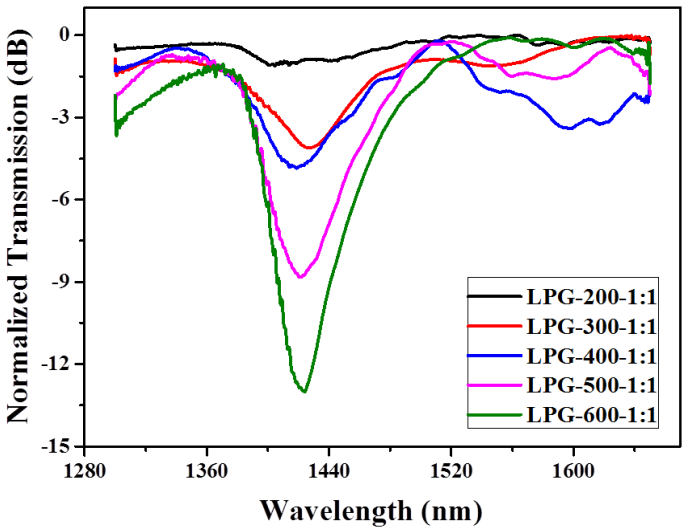


Figure 4.5 Micro-fiber LPG spectra evolution fabricated by PAA ionic hydrogels encapsulation with increasing the size of PAA ionic hydrogel grating pitch.

### 4.3.2 Testing of PAA-LPG pH Sensors

The fabricated fiber-optic pH sensors have been tested in the experiments. From the results in Fig. 4.5, it can be seen the device of LPG-600-1:1 shows much narrower loss band and its resonant peak is the deepest among the five devices. Thus, LPG-600-1:1 is chosen for pH sensing to enhance the signal-to-noise ratio. The device was measured to sense the pH value ranging from 2 to 7. Fig. 4.6 (a) shows the measured responses of LPG-600-1:1 sensor to different pH solutions. One can see that the central resonant wavelength of the sensor shifts to longer wavelength with the increasement of pH value from 2 to 7. It is because that the swelling of PAA ionic hydrogel will induce a decrease of RI [138, 153, 154, 169]. Consequently, the effective RI of the fiber cladding modes will also become lower as their evanescent fields exist in the PAA ionic hydrogel. Therefore, a red-shift of the resonant wavelength

will be induced as the effective-index difference between the fundamental guided mode and fiber cladding modes will increase. Meanwhile, the swelling of PAA micropatterns will induce a drop of strain in the microfiber. The measured sensitivity of the LPG pH sensor is 7.5 nm/pH, which significantly surpasses other reported fiber-optic pH sensors. The reversibility of the pH sensors has also been tested in the experiments. As shown in Fig. 4.7 (a), the difference of response of the sensor between the forward and backward changes of pH values is very small. Therefore, the sensor can be repeatedly used in pH sensing applications.

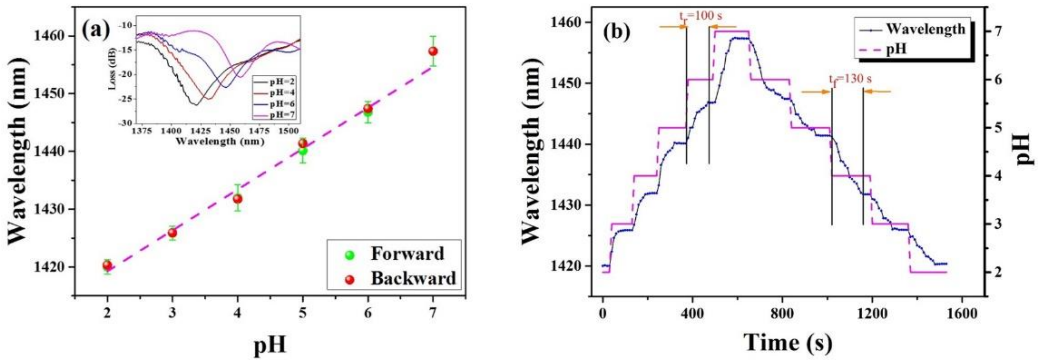


Figure 4.6 (a) Dip wavelength shift with pH increasing of LPG-650-1:1 pH sensor and it can be reversibly responsive to pH change, forward and backward (The error bar is given in the figure). (b) Dynamic response of LPG-600-1:1 pH sensor to different pH solutions.

The dynamic response of LPG-600-1:1 pH sensor is shown in Fig. 4.6 (b). As the swelling transition time is proportional to the square of the gel pattern's size [127] and there is significant difference before and after immersing into solutions, the micro-fiber LPG sensors have been pre-immersed into DI water before testing. The OSA keeps sweeping with period

of 10 s during the testing. It can be observed that the response time of the sensor are 100 s and 130 s for increasing and decreasing the pH, respectively. Although the response time is not very fast (due to the diffusion and swelling process of the PAA hydrogel), it is much better than other reported pH sensors based on PAA ionic hydrogels [170].

The sensitivity of the sensor also depends on the size of PAA ionic hydrogel grating pitch. To further enhance the sensitivity of the sensor, we suggest patterning a larger PAA grating pitch. Therefore, LPG-1000-3:7 was fabricated. LPG-1000-3:7 pH sensor was tested by immersing into different pH solutions. The sensor was tested and the results are shown in Fig. 4.7. It can be seen that the detection range really becomes wider, from 2 to 7, by the LPG-1000-3:7 devices. Meanwhile, the wavelength shift is also similar with the other device. Fortunately, the sensitivity is significantly enhanced, reaching 16.7 nm/pH. But the response time becomes longer, about 120s.

Compared with the pH sensor based on PILs, the detection range of the PAA-LPG pH sensor is relatively narrower (pH detection range is 2 to 7). It is because that PAA hydrogel will be dissolved in high pH solutions. Fortunately, the pH value in human body is usually not high. Therefore, the sensor is still well suitable for potential clinical uses.

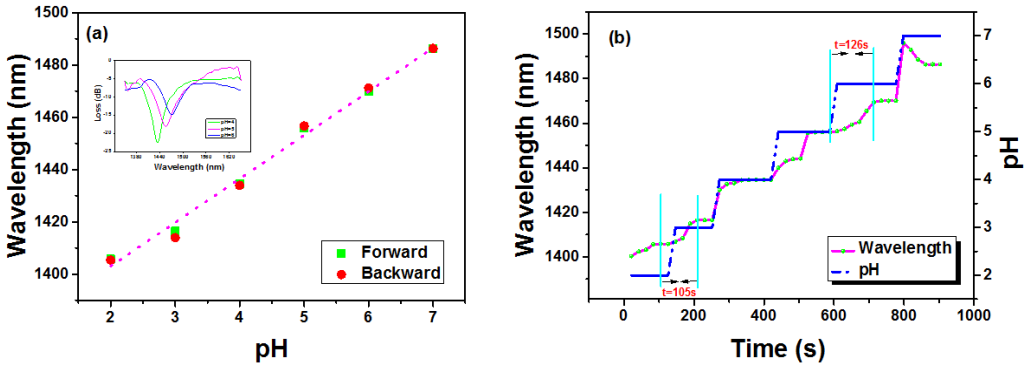


Figure 4.7 (a) Dip wavelength shift of LPG-1000-3:7 devices with pH increasing from pH 2 to 7. (b) Dynamic response of LPG-1000-3:7 pH sensor to different pH solutions.

## 4.4 Summary

In summary, a novel rapid and maskless 3D printing technique has been introduced to fabricate PAA ionic hydrogels microstructure arrays. Various 2D and 3D complex microstructure arrays, including both concave and convex microstructures, were fabricated, with the sizes ranging from several tens to hundreds of micrometers. These microstructure arrays were fabricated in only 5 to 30s. And the pH sensitive PAA hydrogels were printed to enclose tapered fiber for LPG pH sensors fabrication. The pH sensors show very high sensitivity of 16.7 nm/pH. The response of the sensor can reach to be 70s. As the first 3D printed LPG pH sensor, it has great potential for in vivo test as PAA is biocompatible.

## *Chapter 5*

# Fiber-optic DNA Sensor Based on Self-assembled Multilayer Sensing Coating

In this chapter, a highly sensitive fiber-optic DNA sensor was fabricated for DNA hybridization detection. The nanostructured sensing film was coated on the surface of thin-core fiber modal interferometer (TCFMI) by layer-by-layer (LbL) self-assembly technology. Poly (ethylenimine) (PEI), poly (acrylic acid) (PAA) and single-stranded DNA (ssDNA) were used for coating polyelectrolyte multilayer sensing film for DNA detection. The sensing film was characterized by atomic force microscope (AFM) and surface profilometer. The DNA sensors were tested in different ssDNA solutions with concentration of 1 μM. The results show that target ssDNA with different number of match bases can be identified by TCFMI DNA sensors.

## 5.1 Introduction

DNA sensor is one of the most important type among the many kinds of biosensors due to its crucial role in gene engineering, pharmaceutics and clinical medicine [64, 99, 171, 172]. So far, a large number of detection techniques have been developed for DNA detection, including

electrochemical method [173], fiber-optic method [174], fluorescence-labeled method [175] and others [176, 177]. However, fluorescent-labels detection has the problems of limited life-time of fluorescence [64, 171] and the fluorescent signal is instable [178]. Moreover, the light sources are usually UV lights, which are harmful to the health of people [179-181].

To solve those problems, label-free approaches have been developed to fabricate biosensors [171, 182, 183]. In particular, label-free fiber-optic biosensors have gained a great deal of research interests because of their advantages of small size, biocompatibility, multiplexed detection capability, and low-cost. All these features make them highly suitable for clinical and biological applications [184].

Many types of fiber-optic biosensor have been reported, such as fiber-optic biosensors based on surface plasmon resonance (SPR) [185, 186], long-period grating (LPG) [171, 182] and tilted fiber Bragg gratings (TFBG) [187]. However, these types of fiber-optic biosensors have complex architectures [188-190]. Thus, a TCFMI [178, 191], a kind of refractive index (RI) fiber-optic sensor, is adopted to fabricate the DNA sensor. TCFMI DNA sensors have simple structures. In addition, the TCFMI sensors also have the advantages of low fabrication cost, ease of preparation, low temperature cross-sensitivity and high RI sensitivity. Compared with the reported LPG or TFBG fiber-optic DNA sensors [171, 182, 187], the

TCFMI-based DNA sensors exhibit higher sensitivity for ultralow ssDNA concentration detection due to higher sensitivity to RI change. They are also convenient for preparation and potentially lower cost than SPR-based DNA sensors.

However, to implement the TCFMI DNA sensor, a thin sensing film must be coated on the surface of TCFMI. It is known that the sensitivity of TCFMI depending on the thickness of sensing film [26]. Thus, the LbL self-assembly technique would be particularly suitable for the sensing film preparation due to its flexible controllability and tunability of film thickness at nanometer scale [192]. It has also been reported that sensors prepared by LbL self-assembly method can overcome some disadvantages of the biomolecular labelling technique, e.g. the loss of biomolecular activity and the complexity [183].

Thus, LbL self-assembly technique is used to coat sensing film on TCFMI for DNA sensor fabrication. And the TCFMI DNA sensors are disposable after use because of low-cost, which provide convenience for clinical application. Moreover, the TCFMI-based DNA sensors could identify the number of different match bases, while most of previously demonstrated DNA sensors are just able to monitor the occurrence of matched DNA hybridization.

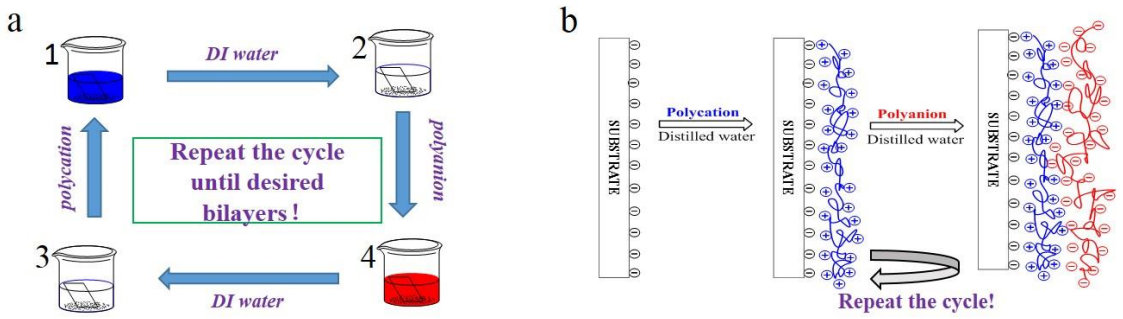


Figure 5.1 Scheme of LbL multilayers sensing film fabrication process: (a) the experiment process; (b) the mechanism for the multilayer film deposition.

## 5.2 Sensing Films Fabrication by LbL Self-Assembly Technique

### 5.2.1 DNA Sensing Film Preparation and Characterization

The concentration of both positively charged PEI and negatively charged PAA were diluted to 2.0 g/L, with pH 9.5 and 3.0, respectively. The concentration of negative charged ssDNA was 1 μM at pH 7.5, a physiological pH value, for both the sensing film fabrication and test solutions. The PEI, PAA and ssDNA multilayer sensing film was deposited on quartz slides (10 × 20 $mm^2$) and TCFMI, respectively, by LbL electrostatic self-assembly technique. The fabrication process was as follows: substrates (i.e. quartz slides and TCFMI) were cleaned with piranha solution (8:2 of 95% $H_2SO_4$ and 50% $H_2O_2$), washed by large number of deionized water and dried with nitrogen, by which the negatively charged substrates could be reached. The substrates were then dipped into the positively charged PEI and negatively charged PAA solutions alternatively, each for 10 minutes

at room temperature. The same process was repeated until 4.5 bilayers were built (one bilayer consists of one PEI layer and one PAA layer and is expressed as $(PEI/PAA)_1$). The substrates were rinsed with deionized water for 1 minute in between the immersions in polycation and polyanion solutions to remove the excess adsorbed components, and dried with nitrogen. The substrates were then dipped into negatively charged ssDNA solution for 30 minutes, and immersed into PBS solution for 10 minute to remove the excess adsorbed ssDNA chains, and dried with nitrogen again. After these processes, $(PEI/PAA)_4(PEI/DNA)_1$ multilayer film was prepared. The process of sensing film fabrication and deposition mechanism are shown in Fig. 5.1. It was finally baked in an oven at 70 °C for 10 hours to enhance its mechanical property and durability [193]. The chemical structures of PEI, PAA and DNA helix structures are given in the inset of Fig. 5.2.

Surface profilometer (Veeco, Germany) was used for monitoring the thickness growth process of $(PEI/PAA)_4(PEI/DNA)_1$ multilayer film. And the thickness change with layer numbers is given in Fig 5.2. As illustrated, the $(PEI/PAA)_4PEI$ layers display an exponential growth in thickness. Since the polymers used for film fabrication are weak polyelectrolytes and many charges on the polymer chain are screened during the layer-by-layer deposition process, more chains are needed to compensate the charges on the former layer, which leads to the exponential growth of the film thickness.

The result is similar with previous work [194]. But when the ssDNA layer was deposited, the thickness increases only a little because of low ssDNA concentration used for film fabrication [47]. It has been reported that the length of ssDNA chain was just about 2 nm with 20 bases [195]. In our work, each ssDNA chain contains 10 bases, and thus the thickness of sensing DNA layer is estimated as ~1 nm. It can be seen ssDNA layer is about 8 nm in our sensing film, from which we could conclude that many probe ssDNA chains have been absorbed on the surface of sensing film.

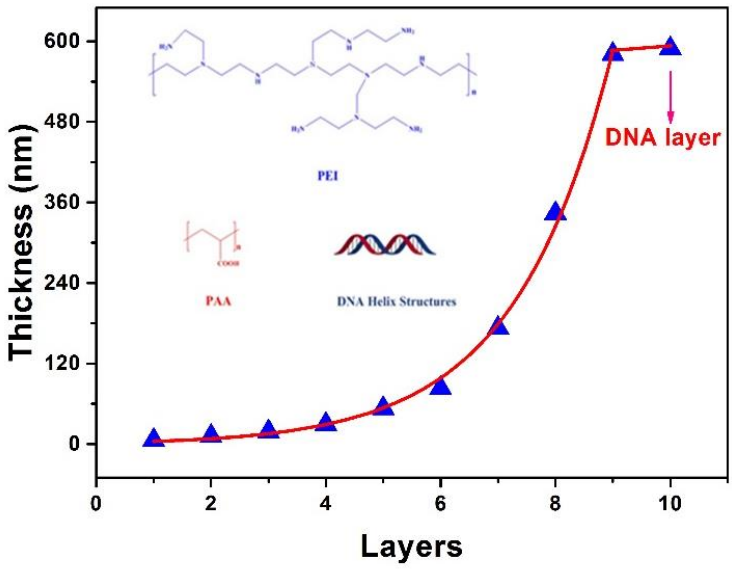


Figure 5.2 Thickness growth of $(PEI/PAA)_4(PEI/DNA)_1$ multilayer sensing film with layer numbers. The inset shows chemical structures of positively charged PEI and negatively charged PAA used for multilayer film fabrication. And the scheme of DNA helix structure is also given.

Scanning probe microscope (DI Nano Scope 8, Veeco, Germany) in AFM mode, in which the silicon tip (NSG10, NT-MDT) was operated with

a resonance frequency of ca. 288 kHz.), was used to characterize the morphologies of the multilayer sensing films. Fig. 5.3 (a), (b), and (c) show the AFM surface images of $(PEI/PAA)_4$, $(PEI/PAA)_4PEI$ and $(PEI/PAA)_4(PEI/DNA)_1$ multilayer film, respectively. The surface of $(PEI/PAA)_4$ multilayer film shows wormlike or vermiculate patterns. Similar patterns have been discovered when PAA was the outmost layer [126, 196]. The measured root mean square (RMS) is 8.18 nm for PAA layer, which could be also seen in Fig. 5.3 $a_2$. When a PEI layer is deposited on the surface of PAA layer (Fig. 5.3 b), the RMS decreased to be 2.47 nm. It is attributed to the outer PEI layer covering up most of the surface texture [194]. We could observe from Fig. 5.3 $b_2$ PEI chains are agglomerated on the surface and show smooth surface. After depositing the probe ssDNA layer (Fig. 5.3 c), the surface of sensing film becomes denser and smoother. And more agglomerate of macromolecule chains appear on the surface [173]. Meanwhile, RMS further decreases to be 1.07 nm. The surface morphologies change indicates that probe ssDNA have been deposited on the surface of PEI layer successfully, as the ssDNA chains are negatively charged polymer at pH=7.5. Therefore, the multilayer sensing films could be applied for DNA sensors fabrication.

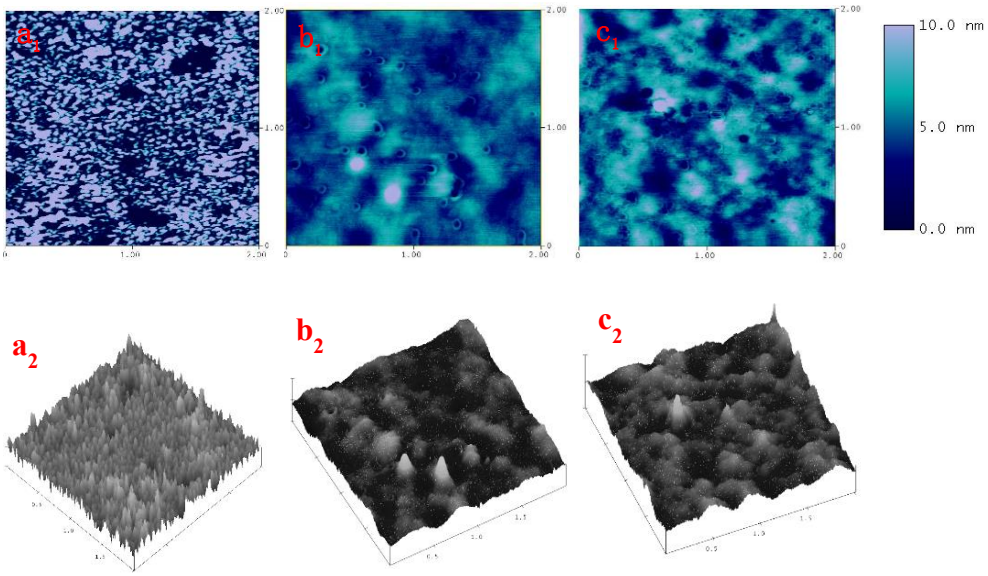


Figure 5.3 AFM images for $(PEI/PAA)_4$ (a), $(PEI/PAA)_4PEI$ (b) and $(PEI/PAA)_4(PEI/DNA)_1$ (c) multilayer films: the left are surface morphologies and the right are their 3D presentations.

### 5.2.2 Sensing Property of $(PEI/PAA)_4(PEI/DNA)_1$ Multilayer Film

UV-vis spectrophotometer (Cary 100Bio) was used for characterizing the absorption of the film after immersing into different kinds of target ssDNA solutions, as DNA has a maximum UV absorption at about 260 nm. Thus, the absorption peak was applied to test if the $(PEI/PAA)_4(PEI/DNA)_1$ multilayer film could be adopted as a DNA sensor. The multilayer coating was deposited on the surface of quartz slides for the tests. Fig. 5.4 shows absorption spectrum of $(PEI/PAA)_4(PEI/DNA)_1$ multilayer film and the inset shows the dependency of UV absorption intensity on different kinds of target ssDNA solutions. It can be seen that the absorption intensity grows when the match base numbers increases. The reason for the phenomenon is that more

target ssDNA chains are absorbed by $(PEI/PAA)_4(PEI/DNA)_1$ multilayer film when the number of match bases increase due to the linking force stronger for target and probe ssDNA as more hydrogen bond formation. Consequently, the UV absorption became larger [183, 197]. These results demonstrate that $(PEI/PAA)_4(PEI/DNA)_1$ multilayer film has the potential to be used as DNA sensors.

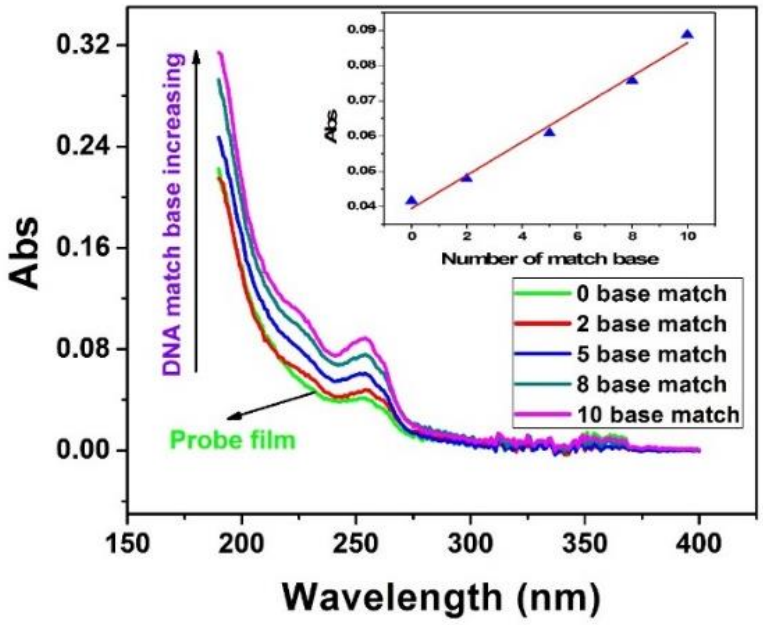


Figure 5.4 UV absorption of $(PEI/PAA)_4(PEI/DNA)_1$ multilayer film and after its hybridization with different types of target DNA single chain at 260nm.

The working principle of $(PEI/PAA)_4(PEI/DNA)_1$ multilayer sensing film for ssDNA detection is schematically shown in Fig. 5.5. With the number of match bases rising for target ssDNA, the force between the probe ssDNA chains and target ssDNA chains also becomes stronger. As a result, more target ssDNA chains could be tightly absorbed into sensing film. Thus,

the RI of the sensing film increases with denser and thicker sensing film. The RI change could be detected by TCFMI sensor for the latter is sensitive to RI change of surrounding environments.

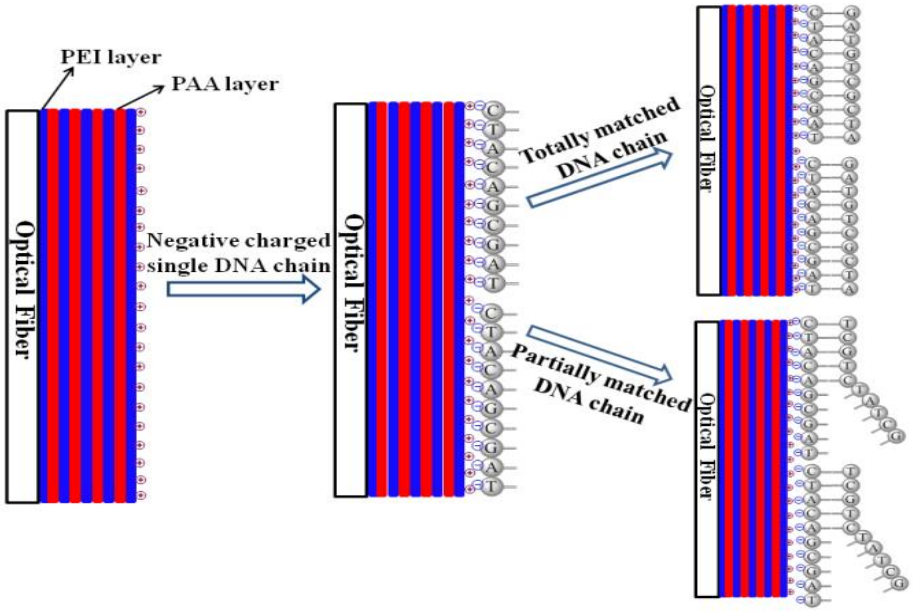


Figure 5.5 Principle of TCFMI DNA sensor: the force between two match bases accelerating ssDNA chains adsorbed onto $(PEI/PAA)_4(PEI/DNA)_1$ sensing film which will change the RI of sensing film.

## 5.3 TCFMI DNA Sensors Fabricated by LbL Self-assembly Technique

### 5.3.1 Fabrication of TCFMI DNA Sensors

The fabrication process of TCFMI sensor is as follows: a commercial 1.5-cm-long thin-core optical fiber section (Nufern 460-HP, core diameter of the fiber is 2.5 μm, and the cutoff wavelength is ~450 nm) is connected between two standard single-mode optical fibers by fusion splicing. And the principle

of the TCFMI sensor has been shown in Chapter 3. Before the DNA sensing nanocoatings fabrication, it is necessary to determine the number of PEI/PAA bilayers to achieve the better performance.

$(PEI/PAA)_n$ multilayer films were firstly deposited on TCFMI by LbL self-assembly technique, to investigate the optimum thickness for DNA sensor fabrication. Fig. 5.6 illustrates the spectra change of TCFMI with and without $(PEI/PAA)_n$ multilayer film. It can be seen that the wavelength shift becomes larger with the number of bilayer, which indicates that the RI of $(PEI/PAA)_n$ multilayer film increases. However, the interference peak firstly becomes deeper and then weaker. The phenomenon could be explained by RI changing of $(PEI/PAA)_n$ multilayer. The RI of the multilayer film increases with thickness growth, and eventually larger than $SiO_2$ [196]. As a result, the mode distribution and effective index of the cladding is changed, and the interference between the core and cladding modes is also altered. So, though more layers lead to more probe ssDNA chains deposition, the interference peak disappears gradually. Since more PEI will be contained in thicker sensing film, more ssDNA chains will be deposited which will lead to higher sensitivity. After a comprehensive comparison, the film with five bilayers is finally chosen for DNA sensor fabrication.

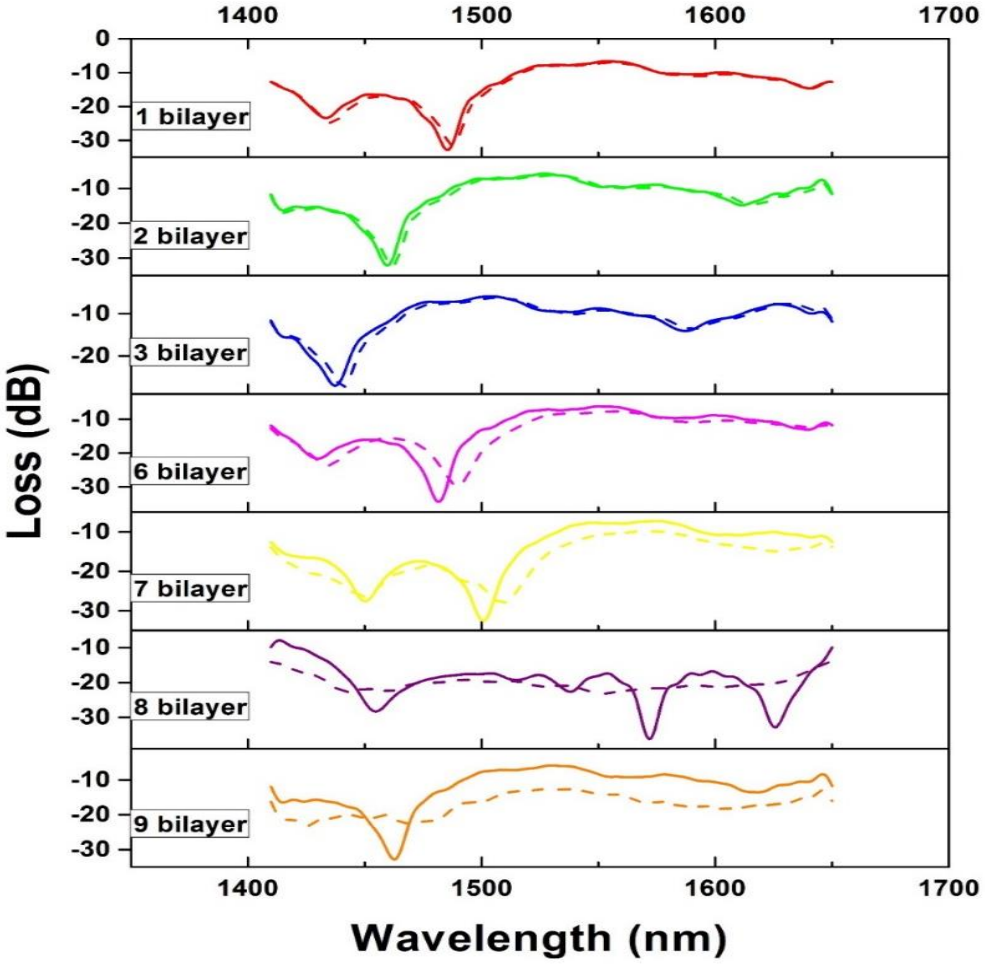


Figure 5.6 Transmission spectra of TCFMI before (solid line) and after (dashed line) the coating of $(PEI/PAA)_n$ multilayer film with different bilayer numbers (bilayer numbers increasing from the top to bottom).

The multilayer sensing film is coated on the surface of TCFMI to fabricate TCFMI DNA sensors. Transmission spectra of the TCFMI before and after $(PEI/PAA)_4(PEI/DNA)_1$ multilayer film coating are shown in Fig. 5.7. The absorption peak at 1592.4 nm shifts to 1596.6 nm after the multilayer film depositing on the TCFMI surface. The change is due to the RI of sensing film is larger than that of air. It indicates that

$(PEI/PAA)_4(PEI/DNA)_1$ multilayer film has been successfully coated on the TCFMI.

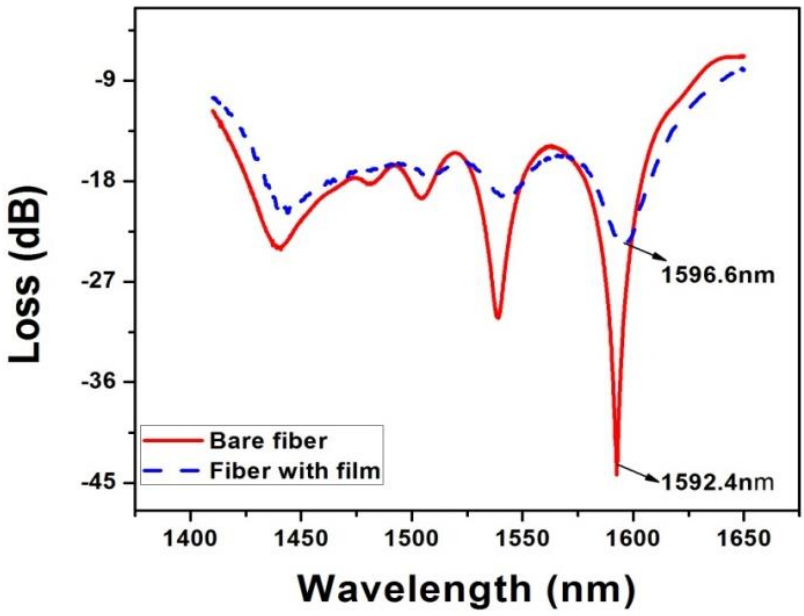


Figure 5.7 Transmission spectra change of TCFMI before (solid line) and after (dashed line) the deposition of $(PEI/PAA)_4(PEI/DNA)_1$ multilayer sensing film by LbL self-assembly technique.

### 5.3.2 Testing of TCFMI DNA Sensors

The setup used for the TCFMI DNA sensors' tests is shown in Fig. 5.8. The TCFMI DNA sensor was packaged in an aluminum groove and connected with OSA and BBS. 1 μM of different target ssDNA solutions were prepared and injected into the aluminium groove for the test.

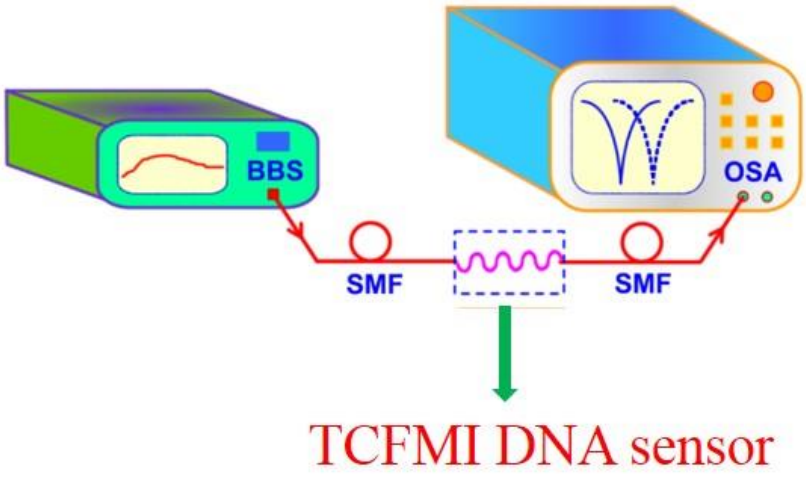


Figure 5.8 Setup for TCFMI DNA sensor test.

Fig. 5.9 shows the wavelength shift of TCFMI DNA sensors in different target ssDNA solutions. The sensor is tested continuously in each target ssDNA solutions for 1 h. It can be seen that the equilibrium time decreases with the number of match bases increasing. The results could be explained by the force change between probe ssDNA and different kinds of target ssDNA: when the number of target ssDNA match bases increases, the force between the probe ssDNA chains and target ssDNA chains becomes larger and larger [198]. As a result, the target ssDNA chains own more energy to hybridize with probe ssDNA chains, speeding up their mobility.

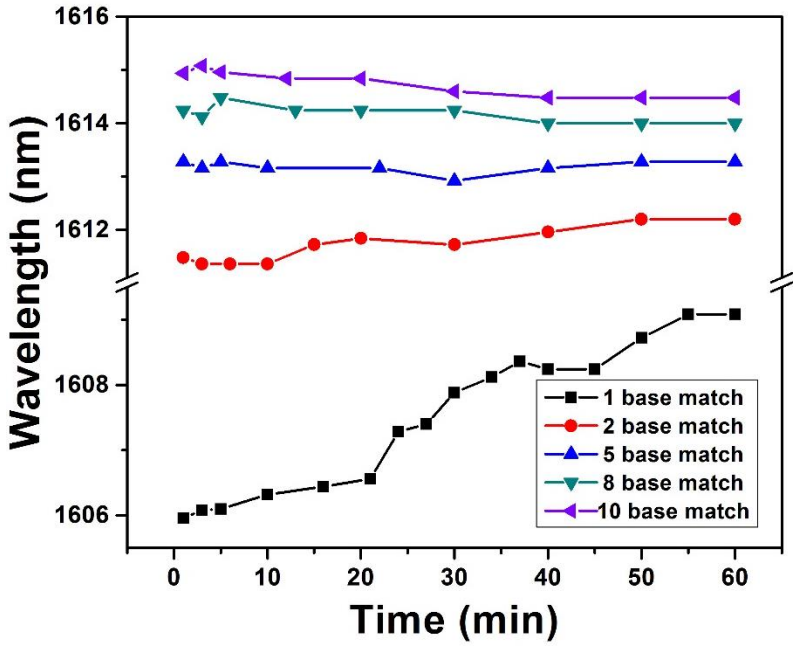


Figure 5.9 Time dependence of TCFMI-based DNA sensor in different types of target ssDNA solution.

Fig. 5.10 illustrates the wavelength change of DNA sensor in different target ssDNA solutions, which was recorded after reaching equilibrium. It can be seen the wavelength of TCFMI DNA sensor has nearly no change detecting target ssDNA solution with 1 match base, comparing with that in PBS solution. It means that the target ssDNA chain with 1 match base could not be adsorbed onto the surface of sensing film because of very weak force. With the match bases increasing (from 2 to 10), however, the spectra of DNA sensors shift linearly to longer wavelengths. As more target ssDNA chains have adsorbed on the sensing film, RI of sensing film increases, which lead to red shift of the wavelength. The inset of Fig. 5.10 gives the spectra evolution in different types of target ssDNA solutions.

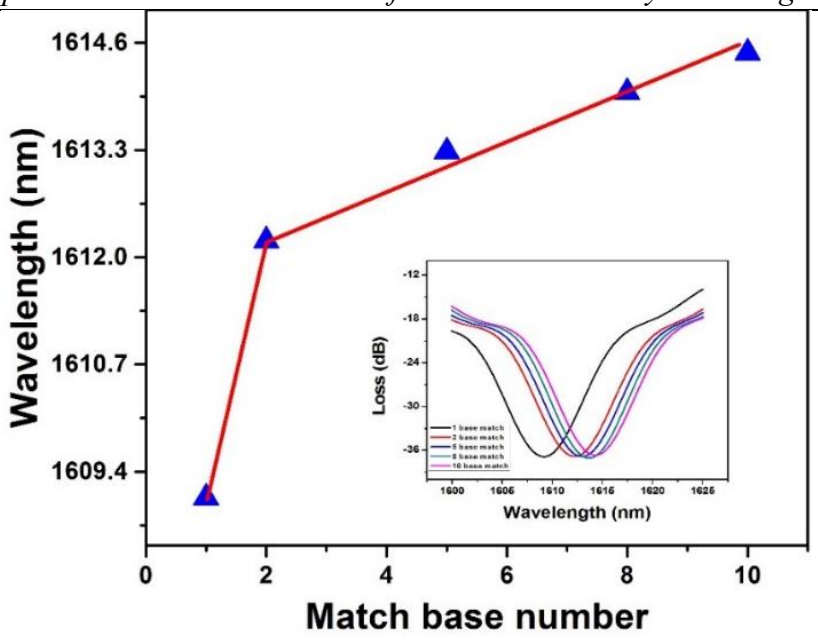


Figure 5.10 Wavelength shift of TCFMI based DNA sensor in detecting different types of target ssDNA. Inset gives spectra evolution the sensor in different target ssDNA solutions.

After hybridization with target ssDNA, the DNA sensor was immersed into PBS solution to remove excess target ssDNA chains. The wavelength of the TCFMI based DNA sensor was tested after extracting the PBS solution and drying. Fig. 5.11 shows that the wavelength of the TCFMI DNA sensor washed with PBS solution is 1595.64 nm. However, the wavelengths are still the same after hybridization with target ssDNA with 1 or 2 match bases. The reason is that their hybridization force is too weak to keep the hybridized target ssDNA attached on the surface. The results indicate that if 5 match bases ssDNA solution is tested after 2 match bases test, no influence on the results as 2 match bases ssDNA have been washed away. After hybridization with ssDNA with 5 match bases or more, however, the target ssDNA chains are strongly adsorbed onto the sensing film after

washing with PBS solution, which could have influence on the following tests. The wavelength shift is very small, which means they could also be washed away a little even the number of match base is larger for target ssDNA. All the results indicate that the sensor is suitable for DNA detection in solution environment, which meets the requirement of clinical tests.

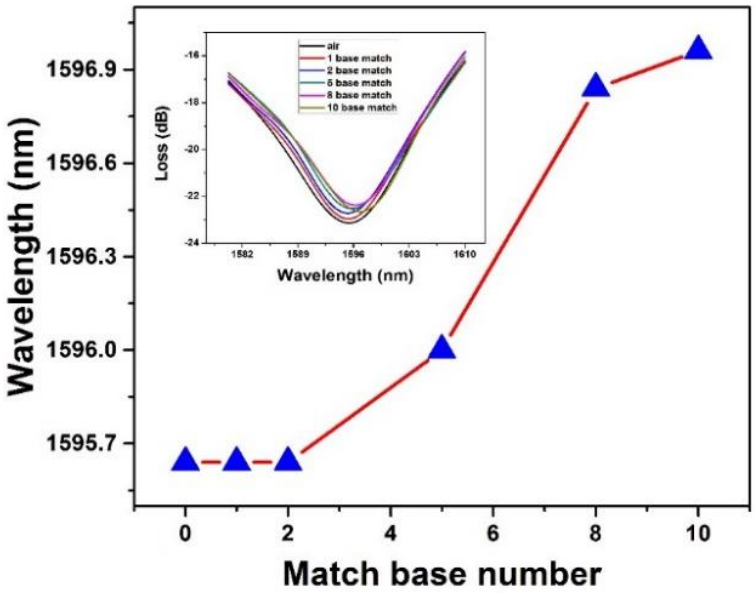


Figure 5.11 Wavelength shift of TCFMI based DNA sensor in detecting different types of target ssDNAs after washed with PBS solution and dry. The inset is corresponding spectra evolution the sensor.

As our test was conducted consecutively without washing between the two target ssDNA solutions test, the former tests may have influence on the later. To exclude the influence of previous accumulation, we have directly tested 8 and 10 match bases target ssDNA solutions respectively, using another two TCFMI DNA sensors (fabricated in the same condition). Fig.

5.12 shows the spectra change of TCFMI based DNA sensor after testing with target ssDNA solutions with match base number 8 and 10. It can be seen from the results that the change of wavelength is similar to the results in Fig. 5.10. Besides, we also fabricated another TCFMI based DNA sensors for directly detecting the target ssDNA with fully complementary bases. The results are shown in Fig. 5.13. The results also show a similar wavelength change value to the results in Fig. 5.10.

From the above results and discussions, we can conclude that the former tests of target ssDNA with fewer match bases have little influence on the latter tests, as the forces were very weak.

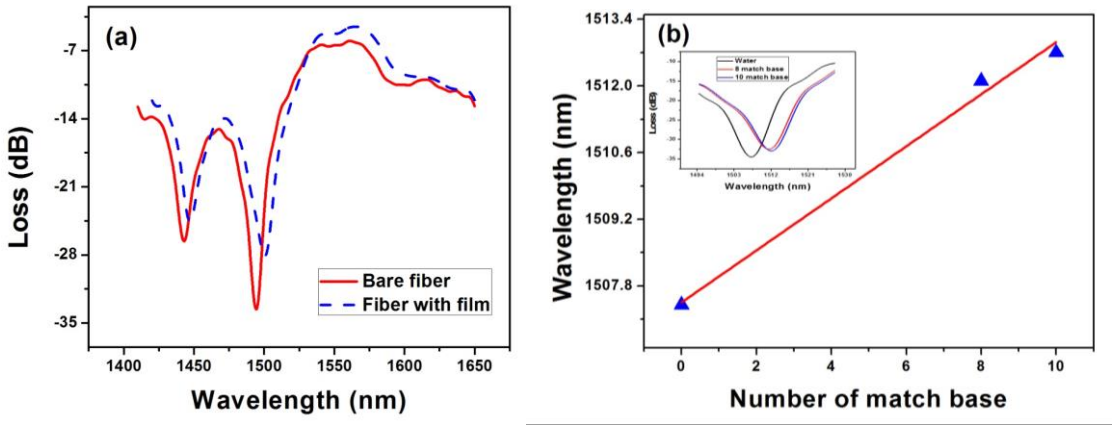


Figure 5.12 (a) Spectrum change of TCFMI before (solid line) and after (dashed line) the deposition of $(PEI/PAA)_4(PEI/DNA)_1$ multilayer film. (b) Wavelength shift of TCFMI based DNA sensor in target DNA solution with match base number 8 and 10.

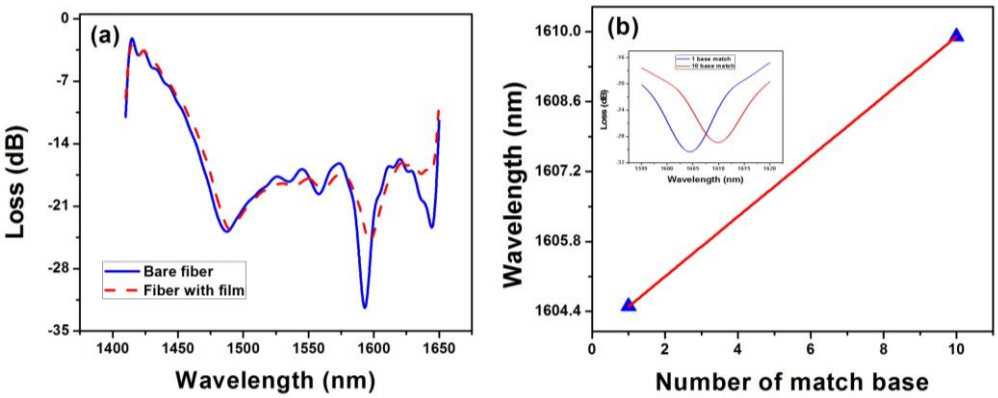


Figure 5.13 (a) Spectrum change of TCFMI before (solid line) and after (dashed line) the deposition of $(PEI/PAA)_4(PEI/DNA)_1$ multilayer film. (b) Wavelength shift of TCFMI based DNA sensor in target DNA solution with match base number 10.

The wavelength shift values in detection of different target ssDNA solutions are presented in Fig. 5.14. From the measured date, we can deduce that the sensitivity of the fabricated TCFMI DNA sensor is 0.27 nm/ match-base (the sensitivity is defined as the wavelength shift per match-base number). The sensitivity is higher than some other LPG-based fiber-optic DNA sensors [199]. Moreover, the TCFMI based DNA sensor is able to identify the number of mismatch bases in target ssDNA chains in very low concentration (only 1 μM), which is very useful in the clinical tests to find the origins of the new diseases.

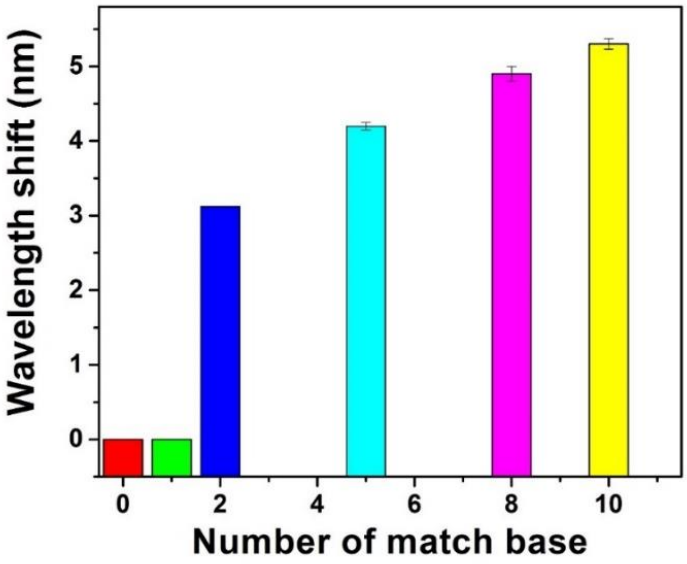


Figure 5.14 Performance of TCFMI based DNA sensors for different types of target ssDNA detection (The concentration of target ssDNA solution is 1μM, each data is tested three times and error bar is shown).

## 5.4 Summary

In summary, highly sensitive and disposable TCFMI based DNA sensors have been prepared by coating multilayer sensing film on the fiber, adopting LbL self-assembly technique. The TCFMI DNA sensors have been tested with different kinds of target ssDNA solutions. The results show that the sensor could not detect target ssDNA with 1 match base. But a linearly growth of signal with the base numbers could be achieved when the match base numbers are larger than one. And the sensitivity is 0.27 nm/ match-base. Fabrication of the TCFIM based sensor is simple and low-cost, so it would be a good candidate for real application in biological fields.

## *Chapter 6*

# Optical Fiber Sensor Integrated Biochips for Ultrasensitive Glucose Detection

A miniature biomedical device for highly sensitive and rapid detection of glucose (GO) is a very appealing technology for both healthcare and clinical diagnosis. In this paper, we present an optical fiber sensor integrated microfluidic biochip for ultrasensitive GO detection. A long-period grating (LPG) is inscribed in a small-diameter single-mode fiber (SDSMF) as an optical refractive-index (RI) sensor. With the layer-by-layer (LbL) self-assembly technique, poly (ethylenimine) (PEI) and poly (acrylic acid) (PAA) multilayer film is deposited on the surface of the SDSMF-LPG sensor as the supporting film, and then a negatively charged glucose oxidase (GOD) layer is immobilized on the outer layer for GO sensing. A GO biochip is fabricated after integrating the SDSMF-LPG GO sensor into a microfluidic chip. Experimental results show that the SDSMF-LPG GO sensor can detect GO concentration as low as 1 nM. After integration into the microfluidic chip, the biosensor's detection range is extended from 2 μM to 10 μM, and the response time is shortened from 6 minutes to 70 seconds.

## 6.1 Introduction

Diabetes mellitus has become a worldwide health problem and it often induces numerous diseases, such as heart disease, kidney failure, or blindness [93]. Two well-known main causes of the disease are insulin deficiency and hyperglycemia in human body. Both of the two parameters can be reflected by blood glucose (GO) concentrations [94]. Therefore, it is much demanded to develop biomedical diagnostic devices for highly sensitive and rapid detection of GO content in the blood.

The GO sensor was firstly demonstrated by using electrochemical glucose enzyme electrodes in 1962 [95]. Thereafter, many efforts have been devoted to exploring novel GOD immobilization techniques, electrode materials and matrix for GOD [93]. For instance, the conductive polypyrrole encapsulated by pHEMA hydrogel was adopted as matrix for GOD, and then deposited on Pt electrode for GO detection [200]. Later, GOD-graphene-chitosan nanocomposite was demonstrated as active component and glassy carbon was used as electrode for GO sensor fabrication [201]. However, the electron transfer between GOD and electrode is not efficient. To solve the problem, Luong et al. [202] suggested using nanoporous $TiO_2$ as matrix for GOD adsorption. It was deposited on FePc modified CNT electrodes to monitor GO concentration. However, those GO sensors are usually too bulky and costly for daily use and their sample consumption is relatively high.

One of promising solutions to these problems is to use microfluidic chips due to its advantages of compactness, low-sample consumption, and low cost [203, 204]. Moreover, microfluidic chip technology offers a platform to integrate sensors with functional components (e.g. microfluidic mixers) to achieve the lab-on-a-chip analysis system [205]. Recently, it was demonstrated electrochemical GO biosensors can be integrated into microfluidic chips to develop easy-handle, low-cost and portable biochips [206-209]. However, electroactive interference problems often appear in electrochemical sensors because some endogenous reducing species (e.g. ascorbic and uric acids) and drugs (e.g., acetaminophen) are electroactive [93].

This limitation can be overcome by using optical fiber sensor technology due to its well-known immunity to electromagnetic interferences. Moreover, some unique features of fiber-optic sensors, such as small size, high sensitivity and multiplexed detection capability, render them ideal candidates to be integrated within microfluidic chip to develop high-performance biochips. For instance, Lyu et al. [210] integrated a fiber-optic particle plasmon resonance biosensor into microfluidic chip for anti-biotin detection. Dong et al. [211] proposed an integrated fiber-optic microfluidic device for muscular force monitoring.

In our study, an optical fiber sensor self-assembled with $(PEI/PAA)_9(PEI/GOD)_1$ multilayer film is fabricated and integrated into a microfluidic chip to develop a biochip, as shown in Fig. 6.1, for GO detection. A fiber-optic refractive-index (RI) sensor based on a cladding mode dependent resonant device, i.e. long-period grating (LPG), is used to monitor the reaction between the sensing film and surrounding medium. Although LPG sensors were proposed for detection of pH value, DNA, antibody and so on [38, 212, 213], the LPG technology was firstly, to the best of our knowledge, demonstrated to detect GO concentration. Furthermore, the LPG GO sensor will be integrated into a microfluidic chip for fast low-sample-consumption bioanalysis. Experimental results reveal that the performances of the biosensor, in terms of both detection range and response time, have been greatly improved after integrated into the microfluidic chip.

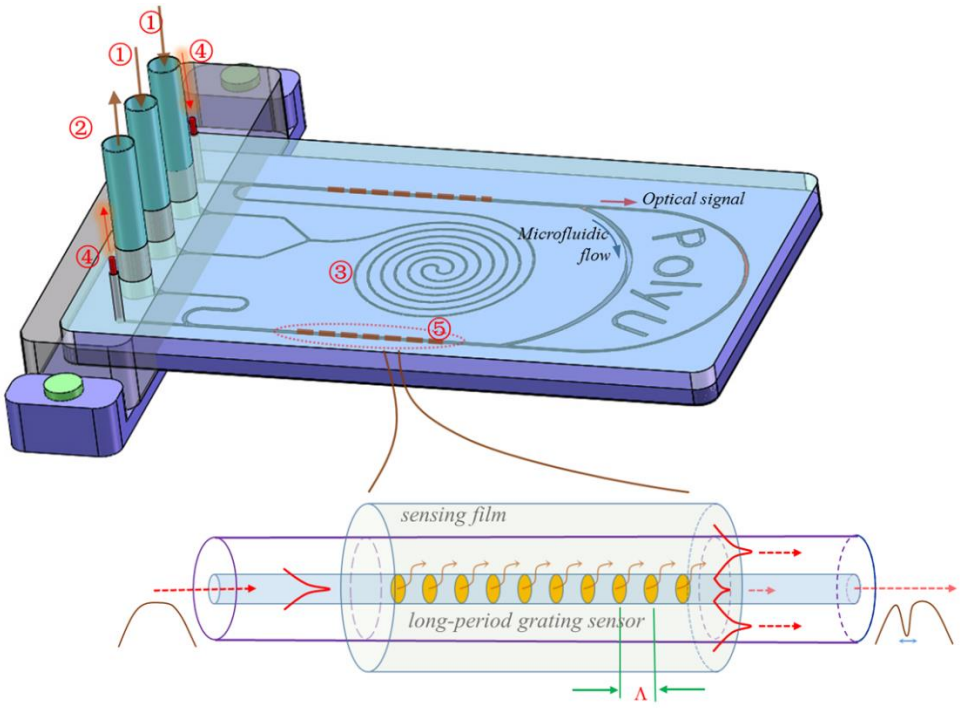


Figure 6.1 Schematic design of the optical fiber sensor integrated microfluidic chip for GO detection: two inlets ① for GO concentration control; one outlet ② to outgo the waste solution; a spiral mixture ③ to homogeneously mix the GO solutions; small diameter single-mode optical fiber ④ and the embedded LPG GO sensor ⑤. The bottom shows a resonant scattering of light in the LPG GO sensor.

## 6.2 Fabrication of Optical Fiber GO Sensor

### 6.2.1 Fabrication of LPG RI Sensor

The LPG used in the experiment were inscribed in a small-diameter single mode fibers (80 μm in diameter, Yangtze Optical Fibre and Cable Joint Stock Limited Company). The fiber was hydrogen loaded at a pressure of 1500psi at room temperature for a week to increase the fiber photosensitivity. A point-to-point technique was used for preparing LPGs by means of ArF/KrF pulsed

Excimer laser (Braggstar-500 Tuilaser, Germany) operating at a wavelength of 248nm.

When an optical fiber was inscribed with an LPG structure, a resonant mode coupling between the guided core mode and a forward-propagating cladding mode can be excited at the wavelength [65]:

$$\lambda = [n_{eff}(\lambda) - n_{clad}^{i}(\lambda)]\Lambda \qquad (1)$$

where $n_{eff}(\lambda)$ is the effective RI of the core mode at the wavelength of $\lambda$, $n_{clad}^{i}(\lambda)$ is the RI of the $i$ th cladding mode and $\Lambda$ is the period of the LPG. It can be seen from Eqn. (1) that the resonant wavelength $\lambda$ is determined by $n_{clad}^{i}(\lambda)$ which depends on the evanescent field of the cladding mode. Therefore, LPG is a versatile technology for label-free RI sensing.

In the experiments, 2-cm length LPGs with the period of 390 μm were inscribed in the SDSMF. The measured transmission spectrum of SDSMF-LPG is shown in Fig. 6.2a. The resonant peak corresponding to the 5$^{th}$ order cladding mode at the wavelength of about 1510 nm is chosen for sensing as this wavelength is at the optical fiber communication window [65, 214].

A number of RI solutions ($CaCl_2$ aqueous solution with different concentration) were used to measure the responses of the SDSMF-LPG sensor to RI changes. The measured results are shown in Fig. 6.2b. It can be seen the central wavelength of the spectrum dip decreased linearly with the increment of RI and its RI sensitivity is about 205 nm/RIU. It is noteworthy

that its RI sensitivity is higher than LPGs fabricated in standard SMF with the diameter of 125 μm [214-216], which means SDSMF-LPG has higher potential to develop high-performance fiber-optic biosensors for e.g. on-chip integration.

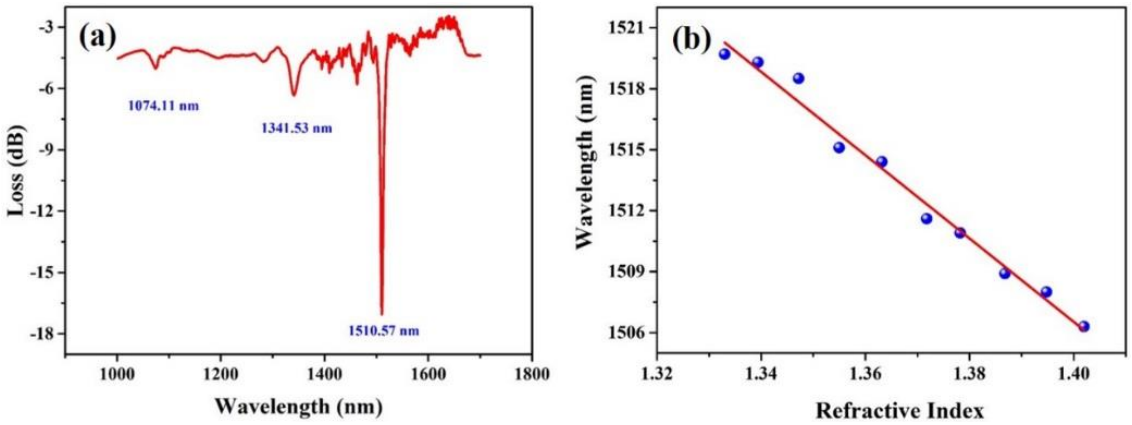


Figure 6.2 Measured transmission spectrum of SDSMF-LPG (a) and its response to the RI change of surrounding medium (b).

### 6.2.2 Preparation of GO Sensing Nanocoating

The concentrations of both positively charged PEI and negatively charged PAA were diluted to 2.0 g/L, with the pH of 11.0 and 3.0, respectively. The concentration of negatively charged GOD was 50 mg/L at pH 7.0. The LbL electrostatic self-assembly of PEI, PAA, and GOD was carried out on silicon wafers (10×10 $mm^2$) for testing and characterization and then applied on SDSMF LPGs, respectively. The substrates were cleaned with piranha solution (7:3 of 98% $H_2SO_4$ and 30% $H_2O_2$), washed with large volumes of

DI water and dried with nitrogen to get negatively charged surface. The negatively charged substrates were then dipped into the positively charged PEI and negatively charged PAA solutions alternatively, each for 10 minutes at room temperature. The substrates were rinsed with DI water for 1 minute in between the immersions in polycation and polyanion solutions to remove the excess adsorbed components, and dried with nitrogen. The process was repeated until desired numbers of bilayers were fabricated (one bilayer consists of one PEI layer and one PAA layer and is expressed as $(PEI/PAA)_1$). The substrates were then dipped into a negatively charged GOD solution for 60 minutes, and immersed in DI water for 3 minutes, and dried with nitrogen again.

The morphologies of the multilayer films were characterized by atomic force microscopy (AFM). Fig. 6.3 (a)–(c) show the AFM surface images of $(PEI/PAA)_9$, $(PEI/PAA)_9PEI$ and $(PEI/PAA)_9(PEI/GOD)_1$ multilayer films, respectively. For the $(PEI/PAA)_9$ multilayer film (Fig. 6.3 a), the surface is very rough, obvious bumps and holes can be seen. And the measured root mean square (RMS) is 22.4 nm. The RMS reduced to be 0.18 nm after the adsorption of PEI layer (Fig. 6.3 b). It means the PEI layer fully covers the bumps and holes on the PAA layer. When the sensing layer, negatively charged GOD, is deposited on the surface of PEI layer, RMS becomes to be 6.73 nm (Fig. 6.3 c). It provides an obvious evidence that GOD is

successfully deposited and can be used for GO sensor fabrication.

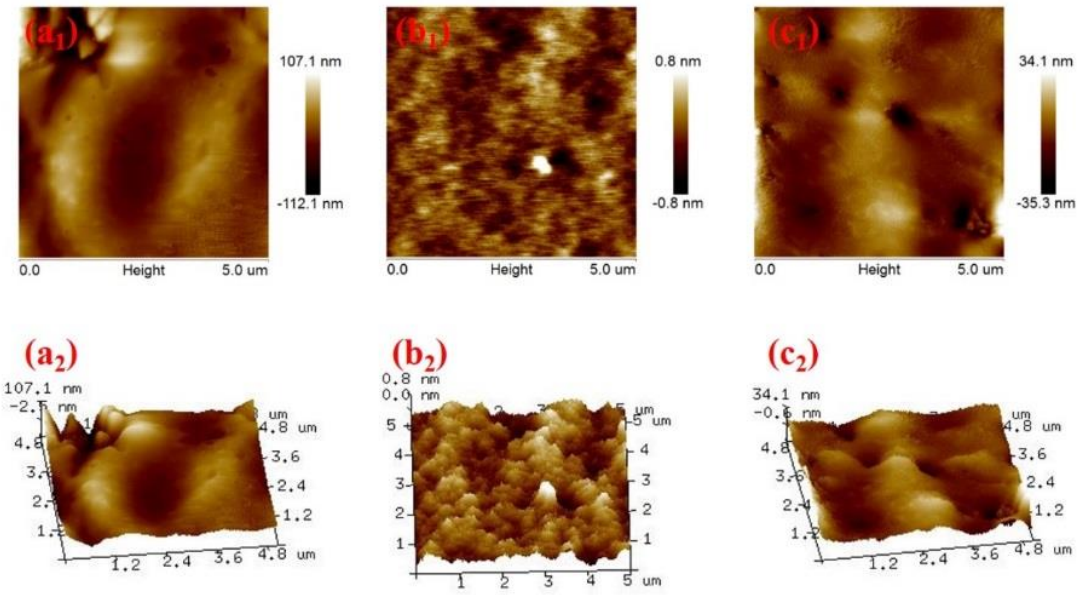


Figure 6.3 AFM images of $(PEI/PAA)_9$ (a), $(PEI/PAA)_9PEI$ (b) and $(PEI/PAA)_9(PEI/GOD)_1$ (c) multilayer films: the top images are the surface morphologies and the bottom images are their 3D presentations.

The $(PEI/PAA)_9(PEI/GOD)_1$ multilayer film was measured by using a surface profilometer. It can be seen from Fig. 6.4 that the $(PEI/PAA)_n$ layers display an exponential growth in thickness [153, 194]. On the other hand, the active GOD layer is very thin (about 22 nm) due to the low concentration of GOD used in the film preparation. The thin active GOD layer is useful for the solution fast diffusing into, to achieve fast response.

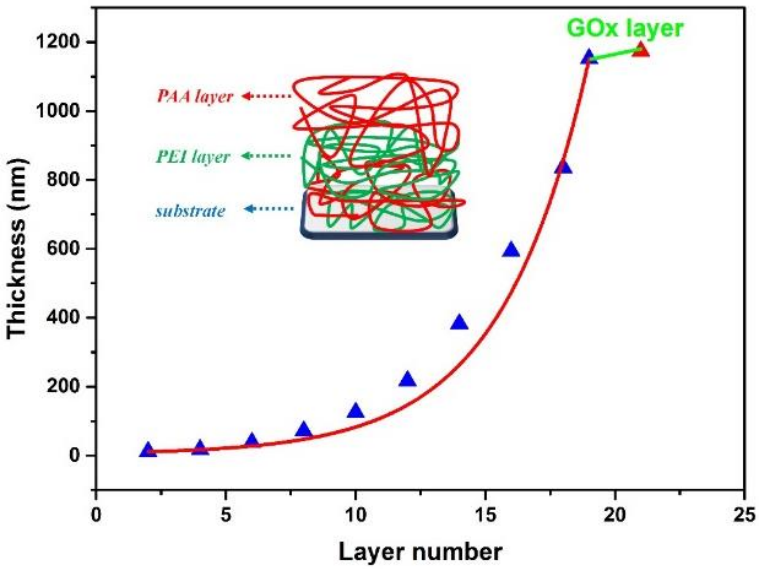


Figure 6.4 Thickness growth of the $(PEI/PAA)_9(PEI/GOD)_1$ multilayer film. The inset shows the growth scheme of the multilayer film.

### 6.2.3 Testing of SDSMF-LPG GO sensors

$(PEI/PAA)_n(PEI/GOD)_1$ multilayers with different number of layers were prepared on the surface of SDSMF-LPG and tested by using a broadband light source and an optical spectra analyzer (OSA). Fig. 6.5a and Fig. 6.5b show the measured transmission spectra of the two SDSMF-LPGs before and after $(PEI/PAA)_9(PEI/GOD)_1$ and $(PEI/PAA)_{19}(PEI/GOD)_1$ multilayer film, respectively. It can be seen that both spectral dips appear blue shift after deposition of sensing films. The result agrees with the data shown in Fig. 2b that the higher RI of multilayer sensing film induces a blue shift of spectral dip. It indicates that the multilayer sensing films have been successfully deposited on the surface of SDSMF-LPG [169].

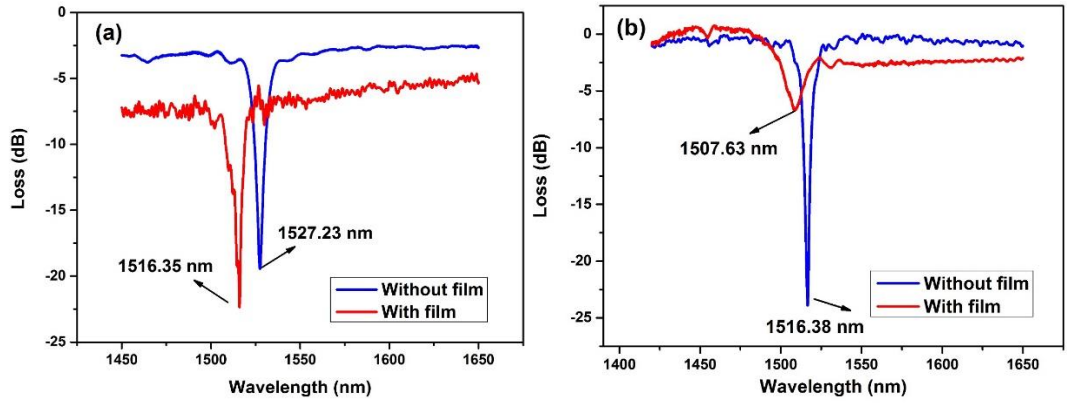


Figure 6.5 Transmission spectra of the SDSMF-LPG before and after $(PEI/PAA)_9(PEI/GOD)_1$ multilayer sensing film (a) and $(PEI/PAA)_{19}(PEI/GOD)_1$ multilayer sensing film deposition.

The sensing mechanism of the GO sensor is shown in Fig. 6.6a. When the GO is oxidized with the GOD catalyst, gluconic acid will be produced and then changes the pH of mixture solution [79]. Since the swelling degree of the $(PEI/AA)_n$ multilayer sensing film depends on the pH of surrounding medium, the sensing film will thus swell with GO concentration increasing and the induced RI change leads to a spectra shift of the SDSMF-LPG sensor [154].

The fabricated SDSMF-LPG sensors were tested in GO solutions with different concentrations. Fig. 6.6b shows the response of the SDSMF-LPG sensor (with $(PEI/PAA)_9(PEI/GOD)_1$ multilayer film) to different GO concentrations. It can be seen that the resonant wavelength shifts to longer values when the concentration of GO increases. It is because the reaction product (i.e. gluconic acid) decreases the pH of solution. As a result, more $-COO^-$ groups are pronated to –COOH in the PAA layer and more positive

charges appear on the PEI chains. Consequently, the complexation between PEI and PAA becomes weaker and the swelling degree of PEI/PAA multilayer film increases. Therefore, the RI of the sensing film will decrease, which thus induces a red shift of the spectral dip of the sensor [138]. The spectral dip stops red shift when the GO concentration increases to 2 μM. It is mainly because that the pH no longer changes after reacting for a specific period of time.

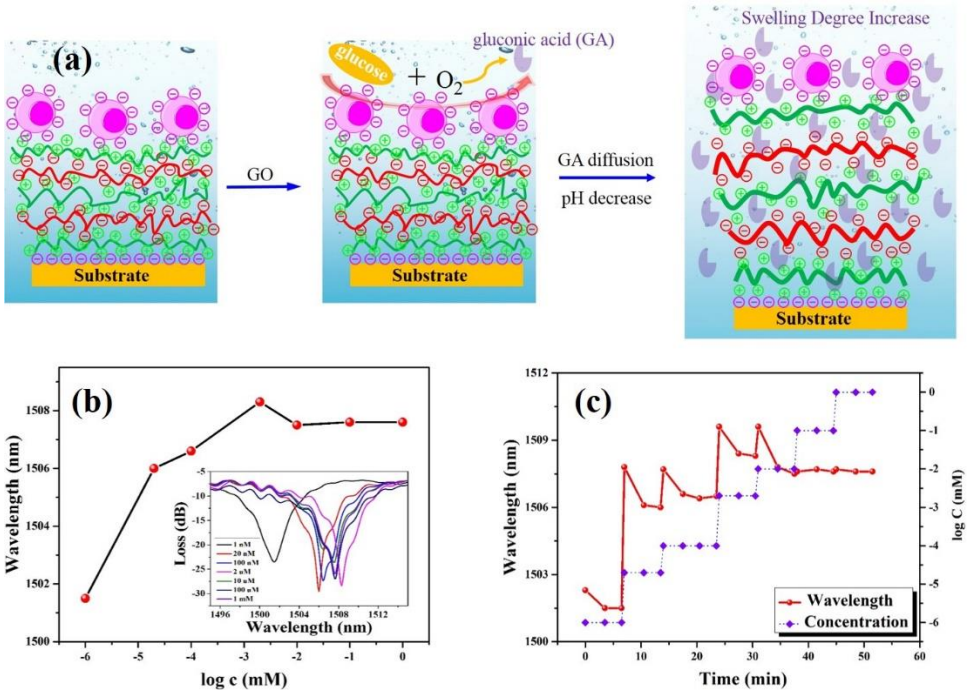


Figure 6.6 (a) Working principle of the GO sensing film; (b) the measured response of the LPG GO sensor to different GO concentrations. The inset shows the measured transmission spectra; (c) the measured dynamic response of the GO sensor.

The dynamic response of the LPG GO sensor is shown in Fig. 6.6c. One can see that the response time of biosensor is around 6 min. Moreover, the detection limit of the sensor is 1 nM. It can also be seen that the wavelength

shifts about 5 nm when the GO concentration changing from 1 nM to 20 nM. As the resolution of OSA is 0.02 nm, it reveals the fabricated LPG sensor can resolve the GO concentration change as low as 1 nM.

The test results of the GO sensor with thicker sensing film, i.e. $(PEI/PAA)_{19}(PEI/GOD)_1$ multilayer film are presented in Fig. 6.7. One can see that the detection range of such a GO sensor was extended to 10 μM while the sensitivity decreased a little. It is because more PEI and PAA chains are contained in the thicker sensing film, and thus offer more sites to react with $H^+$. Consequently, more GO can be consumed for gluconic acid production, which improves the detection range. Meanwhile, the higher content of PAA in the sensing film eases the reduction of complexation sites, which will decelerate the RI decrease. As a result, the sensitivity of the sensor becomes lower.

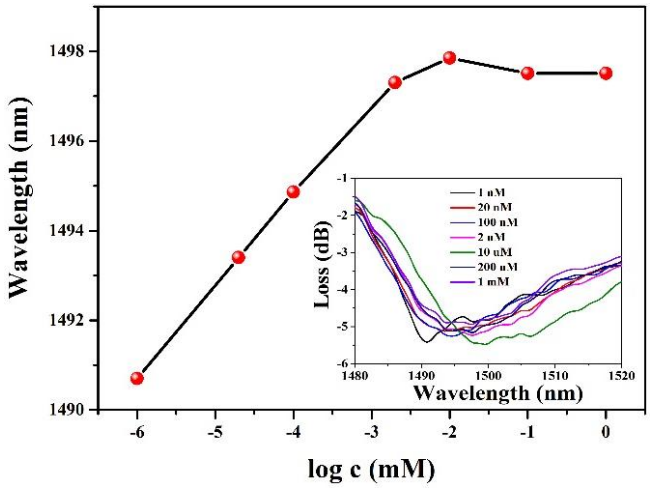


Figure 6.7 Measured response of the LPG GO sensor to different GO concentrations. The inset shows the measured transmission spectra.

## 6.3 Fiber-Optic GO Sensor and Biochip Fabrication

### 6.3.1 Fabrication of Microfluidic GO Biochip

SU-8 was dissolved into cyclopentanone with the concentration of 70 wt%. 0.5 wt% TBA and 2 wt% OPPI were added into solution under stirring and fully dissolved. The solutions were firstly spin-coated on the surface of pretreat silicon wafer (2×2 $cm^2$) at a speed of 1000 rpm. Then the substrate was soft baked at 65 and 95 $^oC$ for 10 and 30 min, respectively. The designed microfluidic chip was converted into a series of image data and then loaded onto a digital micromirror device based maskless lithography system for generation of optical patterns. UV light source (365 nm) was used for optically patterning the SU-8 photoresist. After exposure, the substrate was post baked at 65 and 95 $^oC$ for 1 and 10 min, respectively, to selectively crosslink the exposed portions of the film. The master of designed biochip was then fabricated after the development process.

The PDMS microfluidic chip was fabricated by using molding and thermally crosslinking method. A 10:1 mixture of PDMS and crosslinker was used for the chip fabrication. The mixture was degassed in a vacuum chamber for 30 minute. Thereafter, the PDMS mixture was poured onto the SU-8 master and cured upon the mold in an oven at 75 $^oC$ for 1 hour. The PDMS slice with microfluidic channels were then peeled off from the mold

and three holes were drilled by using the puncher. Then, we directly placed the SDSMF-LPG GO sensor into the microfluidic channel with little pre-stress. Finally, the microfluidic chip was sealed on a glass slide after treating with oxygen plasma for 3 minutes.

The SDSMF-LPG GO sensor with $(PEI/PAA)_9(PEI/GOD)_1$ multilayer film was integrated into the microchannel of a PDMS chip for microfluidic GO sensing. As shown in Fig. 6.1, two fiber-optic GO sensors can be integrated into the chip for dual-parameter microfluidic sensing. A spiral microfluidic mixer is employed to mix the solutions homogeneously before passing through the two LPG sensors. It was reported that such a pre-mixing process can dramatically improve the performance of sensors [127, 217].

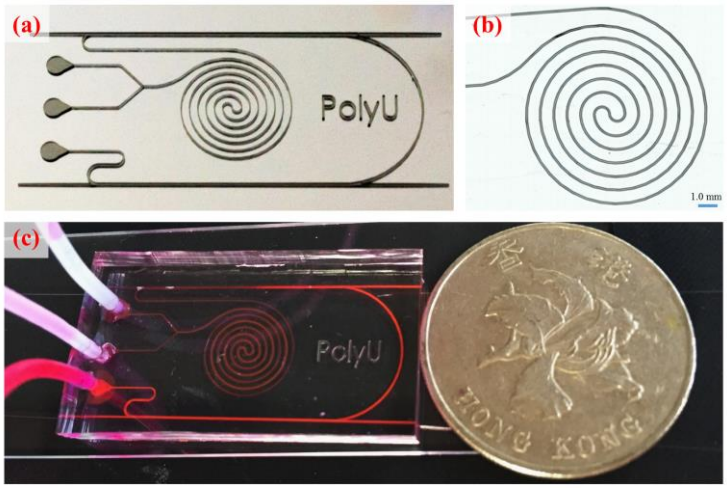


Figure 6.8 Photos of the SU-8 master mold for biochip fabrication (a) and its mixture part (b); the photo of real biochip fabricated by casting PDMS on the SU-8 mold and sealed with glass slide by $O_2$ plasma (c).

Fig. 6.8a shows a photo (taken by using a camera) of the SU-8 master

of the biochip fabricated on the silicon substrate. An enlarge image (taken by laser scanning confocal microscope) of the spiral mixer is given in Fig. 6.8b. The width and depth of the microchannel are about 110 and 260 μm, respectively (a detailed profile and size information are presented in Fig. 6.9). It can be seen that the spiral microstructure is very uniform and its surface is pretty smooth. With the SU-8 master, a PDMS microfluidic chip was fabricated by using the molding method. The SDSMF-LPG GO sensor was embedded into the chip before bonding the PDMS microfluidic chip on the glass substrate. Fig. 6.8c shows the fabricated PDMS microfluidic chip integrated with the LPG GO sensor. The size of the biochip is small, which can thus save solution consumption greatly.

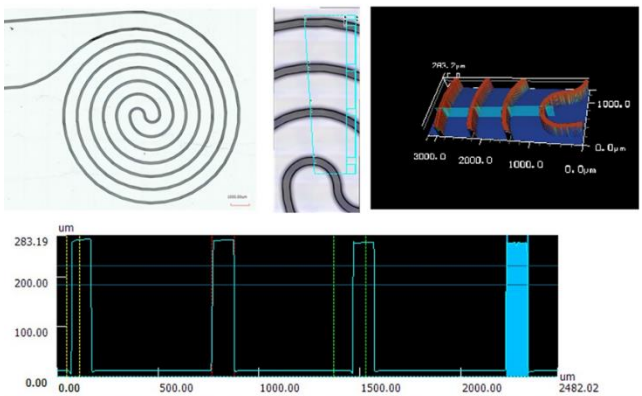


| Profile1 | Horz. dist. | Hght. diff. | Hght. ave. | Angle | C.S. length | C.S. area |
|---|---|---|---|---|---|---|
| All | 2482.02um | 0.51um | 55.73um | 0.01° | 4550.72um | 138388.33um2 |
| Seg.1 | 63.56um | 263.11um | 164.17um | 76.42° | 327.88um | 10704.71um2 |
| Seg.2 | 110.39um | 206.28um | 263.06um | 61.85° | 358.05um | 29197.30um2 |
| Seg.3 | 160.56um | 256.28um | 108.03um | 57.93° | 425.33um | 17386.08um2 |
| Seg.4 | 103.70um | 37.74um | 265.64um | 20.00° | 238.68um | 28009.59um2 |

Figure 6.9 Images and profile parameters of the mixer part of SU-8 master mold for the microfluidic chip.

### 6.3.2 Testing of Biochip

The response of the biochip was tested by injecting GO solution at the flow rate of 5 μL/min. Fig. 6.10a shows the spectral response of the biochip to different GO concentrations. Their corresponding transmission spectra are given in the inset. The sensitivity of the biochip is very close to that of the LPG GO sensor measured in the open air, whereas the detection range extended from 2 μM to 10 μM. The dynamic response of the biochip is shown in Fig. 6.10b. One can see that the biochip can distinctly sense tiny GO concentration as low as 1 nM. Meanwhile, the response time of the biochip was dramatically shortened from 6 minutes to 70 seconds. It can be explained that the dramatic reduction of the GO volume used in the test can give rise to a fast reaction between GO and GOD layer. Therefore, the sensing film can also achieve a quick equilibrium of swelling/deswelling according to the induced pH change of the solution. Such an ultrasensitive, fast-response, and low-sample-consumption GO detection device can not only greatly release the pain of patient but also solve coagulation problem [218], and thus is very promising for practical clinical diagnosis.

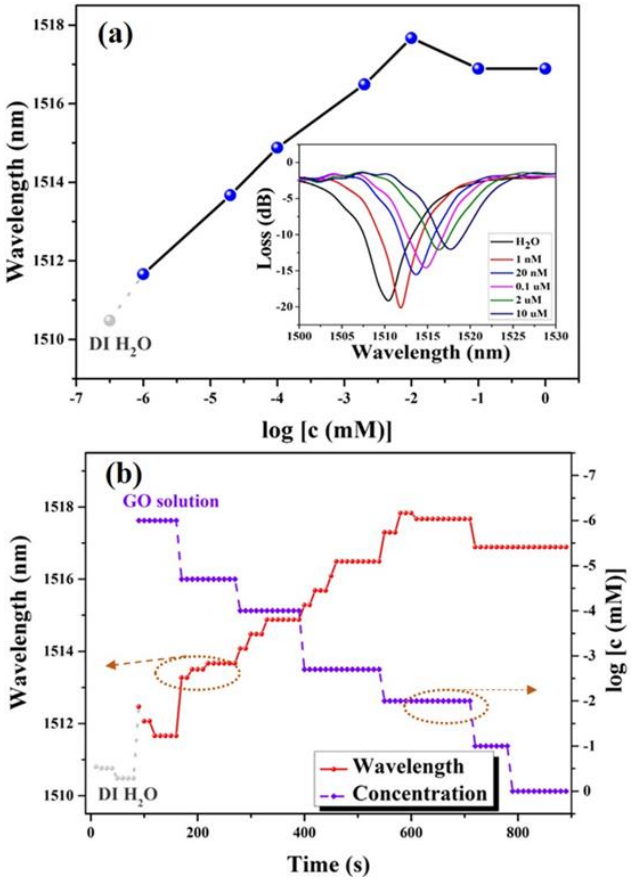


Figure 6.10 (a) Response of the microfluidic biochip to different GO concentrations. The inset shows the measured transmission spectra; (b) the measured dynamic response of the GO biochip.

## 6.4 Summary

A highly sensitive GO biochip based on a specialty optical fiber LPG sensor (fabricated in a small-diameter single-mode fiber) has been demonstrated. A layer-by-layer self-assembly technique has been successfully applied to prepare PEI/PAA multilayers on the surface of the LPG sensor. The negatively charged GOD layer was then immobilized on the multilayer film (with the positively charged PEI as outmost layer) for GO sensing. The

SDSMF-LPG GO biosensor with $(PEI/PAA)_9(PEI/GOD)_1$ multilayer sensing film has been fabricated and embedded into a PDMS microfluidic chip for GO detection. Experimental results have revealed that such a low-sample-consumption microfluidic biochip has not only an ultra-low detection limit (1 nM) but also a remarkably fast response time (70 s). It is believed that such an optical fiber sensor integrated microfluidic biochip has great potential for both healthcare and clinical diagnosis.

*Chapter 7*

# Conclusions and Future Outlook

## 7.1 Conclusion

In conclusion, we suggested a thin-core fiber modal interferometer fiber (TCFMI) as the transducer for high-performance fiber-optic pH sensors fabrication as it is sensitive to refractive index (RI) change of surrounding environments. The PEC film, which consisted of a thin layer of surface macropores followed by a thick layer of three-dimensionally interconnected nanopores (50 ~ 100 nm), was robust and stable in water and common organic solvents. The nanostructured PEC film was coated on the surface of TCFMI for fiber-optic pH sensors fabrication by self-assembly method. The sensor is capable of breaking the common "trade-off" rule in sensor applications, showing a superior pH sensing performance with a fast response rate ($t_r$ = 5 s, $t_f$ = 12 s) and high sensitivity (2.04 nm/pH unit, -2.48 nm/pH unit). And we also compared the nanoporous PEC film sensor with non-porous PEC film sensor, the results show that their sensitivities are similar, but the former gives very fast response due to the nanoporous property of the sensing film. So the nanoporous PEC film pH sensor has greatly potential for application in biological fields.

Furthermore, a novel type of pH sensor was proposed. Long-period

grating (LPG) pH sensor was rapidly fabricated by rapid and maskless 3D printing technique. pH sensitive PAA ion hydrogels were periodically printed to encapsulate tapered fiber for LPG pH sensors fabrication. The pH sensors show very high sensitivity of 7.5 nm/pH with a response time of 70 s. As the first 3D printed, LPG pH sensor, it has great potential for in vivo test as PAA biocompatible properties.

In addition, the TCFMI fiber was adopted for DNA sensor fabrication for ultralow DNA hybridization detection. The DNA sensors prepared by layer-by-layer (LbL) self-assembly polyelectrolyte multilayer film and probe ssDNA on the surface of TCFMI. The TCFMI DNA sensors have been tested in different types of target ssDNA solutions with concentration as low as 1 μM. It has been demonstrated that the sensor cannot absorb the target ssDNA with 1 match base. But the target ssDNA with more match bases can be absorbed onto the sensor's surface. And it can be detected due to RI increase after the adsorption. The response of the TCFMI based DNA sensor to target ssDNA with more than one match base is linearly proportion to the number of match bases. And the sensitivity was 0.27 nm/ match-base. So the sensor could identify the number of match bases of target ssDNA. Fabrication of the TCFIM based sensor is simple, low-cost with the small size of the sensor, it will be a good candidate for real application in biological fields.

Finally, a highly sensitive GO biochip based on a specialty optical

fiber LPG sensor (fabricated in a small-diameter single-mode fiber) has been demonstrated. A layer-by-layer self-assembly technique has been successfully applied to prepare PEI/PAA multilayers on the surface of the LPG sensor. The negatively charged GOD layer was then immobilized on the multilayer film (with the positively charged PEI as outmost layer) for GO sensing. The SDSMF-LPG GO biosensor with $(PEI/PAA)_9(PEI/GOD)_1$ multilayer sensing film has been fabricated and embedded into a PDMS microfluidic chip for GO detection. Experimental results have revealed that such a low-sample-consumption microfluidic biochip has not only an ultra-low detection limit (1 nM) but also a remarkably fast response time (70 s). It is believed that such an optical fiber sensor integrated microfluidic biochip has great potential for both healthcare and clinical diagnosis.

## 7.2 Future Outlook

As mentioned before, many kinds of fiber-optic sensors are based on the principle of RI change sensing of the fibers, such as TCFMI and LPG. Thus, by coating different kinds of sensing films, these optical fibers can achieve different kinds of parameters detection, including gas, ions, pH, humidity, dopamine, DNA, antigen, glucose and other biological species. Among them, stimulus responsive hydrogels are good candidate for fiber-optic sensors fabrication for biological applications, as they are biocompatible and similar

to the native extracellular matrix. By choosing the suitable hydrogel materials, novel kinds of fiber-optic sensors can be achieved, which will extend the detection species of fiber-optic sensors.

Similarly, 3D printing LPG sensors provides a platform for novel kinds of fiber-optic sensors preparation. The sensing property of the fiber-optic sensors depends on the photopolymerized materials, a wide range of responsive materials that can be polymerized by light can be adopted for LPG sensor fabrication without further surface modification. In addition, the sensors type can also be enlarged by modifying the surface of photopolymerized polymers, which have the ability to influence the swelling properties by detecting the analytes. So many works can be done in this field in the future.

Furthermore, the miniaturization of fiber-optic sensors device is an interesting subject, which can provide lab-on-a-chip tests and greatly reduce quantity of analytes consumption. Though the integration of fiber-optic sensors into microfluidic channels have been done in some reports, the biochips are still larger as the limitation of fiber sizes. Therefore, future work can be developed towards exploring novel kinds of optical fibers to minimize the size of the biochips. In addition, fiber-optic based biochips are still at their early stage, different kinds of fiber-optic sensors can be integrated into the microfluidic channels to detect more analytes.

# References

[1] Deutsche Agenda Optische Technologien für das 21. Jahrhundert

[2] J. Haus, Optical Sensors: Basics and Applications, Wiley, 2010.

[3] P.R. Ohodnicki, J.P. Baltrus, T.D. Brown, Pd/$SiO_2$ and AuPd/$SiO_2$ nanocomposite-based optical fiber sensors for $H_2$ sensing applications, *Sensors and Actuators B-Chemical,* **2015,** 214, 159-168.

[4] F. Long, C. Gao, H.C. Shi, M. He, A.N. Zhu, A.M. Klibanov, A.Z. Gu, Reusable evanescent wave DNA biosensor for rapid, highly sensitive, and selective detection of mercury ions, *Biosensors and Bioelectronics,* **2011,** 26, 4018-4023.

[5] M. Yin, B. Gu, J. Qian, A.P. Zhang, Q. An, S. He, Highly sensitive and selective fiber-optic modal interferometric sensor for detecting trace mercury ion in aqueous solution, *Analytical Methods,* **2012,** 4, 1292-1297.

[6] J.M. Corres, I.R. Matias, I. del Villar, F.J. Arregui, Design of pH Sensors in Long-Period Fiber Gratings Using Polymeric Nanocoatings, *Sensors Journal, IEEE,* **2007,** 7, 455-463.

[7] Z.L. Gui, J.W. Qian, M.J. Yin, Q.F. An, B.B. Gu, A. Zhang, A novel fast response fiber-optic pH sensor based on nanoporous self-assembled multilayer films, *Journal of Materials Chemistry,* **2010,** 20,

7754-7760.

[8] S.K. Mishra, B.D. Gupta, Surface plasmon resonance based fiber optic pH sensor utilizing Ag/ITO/Al/hydrogel layers, *Analyst,* **2013,** 138, 2640-2646.

[9] S.R. Ankireddy, J. Kim, Fabrication of Optical Fiber pH Sensor Based on Near-Infrared (NIR) Quantum Dots, *Science of Advanced Materials,* **2014,** 6, 2562-2565.

[10] J.M. Corres, I. del Villar, I.R. Matias, F.J. Arregui, Two-Layer Nanocoatings in Long-Period Fiber Gratings for Improved Sensitivity of Humidity Sensors, *Nanotechnology, IEEE Transactions on,* **2008,** 7, 394-400.

[11] L.H. Chen, T. Li, C.C. Chan, R. Menon, P. Balamurali, M. Shaillender, B. Neu, X.M. Ang, P. Zu, W.C. Wong, K.C. Leong, Chitosan based fiber-optic Fabry–Perot humidity sensor, *Sensors and Actuators B: Chemical,* **2012,** 169, 167-172.

[12] L. Xia, L. Li, W. Li, T. Kou, D. Liu, Novel optical fiber humidity sensor based on a no-core fiber structure, *Sensors and Actuators A: Physical,* **2013,** 190, 1-5.

[13] M.R.R. Khan, S.-W. Kang, A High Sensitivity and Wide Dynamic Range Fiber-Optic Sensor for Low-Concentration VOC Gas Detection, *Sensors,* **2014,** 14, 23321-23336.

[14] X. Wang, K.L. Cooper, A. Wang, J. Xu, Z. Wang, Y. Zhang, Z. Tu, Label-free DNA sequence detection using oligonucleotide functionalized optical fiber, *Applied Physics Letters,* **2006,** 89, 163901.

[15] A. Leung, P.M. Shankar, R. Mutharasan, Label-free detection of DNA hybridization using gold-coated tapered fiber optic biosensors (TFOBS) in a flow cell at 1310 nm and 1550 nm, *Sensors and Actuators B: Chemical,* **2008,** 131, 640-645.

[16] D. Sun, T. Guo, Y. Ran, Y. Huang, B.-O. Guan, In-situ DNA hybridization detection with a reflective microfiber grating biosensor, *Biosensors and Bioelectronics,* **2014,** 61, 541-546.

[17] S. Tierney, B.M.H. Falch, D.R. Hjelme, B.T. Stokke, Determination of Glucose Levels Using a Functionalized Hydrogel−Optical Fiber Biosensor: Toward Continuous Monitoring of Blood Glucose in Vivo, *Analytical Chemistry,* **2009,** 81, 3630-3636.

[18] X. Zhang, Y. Guan, Y. Zhang, Ultrathin Hydrogel Films for Rapid Optical Biosensing, *Biomacromolecules,* **2012,** 13, 92-97.

[19] E. Eltzov, R.S. Marks, S. Voost, B.A. Wullings, M.B. Heringa, Flow-through real time bacterial biosensor for toxic compounds in water, *Sensors and Actuators B: Chemical,* **2009,** 142, 11-18.

[20] G. Thouand, H. Horry, M.J. Durand, P. Picart, L. Bendriaa, P. Daniel, M.S. DuBow, Development of a biosensor for on-line

detection of tributyltin with a recombinant bioluminescent Escherichia coli strain, *Appl Microbiol Biotechnol,* **2003,** 62, 218-225.

[21] T. Fine, P. Leskinen, T. Isobe, H. Shiraishi, M. Morita, R.S. Marks, M. Virta, Luminescent yeast cells entrapped in hydrogels for estrogenic endocrine disrupting chemical biodetection, *Biosensors and Bioelectronics,* **2006,** 21, 2263-2269.

[22] F.B. Myers, L.P. Lee, Innovations in optical microfluidic technologies for point-of-care diagnostics, *Lab on a Chip,* **2008,** 8, 2015-2031.

[23] B. Kuswandi, Nuriman, J. Huskens, W. Verboom, Optical sensing systems for microfluidic devices: A review, *Analytica Chimica Acta,* **2007,** 601, 141-155.

[24] B. Gu, M.-J. Yin, A.P. Zhang, J.-W. Qian, S. He, Low-cost high-performance fiber-optic pH sensor based on thin-core fiber modal interferometer, *Opt. Express,* **2009,** 17, 22296-22302.

[25] M. Yin, B. Gu, Q. Zhao, J. Qian, A. Zhang, Q. An, S. He, Highly sensitive and fast responsive fiber-optic modal interferometric pH sensor based on polyelectrolyte complex and polyelectrolyte self-assembled nanocoating, *Anal Bioanal Chem,* **2011,** 399, 3623-3631.

[26] L. Yang, W. Liwei, Z. Min, T. Dongsheng, M. Xianhui, L. Yanbiao, Long-Period Grating Relative Humidity Sensor With Hydrogel Coating, *Photonics Technology Letters, IEEE,* **2007,** 19,

880-882.

[27] M. Yinping, L. Bo, Z. Hao, Y. Li, Z. Haibin, S. Hua, Z. Weihua, Z. Qida, Relative Humidity Sensor Based on Tilted Fiber Bragg Grating With Polyvinyl Alcohol Coating, *Photonics Technology Letters, IEEE,* **2009,** 21, 441-443.

[28] A. Leung, P.M. Shankar, R. Mutharasan, Real-time monitoring of bovine serum albumin at femtogram/mL levels on antibody-immobilized tapered fibers, *Sensors and Actuators B: Chemical,* **2007,** 123, 888-895.

[29] W.C. Wong, C.C. Chan, L.H. Chen, T. Li, K.X. Lee, K.C. Leong, Polyvinyl alcohol coated photonic crystal optical fiber sensor for humidity measurement, *Sensors and Actuators B: Chemical,* **2012,** 174, 563-569.

[30] L.V. Nguyen, S.C. Warren-Smith, A. Cooper, T.M. Monro, Molecular beacons immobilized within suspended core optical fiber for specific DNA detection, *Opt. Express,* **2012,** 20, 29378-29385.

[31] O.S. Wolfbeis, Fiber optic chemical sensors and biosensors, *Analytical Chemistry,* **2000,** 72, 81R-89R.

[32] O.S. Wolfbeis, Fiber-optic chemical sensors and biosensors, *Analytical Chemistry,* **2002,** 74, 2663-2677.

[33] O.S. Wolfbeis, Fiber-optic chemical sensors and biosensors,

*Analytical Chemistry,* **2004,** 76, 3269-3283.

[34] O.S. Wolfbeis, Fiber-optic chemical sensors and biosensors, *Analytical Chemistry,* **2006,** 78, 3859-3873.

[35] O.S. Wolfbels, Fiber-optic chemical sensors and biosensors, *Analytical Chemistry,* **2008,** 80, 4269-4283.

[36] X.D. Wang, O.S. Wolfbeis, Fiber-Optic Chemical Sensors and Biosensors (2008-2012), *Analytical Chemistry,* **2013,** 85, 487-508.

[37] W.J. Stephen, P.T. Ralph, Fibre optic sensors with nano-structured coatings, *Journal of Optics A: Pure and Applied Optics,* **2006,** 8, S430.

[38] M.J. Yin, Q.F. An, J.W. Qian, A.P. Zhang, Preparation and Application of Fiber-Optic Sensors Based on Layer-by-Layer Self-Assembly Multilayers, *Prog. Chem.,* **2011,** 23, 2568-2575.

[39] X.L. Li, G.Y. Zhang, X.D. Bai, X.M. Sun, X.R. Wang, E. Wang, H.J. Dai, Highly conducting graphene sheets and Langmuir-Blodgett films, *Nature Nanotechnology,* **2008,** 3, 538-542.

[40] Z.P. Chen, W.C. Ren, L.B. Gao, B.L. Liu, S.F. Pei, H.M. Cheng, Three-dimensional flexible and conductive interconnected graphene networks grown by chemical vapour deposition, *Nature Materials,* **2011,** 10, 424-428.

[41] S.M. George, Atomic Layer Deposition: An Overview, *Chemical Reviews,* **2010,** 110, 111-131.

[42] G. Decher, Fuzzy nanoassemblies: Toward layered polymeric multicomposites, *Science,* **1997,** 277, 1232-1237.

[43] G. Decher, J.D. Hong, J. Schmitt, Buildup of ultrathin multilayer films by a self-assembly process: III. Consecutively alternating adsorption of anionic and cationic polyelectrolytes on charged surfaces, *Thin Solid Films,* **1992,** 210–211, Part 2, 831-835.

[44] R.R. Costa, J.F. Mano, Polyelectrolyte multilayered assemblies in biomedical technologies, *Chemical Society Reviews,* **2014,** 43, 3453-3479.

[45] J.J. Richardson, M. Björnmalm, F. Caruso, Technology-driven layer-by-layer assembly of nanofilms, *Science,* **2015,** 348.

[46] X. Zhang, H. Chen, H. Zhang, Layer-by-layer assembly: from conventional to unconventional methods, *Chemical Communications,* **2007,** 1395-1405.

[47] K. Ariga, J.P. Hill, Q. Ji, Layer-by-layer assembly as a versatile bottom-up nanofabrication technique for exploratory research and realistic application, *Physical Chemistry Chemical Physics,* **2007,** 9, 2319-2340.

[48] P.T. Hammond, Form and Function in Multilayer Assembly: New Applications at the Nanoscale, *Advanced Materials,* **2004,** 16, 1271-1293.

[49] M.N. Hyder, S.W. Lee, F.C. Cebeci, D.J. Schmidt, Y. Shao-Horn, P.T. Hammond, Layer-by-Layer Assembled Polyaniline Nanofiber/Multiwall Carbon Nanotube Thin Film Electrodes for High-Power and High-Energy Storage Applications, *Acs Nano,* **2011,** 5, 8552-8561.

[50] S.W. Lee, N. Yabuuchi, B.M. Gallant, S. Chen, B.-S. Kim, P.T. Hammond, Y. Shao-Horn, High-power lithium batteries from functionalized carbon-nanotube electrodes, *Nat Nano,* **2010,** 5, 531-537.

[51] X. Ou, L. Jiang, P. Chen, M. Zhu, W. Hu, M. Liu, J. Zhu, H. Ju, Highly Stable Graphene-Based Multilayer Films Immobilized via Covalent Bonds and Their Applications in Organic Field-Effect Transistors, *Advanced Functional Materials,* **2013,** 23, 2422-2435.

[52] G. Zotti, B. Vercelli, A. Berlin, T. Virgili, Multilayers of CdSe Nanocrystals and Bis(dithiocarbamate) Linkers Displaying Record Photoconduction, *The Journal of Physical Chemistry C,* **2012,** 116, 25689-25693.

[53] X. Wang, F. Liu, X. Zheng, J. Sun, Water-Enabled Self-Healing of Polyelectrolyte Multilayer Coatings, *Angewandte Chemie International Edition,* **2011,** 50, 11378-11381.

[54] U. Manna, A.H. Broderick, D.M. Lynn, Chemical Patterning and

Physical Refinement of Reactive Superhydrophobic Surfaces, *Advanced Materials,* **2012,** 24, 4291-4295.

[55] C.J. Ochs, G.K. Such, F. Caruso, Modular Assembly of Layer-by-Layer Capsules with Tailored Degradation Profiles, *Langmuir,* **2011,** 27, 1275-1280.

[56] G.K. Such, J.F. Quinn, A. Quinn, E. Tjipto, F. Caruso, Assembly of Ultrathin Polymer Multilayer Films by Click Chemistry, *Journal of the American Chemical Society,* **2006,** 128, 9318-9319.

[57] W. Xu, I. Choi, F.A. Plamper, C.V. Synatschke, A.H.E. Müller, V.V. Tsukruk, Nondestructive Light-Initiated Tuning of Layer-by-Layer Microcapsule Permeability, *ACS Nano,* **2013,** 7, 598-613.

[58] J. Barthes, D. Mertz, C. Bach, M.-H. Metz-Boutigue, B. Senger, J.-C. Voegel, P. Schaaf, P. Lavalle, Stretch-Induced Biodegradation of Polyelectrolyte Multilayer Films for Drug Release, *Langmuir,* **2012,** 28, 13550-13554.

[59] Z. Zhou, A.C. Anselmo, S. Mitragotri, Synthesis of Protein-Based, Rod-Shaped Particles from Spherical Templates using Layer-by-Layer Assembly, *Advanced Materials,* **2013,** 25, 2723-2727.

[60] C.A. Holmes, M. Tabrizian, Substrate-Mediated Gene Delivery from Glycol-Chitosan/Hyaluronic Acid Polyelectrolyte Multilayer Films, *ACS Applied Materials & Interfaces,* **2013,** 5, 524-531.

[61] F. Cuomo, F. Lopez, A. Ceglie, L. Maiuro, M.G. Miguel, B. Lindman, pH-responsive liposome-templated polyelectrolyte nanocapsules, *Soft Matter,* **2012,** 8, 4415-4420.

[62] M. Bosch, A. Sánchez, F. Rojas, C. Ojeda, Recent Development in Optical Fiber Biosensors, *Sensors,* **2007,** 7, 797-859.

[63] G. Orellana, D. Haigh, New Trends in Fiber-Optic Chemical and Biological Sensors, *Current Analytical Chemistry,* **2008,** 4, 273-295.

[64] A. Leung, P.M. Shankar, R. Mutharasan, A review of fiber-optic biosensors, *Sensors and Actuators B: Chemical,* **2007,** 125, 688-703.

[65] W.J. Stephen, P.T. Ralph, Optical fibre long-period grating sensors: characteristics and application, *Meas. Sci. Technol.,* **2003,** 14, R49.

[66] L. Alwis, T. Sun, K.T.V. Grattan, Fibre optic long period grating-based humidity sensor probe using a Michelson interferometric arrangement, *Sensors and Actuators B: Chemical,* **2013,** 178, 694-699.

[67] S. Zhu, F. Pang, S. Huang, F. Zou, Y. Dong, T. Wang, High sensitivity refractive index sensor based on adiabatic tapered optical fiber deposited with nanofilm by ALD, *Opt. Express,* **2015,** 23, 13880-13888.

[68] R. Zengling, R. Yunjiang, Z. Jian, L. Zhiwei, X. Bing, A Miniature Fiber-Optic Refractive-Index Sensor Based on Laser-Machined Fabry–Perot Interferometer Tip, *Lightwave*

*Technology, Journal of,* **2009,** 27, 5426-5429.

[69] J. Cao, M.H. Tu, T. Sun, K.T.V. Grattan, Wavelength-based localized surface plasmon resonance optical fiber biosensor, *Sensors and Actuators B: Chemical,* **2013,** 181, 611-619.

[70] D.A. Jackson, Recent progress in monomode fibre-optic sensors, *Measurement Science and Technology,* **1994,** 5, 621.

[71] Anon, Investigating the surface chemistry of Mars, *Analytical Chemistry,* **1995,** 67, 605A-610A.

[72] B. Sepúlveda, P.C. Angelomé, L.M. Lechuga, L.M. Liz-Marzán, LSPR-based nanobiosensors, *Nano Today,* **2009,** 4, 244-251.

[73] C.M.C.P. Gouvêa (2011) *Biosensors for health applications*.

[74] K. Urmann, J.-G. Walter, T. Scheper, E. Segal, Label-Free Optical Biosensors Based on Aptamer-Functionalized Porous Silicon Scaffolds, *Analytical Chemistry,* **2015,** 87, 1999-2006.

[75] Q. Cui, W. Wang, B. Gu, L. Liang, A Combined Physical–Chemical Polymerization Process for Fabrication of Nanoparticle–Hydrogel Sensing Materials, *Macromolecules,* **2012,** 45, 8382-8386.

[76] C. Zhang, D. Gao, G. Zhou, L. Chen, X.-a. Zhang, Z. Cui, Z. He, Label-Free Homogeneous Immunosensor Based on FRET for the Detection of Virus Antibody in Serum, *Chemistry – An Asian Journal,* **2012,** 7, 1764-1767.

[77] Y. Zhao, X. Zhao, B. Tang, W. Xu, J. Li, J. Hu, Z. Gu, Quantum-Dot-Tagged Bioresponsive Hydrogel Suspension Array for Multiplex Label-Free DNA Detection, *Advanced Functional Materials,* **2010,** 20, 976-982.

[78] L. Römhildt, C. Pahlke, F. Zörgiebel, H.-G. Braun, J. Opitz, L. Baraban, G. Cuniberti, Patterned Biochemical Functionalization Improves Aptamer-Based Detection of Unlabeled Thrombin in a Sandwich Assay, *ACS Applied Materials & Interfaces,* **2013,** 5, 12029-12035.

[79] I. Tokarev, I. Tokareva, V. Gopishetty, E. Katz, S. Minko, Specific Biochemical-to-Optical Signal Transduction by Responsive Thin Hydrogel Films Loaded with Noble Metal Nanoparticles, *Adv. Mater.,* **2010,** 22, 1412-1416.

[80] O. Korostynska, K. Arshak, E. Gill, A. Arshak, Review paper: Materials and techniques for in vivo pH monitoring, *Ieee Sensors Journal,* **2008,** 8, 20-28.

[81] S.-H. Lee, J. Kumar, S.K. Tripathy, Thin Film Optical Sensors Employing Polyelectrolyte Assembly, *Langmuir,* **2000,** 16, 10482-10489.

[82] G. Miesenbock, D.A. De Angelis, J.E. Rothman, Visualizing secretion and synaptic transmission with pH-sensitive green

fluorescent proteins, *Nature,* **1998,** 394, 192-195.

[83] G. Beltrán-Pérez, F. López-Huerta, S. Muñoz-Aguirre, J. Castillo-Mixcóatl, R. Palomino-Merino, R. Lozada-Morales, O. Portillo-Moreno, Fabrication and characterization of an optical fiber pH sensor using sol–gel deposited $TiO_2$ film doped with organic dyes, *Sensors and Actuators B: Chemical,* **2006,** 120, 74-78.

[84] S. Dong, M. Luo, G. Peng, W. Cheng, Broad range pH sensor based on sol–gel entrapped indicators on fibre optic, *Sensors and Actuators B: Chemical,* **2008,** 129, 94-98.

[85] C. Maule, H. Gonçalves, C. Mendonça, P. Sampaio, J.C.G. Esteves da Silva, P. Jorge, Wavelength encoded analytical imaging and fiber optic sensing with pH sensitive CdTe quantum dots, *Talanta,* **2010,** 80, 1932-1938.

[86] I. Oehme, O.S. Wolfbeis, Optical sensors for determination of heavy metal ions, *Mikrochimica Acta,* **1997,** 126, 177-192.

[87] G. Aragay, J. Pons, A. Merkoçi, Recent Trends in Macro-, Micro-, and Nanomaterial-Based Tools and Strategies for Heavy-Metal Detection, *Chemical Reviews,* **2011,** 111, 3433-3458.

[88] X. Liu, Y. Tang, L. Wang, J. Zhang, S. Song, C. Fan, S. Wang, Optical Detection of Mercury(II) in Aqueous Solutions by Using Conjugated Polymers and Label-Free Oligonucleotides,

*Advanced Materials,* **2007,** 19, 1471-1474.

[89] J. Ueberfeld, N. Parthasarathy, H. Zbinden, N. Gisin, J. Buffle, Coupling Fiber Optics to a Permeation Liquid Membrane for Heavy Metal Sensor Development, *Analytical Chemistry,* **2002,** 74, 664-670.

[90] T.-W. Sung, Y.-L. Lo, Highly sensitive and selective sensor based on silica-coated CdSe/ZnS nanoparticles for Cu2+ ion detection, *Sensors and Actuators B: Chemical,* **2012,** 165, 119-125.

[91] B. Gu, M.-J. Yin, A.P. Zhang, J.-W. Qian, S. He, Fiber-optic metal ion sensor based on thin-core fiber modal interferometer with nanocoating self-assembled via hydrogen bonding, *Sens. Actuators, B,* **2011,** 160, 1174-1179.

[92] E.-H. Yoo, S.-Y. Lee, Glucose Biosensors: An Overview of Use in Clinical Practice, *SENSORS-BASEL,* **2010,** 10, 4558-4576.

[93] J. Wang, Electrochemical glucose biosensors, *Chem. Rev.,* **2008,** 108, 814-825.

[94] S.K. Vashist, D. Zheng, K. Al-Rubeaan, J.H.T. Luong, F.-S. Sheu, Technology behind commercial devices for blood glucose monitoring in diabetes management: A review, *Anal. Chim. Acta,* **2011,** 703, 124-136.

[95] L.C. Clark, C. Lyons, Electrode systems for continuous monitoring in cardiovascular surgery, *Ann. N.Y. Acad. Sci.,* **1962,** 102, 29-45.

[96] J.H. Holtz, S.A. Asher, Polymerized colloidal crystal hydrogel films as intelligent chemical sensing materials, *Nature,* **1997,** 389, 829-832.

[97] J.M. Corres, A. Sanz, F.J. Arregui, I.R. Matías, J. Roca, Fiber optic glucose sensor based on bionanofilms, *Sensors and Actuators B: Chemical,* **2008,** 131, 633-639.

[98] T. Saxl, F. Khan, M. Ferla, D. Birch, J. Pickup, A fluorescence lifetime-based fibre-optic glucose sensor using glucose/galactose-binding protein, *Analyst,* **2011,** 136, 968-972.

[99] J. Wang, Electrochemical biosensors: Towards point-of-care cancer diagnostics, *Biosensors and Bioelectronics,* **2006,** 21, 1887-1892.

[100] B.S. Gaylord, A.J. Heeger, G.C. Bazan, DNA Hybridization Detection with Water-Soluble Conjugated Polymers and Chromophore-Labeled Single-Stranded DNA, *Journal of the American Chemical Society,* **2003,** 125, 896-900.

[101] X. Wang, U.J. Krull, Synthesis and fluorescence studies of thiazole orange tethered onto oligonucleotide: development of a self-contained DNA biosensor on a fiber optic surface, *Bioorganic & Medicinal Chemistry Letters,* **2005,** 15, 1725-1729.

[102] S.-y. Niu, S.-j. Wang, C. Shi, S.-s. Zhang, Studies on the Fluorescence Fiber-Optic DNA Biosensor Using p-Hydroxyphenylimidazo[f]1,10-phenanthroline Ferrum(III) as

Indicator, *J Fluoresc,* **2008,** 18, 227-235.

[103] S.-y. Niu, Q.-y. Li, R. Ren, S.-s. Zhang, Enzyme-enhanced fluorescence detection of DNA on etched optical fibers, *Biosensors and Bioelectronics,* **2009,** 24, 2943-2946.

[104] P.C.A. Jerónimo, A.N. Araújo, M. Conceição B.S.M. Montenegro, Optical sensors and biosensors based on sol–gel films, *Talanta,* **2007,** 72, 13-27.

[105] S. Wu, W. Cheng, Y. Qiu, Z. Li, S. Shuang, C. Dong, Fiber optic pH sensor based on mode-filtered light detection, *Sensors and Actuators B: Chemical,* **2010,** 144, 255-259.

[106] W. Li, H. Cheng, M. Xia, K. Yang, An experimental study of pH optical sensor using a section of no-core fiber, *Sensors and Actuators A: Physical,* **2013,** 199, 260-264.

[107] C.R. Zamarreño, J. Bravo, J. Goicoechea, I.R. Matias, F.J. Arregui, Response time enhancement of pH sensing films by means of hydrophilic nanostructured coatings, *Sensors and Actuators B: Chemical,* **2007,** 128, 138-144.

[108] G. Bobo, Y. Mingjie, A.P. Zhang, Q. Jinwen, H. Sailing, Biocompatible Fiber-Optic pH Sensor Based on Optical Fiber Modal Interferometer Self-Assembled With Sodium Alginate/Polyethylenimine Coating, *Sensors Journal, IEEE,* **2012,** 12,

1477-1482.

[109] D. Wu, F. Xu, B. Sun, R. Fu, H. He, K. Matyjaszewski, Design and Preparation of Porous Polymers, *Chem. Rev.,* **2012,** 112, 3959-4015.

[110] M.A. Shannon, P.W. Bohn, M. Elimelech, J.G. Georgiadis, B.J. Marinas, A.M. Mayes, Science and technology for water purification in the coming decades, *Nature,* **2008,** 452, 301-310.

[111] D.L. Gin, R.D. Noble, Designing the Next Generation of Chemical Separation Membranes, *Science,* **2011,** 332, 674-676.

[112] R. Dawson, A.I. Cooper, D.J. Adams, Nanoporous organic polymer networks, *Prog. Polym. Sci.,* **2012,** 37, 530-563.

[113] M. Ulbricht, Advanced functional polymer membranes, *Polymer,* **2006,** 47, 2217-2262.

[114] L. Xue, J. Zhang, Y. Han, Phase separation induced ordered patterns in thin polymer blend films, *Prog. Polym. Sci.,* **2012,** 37, 564-594.

[115] M. Hernandez-Guerrero, M.H. Stenzel, Honeycomb structured polymer films via breath figures, *Polym. Chem.,* **2012,** 3, 563-577.

[116] L.A. Baker, Y. Choi, C.R. Martin, Nanopore membranes for biomaterials synthesis, biosensing and bioseparations, *Curr. Nanosci.,* **2006,** 2, 243-255.

[117] K.-V. Peinemann, V. Abetz, P.F.W. Simon, Asymmetric

superstructure formed in a block copolymer via phase separation, *Nat. Mater.,* **2007,** 6, 992-996.

[118] L.-S. Wan, J.-W. Li, B.-B. Ke, Z.-K. Xu, Ordered Microporous Membranes Templated by Breath Figures for Size-Selective Separation, *J. Am. Chem. Soc.,* **2012,** 134, 95-98.

[119] L.M. Pitet, M.A. Amendt, M.A. Hillmyer, Nanoporous Linear Polyethylene from a Block Polymer Precursor, *J. Am. Chem. Soc.,* **2010,** 132, 8230-8231.

[120] L. Le, S. Xiaobo, H. Sung Woo, R.C. Hayward, T.P. Russell, Fabrication of Co-continuous Nanostructured and Porous Polymer Membranes: Spinodal Decomposition of Homopolymer and Random Copolymer Blends, *Angew. Chem. Int. Ed.,* **2012,** 51, 4089-4094.

[121] H. Zhao, W. Gu, E. Sterner, T.P. Russell, E.B. Coughlin, P. Theato, Highly Ordered Nanoporous Thin Films from Photocleavable Block Copolymers, *Macromolecules,* **2011,** 44, 6433-6440.

[122] C. Liu, C. Gao, D. Yan, Honeycomb-patterned photoluminescent films fabricated by self-assembly of hyperbranched polymers, *Angew. Chem. Int. Ed.,* **2007,** 46, 4128-4131.

[123] H.H. Hariri, J.B. Schlenoff, Saloplastic Macroporous Polyelectrolyte Complexes: Cartilage Mimics, *Macromolecules,* **2010,** 43, 8656-8663.

[124] H.-J. Hong, S.-E. Jin, J.-S. Park, W.S. Ahn, C.-K. Kim,

Accelerated wound healing by smad3 antisense oligonucleotides-impregnated chitosan/alginate polyelectrolyte complex, *Biomaterials,* **2008,** 29, 4831-4837.

[125] Z.S. Li, H.R. Ramay, K.D. Hauch, D.M. Xiao, M.Q. Zhang, Chitosan-alginate hybrid scaffolds for bone tissue engineering, *Biomaterials,* **2005,** 26, 3919-3928.

[126] Z. Gui, J. Qian, M. Yin, Q. An, B. Gu, A. Zhang, A novel fast response fiber-optic pH sensor based on nanoporous self-assembled multilayer films, *J. Mater. Chem.,* **2010,** 20, 7754-7760.

[127] D. Buenger, F. Topuz, J. Groll, Hydrogels in sensing applications, *Prog. Polym. Sci.,* **2012,** 37, 1678-1719.

[128] X.H. Yang, L.L. Wang, Fluorescence pH probe based on microstructured polymer optical fiber, *Opt. Express,* **2007,** 15, 16478-16483.

[129] C.-C. Chiang, C.-H. Hsu, C.-H. Ou, A pH Sensor Based on Corrugated Long-Period Fiber Grating, *Sensors and Materials,* **2013,** 25, 359-364.

[130] X.Y. Zhang, Y.S. Yu, C. Chen, C.C. Zhu, R. Yang, Z.J. Liu, J.F. Liang, Q.D. Chen, H.B. Sun, Point-by-Point Dip Coated Long-Period Gratings in Microfibers, *IEEE Photon. Technol. Lett.,* **2014,** 26, 2503-2506.

[131] H. Xuan, W. Jin, M. Zhang, $CO_2$ laser induced long period gratings in optical microfibers, *Opt. Express,* **2009,** 17, 21882-21890.

[132] C.C. Chiang, L.R. Tsai, Perfectly notched long-period fiber grating filter based on ICP dry etching technique, *Opt. Lett.,* **2012,** 37, 193-195.

[133] A.I. Ciuciu, P.J. Cywinski, Two-photon polymerization of hydrogels - versatile solutions to fabricate well-defined 3D structures, *RSC Adv.,* **2014,** 4, 45504-45516.

[134] Y. Samchenko, Z. Ulberg, O. Korotych, Multipurpose smart hydrogel systems, *Adv. Colloid Interface Sci.,* **2011,** 168, 247-262.

[135] O. Azzaroni, K.H.A. Lau, Layer-by-layer assemblies in nanoporous templates: nano-organized design and applications of soft nanotechnology, *Soft Matter,* **2011,** 7, 8709-8724.

[136] X. Wang, X. Liu, X. Wang, Hydrogel diffraction grating as sensor: A tool for studying volume phase transition of thermo-responsive hydrogel, *Sens. Actuators, B,* **2014,** 204, 611-616.

[137] B.L. Rivas, E.D. Pereira, M. Palencia, J. Sánchez, Water-soluble functional polymers in conjunction with membranes to remove pollutant ions from aqueous solutions, *Prog. Polym. Sci.,* **2011,** 36, 294-322.

[138] Q. Zhao, M. Yin, A.P. Zhang, S. Prescher, M. Antonietti, J.

Yuan, Hierarchically Structured Nanoporous Poly(Ionic Liquid) Membranes: Facile Preparation and Application in Fiber-Optic pH Sensing, *J. Am. Chem. Soc.,* **2013,** 135, 5549-5552.

[139] Q. Zhao, J.W.C. Dunlop, X. Qiu, F. Huang, Z. Zhang, J. Heyda, J. Dzubiella, M. Antonietti, J. Yuan, An instant multi-responsive porous polymer actuator driven by solvent molecule sorption, *Nat. Commun.,* **2014,** 5.

[140] Q. Zhao, Q.F.F. An, Y.L. Ji, J.W. Qian, C.J. Gao, Polyelectrolyte complex membranes for pervaporation, nanofiltration and fuel cell applications, *J. Membr. Sci.,* **2011,** 379, 19-45.

[141] P. Akkahat, V.P. Hoven, Introducing surface-tethered poly(acrylic acid) brushes as 3D functional thin film for biosensing applications, *Colloids Surf., B,* **2011,** 86, 198-205.

[142] E.N. Chiang, R. Dong, C.K. Ober, B.A. Baird, Cellular Responses to Patterned Poly(acrylic acid) Brushes, *Langmuir,* **2011,** 27, 7016-7023.

[143] S. Naficy, J.M. Razal, G.M. Spinks, G.G. Wallace, P.G. Whitten, Electrically Conductive, Tough Hydrogels with pH Sensitivity, *Chem. Mater.,* **2012,** 24, 3425-3433.

[144] H. Jiang, F.-J. Xu, Biomolecule-functionalized polymer brushes, *Chem. Soc. Rev.,* **2013,** 42, 3394-3426.

[145] J. Hu, G. Zhang, S. Liu, Enzyme-responsive polymeric assemblies, nanoparticles and hydrogels, *Chem. Soc. Rev.,* **2012,** 41, 5933-5949.

[146] R. Dong, S. Krishnan, B.A. Baird, M. Lindau, C.K. Ober, Patterned Biofunctional Poly(acrylic acid) Brushes on Silicon Surfaces, *Biomacromolecules,* **2007,** 8, 3082-3092.

[147] P. Calvert, Hydrogels for Soft Machines, *Adv. Mater.,* **2009,** 21, 743-756.

[148] M. Krishnamoorthy, S. Hakobyan, M. Ramstedt, J.E. Gautrot, Surface-Initiated Polymer Brushes in the Biomedical Field: Applications in Membrane Science, Biosensing, Cell Culture, Regenerative Medicine and Antibacterial Coatings, *Chem. Rev.,* **2014,** 114, 10976-11026.

[149] S.H. Lim, J. Kim, S.-g. Lee, Y.S. Kim, Water-soluble polymer dielectric with potential for high performance organic thin-film transistors, *Chem. Commun.,* **2010,** 46, 3961-3963.

[150] L. Herlogsson, X. Crispin, N.D. Robinson, M. Sandberg, O.J. Hagel, G. Gustafsson, M. Berggren, Low-Voltage Polymer Field-Effect Transistors Gated via a Proton Conductor, *Advanced Materials,* **2007,** 19, 97-101.

[151] L. Herlogsson, Y.-Y. Noh, N. Zhao, X. Crispin, H. Sirringhaus, M. Berggren, Downscaling of Organic Field-Effect Transistors with a

Polyelectrolyte Gate Insulator, *Advanced Materials,* **2008,** 20, 4708-4713.

[152] L.M. Dumitru, K. Manoli, M. Magliulo, L. Sabbatini, G. Palazzo, L. Torsi, Plain Poly(acrylic acid) Gated Organic Field-Effect Transistors on a Flexible Substrate, *ACS Applied Materials & Interfaces,* **2013,** 5, 10819-10823.

[153] M.J. Yin, C. Wu, L.Y. Shao, W.K.E. Chan, A.P. Zhang, C. Lu, H.Y. Tam, Label-free, disposable fiber-optic biosensors for DNA hybridization detection, *Analyst,* **2013,** 138, 1988-1994.

[154] M.J. Yin, B.B. Gu, Q.A. Zhao, J.W. Qian, A. Zhang, Q.F. An, S.L. He, Highly sensitive and fast responsive fiber-optic modal interferometric pH sensor based on polyelectrolyte complex and polyelectrolyte self-assembled nanocoating, *Anal. Bioanal.Chem.,* **2011,** 399, 3623-3631.

[155] M.-J. Zhang, W. Wang, R. Xie, X.-J. Ju, L. Liu, Y.-Y. Gu, L.-Y. Chu, Microfluidic fabrication of monodisperse microcapsules for glucose-response at physiological temperature, *Soft Matter,* **2013,** 9, 4150-4159.

[156] M.E. Welch, C.K. Ober, Responsive and patterned polymer brushes, *J. Polym. Sci. Part B,* **2013,** 51, 1457-1472.

[157] K.J. Son, S. Kim, J.-H. Kim, W.-D. Jang, Y. Lee, W.-G. Koh,

Dendrimer porphyrin-terminated polyelectrolyte multilayer micropatterns for a protein microarray with enhanced sensitivity, *J. Mater. Chem.,* **2010,** 20, 6531-6538.

[158] N. Annabi, A. Tamayol, J.A. Uquillas, M. Akbari, L.E. Bertassoni, C. Cha, G. Camci-Unal, M.R. Dokmeci, N.A. Peppas, A. Khademhosseini, 25th Anniversary Article: Rational Design and Applications of Hydrogels in Regenerative Medicine, *Adv. Mater.,* **2014,** 26, 85-124.

[159] N. Annabi, K. Tsang, S.M. Mithieux, M. Nikkhah, A. Ameri, A. Khademhosseini, A.S. Weiss, Highly Elastic Micropatterned Hydrogel for Engineering Functional Cardiac Tissue, *Adv. Funct. Mater.,* **2013,** 23, 4950-4959.

[160] Z. Hao, H. Chen, D. Ma, Preparation of Micro Gold Devices on Poly(dimethylsiloxane) Chips with Region-Selective Electroless Plating, *Anal. Chem.,* **2009,** 81, 8649-8653.

[161] I. Abdelhedi-Miladi, D. Montarnal, M.M. Obadia, H. Ben Romdhane, E. Drockenmuller, UV-Patterning of Ion Conducting Negative Tone Photoresists Using Azide-Functionalized Poly(Ionic Liquid)s, *ACS Macro Lett.,* **2014,** 3, 1187-1190.

[162] H. Zeng, D. Martella, P. Wasylczyk, G. Cerretti, J.-C.G. Lavocat, C.-H. Ho, C. Parmeggiani, D.S. Wiersma, High-

Resolution 3D Direct Laser Writing for Liquid-Crystalline Elastomer Microstructures, *Advanced Materials,* **2014,** 26, 2319-2322.

[163] S. Naficy, G.M. Spinks, G.G. Wallace, Thin, Tough, pH-Sensitive Hydrogel Films with Rapid Load Recovery, *ACS Appl. Mater. Interfaces,* **2014,** 6, 4109-4114.

[164] K. Braam, V. Subramanian, A Stencil Printed, High Energy Density Silver Oxide Battery Using a Novel Photopolymerizable Poly(acrylic acid) Separator, *Advanced Materials,* **2015,** 27, 689-694.

[165] J. Torgersen, X.-H. Qin, Z. Li, A. Ovsianikov, R. Liska, J. Stampfl, Hydrogels for Two-Photon Polymerization: A Toolbox for Mimicking the Extracellular Matrix, *Adv. Funct. Mater.,* **2013,** 23, 4542-4554.

[166] B.C. Gross, J.L. Erkal, S.Y. Lockwood, C. Chen, D.M. Spence, Evaluation of 3D Printing and Its Potential Impact on Biotechnology and the Chemical Sciences, *Anal. Chem.,* **2014,** 86, 3240-3253.

[167] V.V. Vasilevskaya, I.I. Potemkin, A.R. Khokhlov, Swelling and Collapse of Physical Gels Formed by Associating Telechelic Polyelectrolytes, *Langmuir,* **1999,** 15, 7918-7924.

[168] D. Klinger, K. Landfester, Dual Stimuli-Responsive Poly(2-hydroxyethyl methacrylate-co-methacrylic acid) Microgels Based on Photo-Cleavable Cross-Linkers: pH-Dependent Swelling and Light-

Induced Degradation, *Macromolecules,* **2011,** 44, 9758-9772.

[169] M.J. Yin, B.B. Gu, J.W. Qian, A.P. Zhang, Q.F. An, S.L. He, Highly sensitive and selective fiber-optic modal interferometric sensor for detecting trace mercury ion in aqueous solution, *Anal. Methods,* **2012,** 4, 1292-1297.

[170] J.M. Corres, I. del Villar, I.R. Matias, F.J. Arregui, Fiber-optic pH-sensors in long-period fiber gratings using electrostatic self-assembly, *Opt. Lett.,* **2007,** 32, 29-31.

[171] H.S. Jang, K.N. Park, J.P. Kim, S.J. Sim, O.J. Kwon, Y.-G. Han, K.S. Lee, Sensitive DNA biosensor based on a long-period grating formed on the side-polished fiber surface, *Opt. Express,* **2009,** 17, 3855-3860.

[172] E. Melnik, R. Bruck, R. Hainberger, M. Lämmerhofer, Multi-step surface functionalization of polyimide based evanescent wave photonic biosensors and application for DNA hybridization by Mach-Zehnder interferometer, *Analytica Chimica Acta,* **2011,** 699, 206-215.

[173] M.Y. Li, S.S. Huang, P.S. Zhu, L.M. Kong, B. Peng, H. Gao, A novel DNA biosensor based on ssDNA/Cyt c/L-Cys/GNPs/Chits/GCE, *Electrochimica Acta,* **2009,** 54, 2284-2289.

[174] X.W. Wang, K.L. Cooper, A.B. Wang, J.C. Xu, Z.A. Wang, Y. Zhang, Z.J. Tu, Label-free DNA sequence detection using

oligonucleotide functionalized optical fiber, *Applied Physics Letters,* **2006,** 89.

[175] G. Jiang, A.S. Susha, A.A. Lutich, F.D. Stefani, J. Feldmann, A.L. Rogach, Cascaded FRET in Conjugated Polymer/Quantum Dot/Dye-Labeled DNA Complexes for DNA Hybridization Detection, *Acs Nano,* **2009,** 3, 4127-4131.

[176] X. Zhou, S. Xia, Z. Lu, Y. Tian, Y. Yan, J. Zhu, Biomineralization-Assisted Ultrasensitive Detection of DNA, *Journal of the American Chemical Society,* **2010,** 132, 6932-6934.

[177] F. Caruso, E. Rodda, D.F. Furlong, K. Niikura, Y. Okahata, Quartz crystal microbalance study of DNA immobilization and hybridization for nucleic acid sensor development, *Analytical Chemistry,* **1997,** 69, 2043-2049.

[178] B. Gu, M.-J. Yin, A.P. Zhang, J.-W. Qian, S. He, Low-cost high-performance fiber-optic pH sensor based on thin-core fiber modal interferometer, *Opt. Express,* **2009,** 17, 22296-22302.

[179] S. Niu, Y. Jiang, S. Zhang, Fluorescence detection for DNA using hybridization chain reaction with enzyme-amplification, *Chemical Communications,* **2010,** 46, 3089-3091.

[180] L. Dong, Z. Yang, Y. Zhang, Y. Zhu, L. Wang, L. Wang, Novel luminescent nanoparticles for DNA detection, *Spectrochimica Acta*

*Part A: Molecular and Biomolecular Spectroscopy,* **2010,** 75, 1530-1534.

[181] Y. Xiang, Z. Wang, H. Xing, N.Y. Wong, Y. Lu, Label-Free Fluorescent Functional DNA Sensors Using Unmodified DNA: A Vacant Site Approach, *Analytical Chemistry,* **2010,** 82, 4122-4129.

[182] X. Chen, L. Zhang, K. Zhou, E. Davies, K. Sugden, I. Bennion, M. Hughes, A. Hine, Real-time detection of DNA interactions with long-period fiber-grating-based biosensor, *Opt. Lett.,* **2007,** 32, 2541-2543.

[183] R. Pei, X. Cui, X. Yang, E. Wang, Assembly of Alternating Polycation and DNA Multilayer Films by Electrostatic Layer-by-Layer Adsorption, *Biomacromolecules,* **2001,** 2, 463-468.

[184] W.J. Stephen, P.T. Ralph, Fibre optic sensors with nano-structured coatings, *Journal of Optics A: Pure and Applied Optics,* **2006,** 8, S430-S444.

[185] A.J. Thiel, A.G. Frutos, C.E. Jordan, R.M. Corn, L.M. Smith, In Situ Surface Plasmon Resonance Imaging Detection of DNA Hybridization to Oligonucleotide Arrays on Gold Surfaces, *Analytical Chemistry,* **1997,** 69, 4948-4956.

[186] J.M. Brockman, A.G. Frutos, R.M. Corn, A Multistep Chemical Modification Procedure To Create DNA Arrays on Gold Surfaces for

the Study of Protein−DNA Interactions with Surface Plasmon Resonance Imaging, *Journal of the American Chemical Society,* **1999,** 121, 8044-8051.

[187] A.N. Chryssis, S.S. Saini, S.M. Lee, Y. Hyunmin, W.E. Bentley, M. Dagenais, Detecting hybridization of DNA by highly sensitive evanescent field etched core fiber Bragg grating sensors, *Selected Topics in Quantum Electronics, IEEE Journal of,* **2005,** 11, 864-872.

[188] W.-C. Law, K.-T. Yong, A. Baev, P.N. Prasad, Sensitivity Improved Surface Plasmon Resonance Biosensor for Cancer Biomarker Detection Based on Plasmonic Enhancement, *Acs Nano,* **2011,** 5, 4858-4864.

[189] R.C. Jorgenson, S.S. Yee, A fiber-optic chemical sensor based on surface plasmon resonance, *Sensors and Actuators B: Chemical,* **1993,** 12, 213-220.

[190] J.N. Anker, W.P. Hall, O. Lyandres, N.C. Shah, J. Zhao, R.P. Van Duyne, Biosensing with plasmonic nanosensors, *Nat Mater,* **2008,** 7, 442-453.

[191] B. Gu, M. Yin, A.P. Zhang, J. Qian, S. He, Optical fiber relative humidity sensor based on FBG incorporated thin-core fiber modal interferometer, *Opt. Express,* **2011,** 19, 4140-4146.

[192] J.L. Lutkenhaus, P.T. Hammond, Electrochemically enabled polyelectrolyte multilayer devices: from fuel cells to sensors, *Soft Matter,* **2007,** 3, 804-816.

[193] F.J. Arregui, I. Latasa, I.R. Matias, R.O. Claus (2003) An optical fiber pH sensor based on the electrostatic self-assembly method. *Sensors, 2003. Proceedings of IEEE*, pp 107-110 Vol.101.

[194] Y.-H. Yang, M. Haile, Y.T. Park, F.A. Malek, J.C. Grunlan, Super Gas Barrier of All-Polymer Multilayer Thin Films, *Macromolecules,* **2011,** 44, 1450-1459.

[195] S. Mouradian, J.W. Skogen, F.D. Dorman, F. Zarrin, S.L. Kaufman, L.M. Smith, DNA Analysis Using an Electrospray Scanning Mobility Particle Sizer, *Analytical Chemistry,* **1997,** 69, 919-925.

[196] J.D. Mendelsohn, C.J. Barrett, V.V. Chan, A.J. Pal, A.M. Mayes, M.F. Rubner, Fabrication of microporous thin films from polyelectrolyte multilayers, *Langmuir,* **2000,** 16, 5017-5023.

[197] F. Wang, J. Wang, Y. Zhai, G. Li, D. Li, S. Dong, Layer-by-layer assembly of biologically inert inorganic ions/DNA multilayer films for tunable DNA release by chelation, *Journal of Controlled Release,* **2008,** 132, 65-73.

[198] J. Homola, Present and future of surface plasmon resonance biosensors, *Analytical and Bioanalytical Chemistry,* **2003,** 377, 528-

539.

[199] X. Chen, L. Zhang, K. Zhou, E. Davies, K. Sugden, I. Bennion, M. Hughes, A. Hine, Real-time detection of DNA interactions with long-period fiber-grating-based biosensor, *Opt. Lett.,* **2007,** 32, 2541-2543.

[200] S. Brahim, D. Narinesingh, A. Guiseppi-Elie, Polypyrrole-hydrogel composites for the construction of clinically important biosensors, *Biosens. Bioelectron.,* **2002,** 17, 53-59.

[201] X. Kang, J. Wang, H. Wu, I.A. Aksay, J. Liu, Y. Lin, Glucose Oxidase-graphene-chitosan modified electrode for direct electrochemistry and glucose sensing, *Biosens. Bioelectron.,* **2009,** 25, 901-905.

[202] H.-F. Cui, K. Zhang, Y.-F. Zhang, Y.-L. Sun, J. Wang, W.-D. Zhang, J.H.T. Luong, Immobilization of glucose oxidase into a nanoporous TiO2 film layered on metallophthalocyanine modified vertically-aligned carbon nanotubes for efficient direct electron transfer, *Biosens. Bioelectron.,* **2013,** 46, 113-118.

[203] D. Janasek, J. Franzke, A. Manz, Scaling and the design of miniaturized chemical-analysis systems, *Nature,* **2006,** 442, 374-380.

[204] G.M. Whitesides, The origins and the future of microfluidics, *Nature,* **2006,** 442, 368-373.

[205] R.G. Blazej, P. Kumaresan, R.A. Mathies, Microfabricated bioprocessor for integrated nanoliter-scale Sanger DNA sequencing, *Proc. Nat. Acad. Sci. U.S.A.,* **2006,** 103, 7240-7245.

[206] Y.-H. Lin, S.-H. Wang, M.-H. Wu, T.-M. Pan, C.-S. Lai, J.-D. Luo, C.-C. Chiou, Integrating solid-state sensor and microfluidic devices for glucose, urea and creatinine detection based on enzyme-carrying alginate microbeads, *Biosens. Bioelectron.,* **2013,** 43, 328-335.

[207] P. Labroo, Y. Cui, Graphene nano-ink biosensor arrays on a microfluidic paper for multiplexed detection of metabolites, *Anal. Chim. Acta,* **2014,** 813, 90-96.

[208] Y. Wang, Q. He, Y. Dong, H. Chen, In-channel modification of biosensor electrodes integrated on a polycarbonate microfluidic chip for micro flow-injection amperometric determination of glucose, *Sens. Actuators, B,* **2010,** 145, 553-560.

[209] M.M. Picher, S. Kupcu, C.-J. Huang, J. Dostalek, D. Pum, U.B. Sleytr, P. Ertl, Nanobiotechnology advanced antifouling surfaces for the continuous electrochemical monitoring of glucose in whole blood using a lab-on-a-chip, *Lab Chip,* **2013,** 13, 1780-1789.

[210] W.-T. Hsu, W.-H. Hsieh, S.-F. Cheng, C.-P. Jen, C.-C. Wu, C.-H. Li, C.-Y. Lee, W.-Y. Li, L.-K. Chau, C.-Y. Chiang, S.-R.

Lyu, Integration of fiber optic-particle plasmon resonance biosensor with microfluidic chip, *Anal. Chim. Acta,* **2011,** 697, 75-82.

[211] P. Liu, D. Mao, R.J. Martin, L. Dong, An integrated fiber-optic microfluidic device for detection of muscular force generation of microscopic nematodes, *Lab Chip,* **2012,** 12, 3458-3466.

[212] C. Carrasquilla, Y. Xiao, C.Q. Xu, Y.F. Li, J.D. Brennan, Enhancing Sensitivity and Selectivity of Long-Period Grating Sensors using Structure-Switching Aptamers Bound to Gold-Doped Macroporous Silica Coatings, *Anal. Chem.,* **2011,** 83, 7984-7991.

[213] A. Cusano, P. Pilla, L. Contessa, A. Iadicicco, S. Campopiano, A. Cutolo, M. Giordano, G. Guerra, High-sensitivity optical chemosensor based on coated long-period gratings for sub-ppm chemical detection in water, *Appl. Phys. Lett.,* **2005,** 87.

[214] A.P. Zhang, S. Li-Yang, D. Jin-Fei, H. Sailing, Sandwiched long-period gratings for simultaneous measurement of refractive index and temperature, *IEEE Photonics Technol. Lett.,* **2005,** 17, 2397-2399.

[215] V. Bhatia, A.M. Vengsarkar, Optical fiber long-period grating sensors, *Opt. Lett.,* **1996,** 21, 692-694.

[216] J.H. Chong, P. Shum, H. Haryono, A. Yohana, M.K. Rao, C. Lu, Y. Zhu, Measurements of refractive index sensitivity using long-period grating refractometer, *Opt. Commun.,* **2004,** 229, 65-69.

[217] P.N. Nge, C.I. Rogers, A.T. Woolley, Advances in Microfluidic Materials, Functions, Integration, and Applications, *Chem. Rev.,* **2013,** 113, 2550-2583.

[218] Y.-A. Yang, C.-H. Lin, Multiple enzyme-doped thread-based microfluidic system for blood urea nitrogen and glucose detection in human whole blood, *Biomicrofluidics,* **2015,** 9, 022402.